GENETIC DISSECTION AND FUNCTIONAL ANALYSIS OF A PUTATIVE

A Dissertation

by

CHENGLONG LIU

Submitted to the Office of Graduate and Professional Studies of
Texas A&M University
in partial fulfillment of the requirements for the degree of

DOCTOR OF PHILOSOPHY

Chair of Committee,	Libo Shan
Committee Members,	Ping He
	Michael Kolomiets
	Elizabeth B. Pierson
Head of Department,	Leland S. Pierson III

May 2019

Major Subject: Plant Pathology

ABSTRACT

Perception of microbe-associated molecular patterns (MAMPs) by pattern recognition receptors (PRRs) elicits MAMP-triggered immunity (MTI) and contributes to plant resistance to pathogen infection. To understand the mechanisms underlying MTI, we have performed a genetic screen for the Arabidopsis genes governing immune gene expression (*AGGIE*) using transgenic plants carrying a luciferase reporter under the control of the promoter of a MTI marker gene *FRK1*(*pFRK1::LUC*), and identified a dominant mutant *aggie5-1* with reduced expression of endogenous MTI marker genes in response to multiple MAMPs and increased susceptibility against bacterial pathogen *Pseudomonas syringae*. Map-based cloning coupled with bulk sequencing and complementation test revealed that the causative mutation in *aggie5-1* occurs on a putative GHSL lipase gene (AGGIE5). AGGIE5 is a plant-specific peroxisome/chloroplast membrane-localized protein and plays a positive role in plant defense against bacterial pathogens. In addition, biochemical and genetic analysis revealed that AGGIE5 contains a NTPase domain with both ATPase and GTPase activities that are indispensable for AGGIE5 function in plant immunity.

A yeast two-hybrid screen identified MPK7, a group C mitogen-activated protein kinase (MPK7) as an AGGIE5 interactor. Importantly, MAMP treatment induces phosphorylation of AGGIE5 at threonine 612 by MPK7, and this phosphorylation is important for AGGIE5 function in plant immunity. CRISPR/Cas9-edited *mpk7* knockout mutants showed reduced disease resistance, suggesting a positive role of MPK7 in plant immunity. Significantly, the *aggie5-1* mutant AGGIE5^{D618N} was no longer phosphorylated

by MPK7. Together, the data indicate the importance of MPK7-mediated AGGIE5 phosphorylation in plant innate immunity.

Oxylipin profiling in WT, *aggie5* and *mpk7* mutants with and without treatment of a nonpathogenic bacterium which triggers MTI revealed that several oxylipin species, in particular dinor-12-oxo-phytodienoic acid (dn-OPDA), were induced upon elicitation of MTI and were further enhanced in the *aggie5* and *mpk7* mutants. Importantly, application of dn-OPDA suppressed the expression of some endogenous MTI marker genes and dampened plant defense against bacterial pathogens. Moreover, the dn-OPDA-mediated suppression was OPR3-independent and partially COI1-dependent, suggesting the direct role of dn-OPDA in immunity and indicating dn-OPDA may function as an important signal facilitating fine-tune of defense responses.

ACKNOWLEDGEMENTS

There are many people that have earned my gratitude for their contribution to my study and life in graduate school. More specifically, I would like to thank five groups of people: my committee members, my lab mates, my collaborators, funding agencies, and my family.

I deeply appreciate my PIs, Dr. Ping He and Dr. Libo Shan, for giving me the great opportunity to study in their lab since 2012 fall, and for their tremendous input on training me how to become an independent researcher in the future from every aspect. Under their supervision, I learned how to define a research problem, find a solution to it, and finally organize the results. I clearly understand how I have transformed from that 1-year graduate student who almost had no any idea about research in plant pathology to what I am today. Their great support and invaluable advice kept me studying hard and inspired me to look forward on academia. To summarize, I would give Dr. Ping He and Dr. Libo Shan most of the credit for becoming the kind of researcher I am today. I sincerely thank them for everything they have done in the past years.

I wound give special thanks to my committee Dr. Martin Dickman (former committee member), Dr. Michael Kolomiets and Dr. Elizabeth Pierson for their continuous help and support. They are always caring about me and my research, bring up constructive comments and suggestions and keep patient and encouraging. I am thankful to Dr. Martin Dickman, who taught me course *Theory of Research*, for his crucial remarks that shaped my research proposal. I am also grateful to Dr. Michael Kolomiets for his insightful comments and for sharing with me his tremendous experience in the oxylipin

field. I am quite appreciative of Dr. Elizabeth Pierson, an excellent scientist in the biocontrol/microbiota area, for agreeing to serve on my committee on such a short notice as a replacement for Dr. Martin Dickman.

I am also grateful to my collaborators. Special thanks to Dr. Kai Tao, Dr. Maoying Li, Dr. Zhangjun Fei, Dr. Zhaohu Li and Dr. Brett Tyler.

Lots of thanks give to past and current lab members from Drs. He and Shan lab especially Dr. Baomin Feng for collaborating in AGGIE2 project. I also really appreciate the guidance I got from several past lab members including Dr. Bo Li, Dr. Wenwei Lin, Dr. Xiangzong Meng and Dr. Xiyu Ma.

Thanks are also due to the China Scholarship Council (CSC) for their CSC Scholarship that I otherwise would not have been able to develop my scientific discoveries.

And great thanks give to department staff for making my life here easy, warm and pleasant. Also, I would like to thank my classmates and friends in College Station who made the past years so enjoyable.

Last but not least, I would like to express my deepest gratitude to my family and friends. I can never appreciate my family enough, especially my dad, mom, wife, son, daughter and my grandparents. I won't be here today without their love, encouragement and unconditional support.

CONTRIBUTORS AND FUNDING SOURCES

This work was supervised by a dissertation committee consisting of Dr. Libo Shan, Dr. Michael Kolomiets, Dr. Elizabeth Pierson of the Department of Plant Pathology and Microbiology and Dr. Ping He of the Department of Biochemistry and Biophysices.

The data analyzed for Chapter 2, 3 and 4 was helped by Dr. Libo Shan and Dr. Ping He. The subcellular localization analyses on AGGIE5 depicted in Chapter 2 were conducted in part by Dr. Kai Tao.

All other work conducted for the dissertation was completed by Chenglong Liu independently.

Graduate study was supported by a Research Assistantship from Texas A&M University and a fellowship from China Student Council (CSC fellowship).

NOMENCLATURE

12-OH-JA	12-Hydroxy Jasmonic Acid
12-OH-JA-Ile	12-Hydroxy Jasmonoyl Isoleucine
12-OPDA	12-oxo-phytodienoic Acid
ABA	Abscisic Acid
AFB1	Auxin Signaling F Box Protein 1
BAK1	BRI1-associated Receptor Kinase 1
BIK1	Botrytis–induced kinase 1
Cas9	CRISPR associated protein 9
CERK1	Chitin-elicitor Receptor Kinase 1
COI1	Coronatine Insensitive 1
CRISPR	Clustered Regularly Interspaced Short Palindromic Repeats
DAMP	Danger Associated Molecular Pattern
dn-OPDA	Dinor-phytodienoic Acid
EDS1	Enhanced Disease Susceptibility 1
EFR	Elongation Factor-Tu Receptor
EF-Tu	Elongation Factor-Tu
EMS	Ethyl Methanesulfonate
FLS2	Flagellin Sensitive 2
FRK1	FLG22-induced receptor-like kinase 1
IAA	Indole-3-acetic Acid
JA	Jasmonic acid

JA-Ile	Jasmonoyl Isoleucine
JAZ	Jasmonate-ZIM-domain Protein
LPS	Lipopolysaccharide
LRR	Leucine-rich Repeat
MAPK	Mitogen-activated Protein Kinase
MEKK	Mitogen-activated Protein kinase kinase kinase
MKK	Mitogen-activated Protein kinase kinase
MPK	Mitogen-activated Protein kinase
MYB15	R2R3-MYB transcription factor 15
OPR3	Oxophytodienoate Reductase 3
PAD4	Phytoalexin Deficient 4
PAL1	Phenylalanine Ammonia Lyase 1
PAMPs/MAMPs	Pathogen-or Microbe-associated molecular patterns
PARG	Poly (ADP-ribose) Glycohydrolase
PARP	Poly (ADP-ribose) Polymerase
PDF1.2	Plant Defensin 1.2
PGN	Peptidoglycan
PR1	Pathogenesis-related Gene 1
RbohD	NADPH/Respiratory Burst Oxidase Protein D
RLCK	Receptor-like Cytoplasmic Kinase
RLK	Receptor-like Kinase
RLP	Receptor-like Protein

ROS	Reactive Oxygen Species
SA	Salicylic Acid
SAG101	Senescence-associated Gene 101
SNP	Single Nucleotide Polymorphism
VSP1	Vegetative Storage Protein 1
WRKY30	WRKY DNA-binding Protein 30

TABLE OF CONTENTS

Page

LIST OF FIGURES

Page

LIST OF TABLES

Page

1. INTRODUCTION AND LITERATURE REVIEW

1.1 MAMP-triggered immunity

Plant innate immunity relies on the ability to effectively detect phytopathogens via recognition of pathogen/microbe-associated molecular patterns (PAMPs/MAMPs), which are derived from peptides, saccharides and lipids that are evolutionarily conserved across a wide distribution of pathogens in different kingdoms and are perceived by pattern recognition receptors (PRRs), which usually are plasma membrane (PM)-localized proteins receptor-like kinases (RLKs) and receptor-like proteins (RLPs) (Yu et al., 2017). Following ligand (MAMP)-receptor (PRR) binding, MAMP-triggered immunity (MTI), a rapid and robust signaling pathway is activated and results in effective restriction of penetration, infection and colonization by pathogens. Hallmarks of MTI activation include a series of MAMP-induced cellular and physiological responses, consist of cytosolic Ca^{2+} ($[Ca^{2+}]$cyt) concentration increasement, extracellular alkalization, apoplastic reactive oxygen species (ROS) bursts, actin filament remodeling, nitric oxide (NO) generation, synthesis of antimicrobial compounds and phytohormones, callose deposition, stomatal closure and plasmodesmata closure (Bent and Mackey, 2007; Boller and Felix, 2009; Meng and Zhang, 2013; Segonzac and Zipfel, 2011; Yu et al., 2017).

1.1.1 MAMP Detection

Microbe-associated molecular patterns (MAMPs) are microbe-derived molecules that are essential for microbes but that can be recognized by pattern recognition receptors (PRRs) of plants. PRRs are usually plasma membrane (PM)-localized proteins receptor-

like kinases (RLKs) and receptor-like proteins (RLPs) with extracellular domains allowing MAMP perception (Bohm et al., 2014). During the past two decades, quite a few PRR/MAMP pairs were identified. One of the most well-studied PRRs is Arabidopsis flagellin-sensitive 2 (FLS2), which recognizes flg22, a 22 amino acid long epitope from the N terminus of flagellin of *Pseudomonas aeruginosa* (Chinchilla et al., 2007; Zipfel et al., 2004).The other one is Arabidopsis EF-Tu receptor (EFR), which perceives elf18, an 18 amino acid long epitope of elongation factor Tu (EF-Tu) from *Escherichia coli* (Zipfel et al., 2006). In addition, upon MAMP perception, some proteins rapidly form immune receptor complexes with PRRs at the plasma membrane. BRI1 associated receptor kinase 1 (BAK1) was shown to bind flg22 in association with FLS2. Compromised early flg22-dependent responses was observed in *bak1* knockout mutant and thus be defined as a co-receptor (Heese et al., 2007; Roux et al., 2011; Segonzac and Zipfel, 2011; Sun et al., 2013). The receptor-like cytoplasmic kinase Botrytis-induced kinase 1 (BIK1) and related PBL (PBS1-like) kinases constitutively associate with FLS2 and become quickly phosphorylated and released from the PRR complexes upon MAMP elicitation (Lu et al., 2010; Zhang et al., 2010). Different autophosphorylation and transphosphorylation events happened in immune receptor complex and those molecular components are indispensable for following signal transduction in MAMP-triggered immunity (Lin et al., 2013).

1.1.2 Ca^{2+} Burst

One of the earliest known physiological response is an influx of extracellular Ca^{2+} into the cytosol (Jeworutzki et al., 2010; Nomura et al., 2012; Ranf et al., 2011). It is

known that cytosolic Ca^{2+} concentrations are regulated by plasma membrane Ca^{2+} channels that mediate Ca^{2+} influx and efflux transporters that reestablish Ca^{2+} homeostasis. This Ca^{2+} influx in the context of MAMP perception and signal transduction induces other membrane transporters opening, which lead to influx of H^+, efflux of K^+, Cl^- and NO^{3-}, and finally result in extracellular alkalization and plasma membrane depolarization (Jeworutzki et al., 2010). Ca^{2+} influx is positively regulated by BIK1 and related PBL (PBS1-like) kinases (Kadota et al., 2014; Li et al., 2014).

In addition to the rapid cytosolic Ca^{2+} concentration increasement upon MAMP perception, a following long-lasting increase of Ca^{2+} concentration was observed in the chloroplast stroma. Inhibitors of serine/threonine protein kinases and mitogen-activated protein kinase kinases (MAPKKs) cause a reduction of both the cytoplasmic and stromal Ca^{2+} oscillations, suggesting a possible involvement of a mitogen-activated protein kinase (MAPK) cascade in the generation of these Ca^{2+} signals (Nomura et al., 2012).

1.1.3 ROS Burst

Upon MAMP perception, an apoplastic reactive oxygen species (ROS) production termed as ROS burst rapidly occurs in extracellular area (Chinchilla et al., 2007; Ranf et al., 2011). In Arabidopsis, the plasma membrane-localized NADPH oxidase named respiratory burst oxidase homolog D (RBOHD) and respiratory burst oxidase homolog F (RBOHF) are responsible for MAMP-induced ROS production (Ranf et al., 2011; Zhang et al., 2007). Ca^{2+} direct bind to the N-terminal EF-hand motifs of RBOHD and regulate its function (Ogasawara et al., 2008). MAMP-induced phosphorylation on different

residues of RBOHD by both Ca^{2+}-induced calcium-dependent protein kinases (CDPKs) and BIK1 is also required for its full activation (Boudsocq et al., 2010; Dubiella et al., 2013; Kadota et al., 2014; Li et al., 2014). With activation of RBOHD, membrane-impermeable superoxide O^{2-} is produced in the apoplast and is converted into hydrogen peroxide (H_2O_2) by superoxide dismutases.

1.2 MAPK signaling in MTI responses

In eukaryotes, mitogen-activated protein kinase (MAPK) cascades are highly conserved signaling pathways that transduce several extracellular stimuli into intracellular responses. MAPK cascades activation is one of the earliest signaling events after MAMP sensing and play pivotal roles in plant defense against attacking pathogens. In MTI, MAPK cascades are involved in multiple defense responses, including defense gene induction, defense hormones biosynthesis/signaling, stomatal closure, biosynthesis of phytoalexin, and cell wall strengthening. Interestingly, MAPK cascades have also emerged as battlegrounds of plant-phytopathogen interactions. Pathogens successfully deliver effectors into plant cell to suppress MAPK activation and downstream defense responses to promote virulence and pathogenicity (Meng and Zhang, 2013).

In general, MAPK signaling is initiated by the activation of a MAP kinase kinase kinase (MAP3K; MEKK). Subsequently, MAP3K activation leads to the phosphorylation and activation of downstream MAP kinase kinases (MAP2K; MKK; MEK). Then, the MAP2K in turn phosphorylates the downstream MAP kinase (MAPK; MPK) and sequentially render MPK ability to phosphorylate its substrates (Meng and Zhang, 2013).

In Arabidopsis, there are 20 MAPKs, 10 MAPKKs, and about 60 MAPKKKs (Meng and Zhang, 2013). MAMP flg22 and elf18 can trigger a strong but transient activation of MAPKs, including MPK3, MPK6, MPK4, and MPK11. Absence of BAK1 results in marked reduction of flg22- and elf18-triggered activation of MPK3, MPK6, and MPK4 (Chinchilla et al., 2007). SERK4 was shown to also be required for flg22 and elf18-induced MAPK activation by acting cooperatively with BAK1 in the MAMP signaling (Roux et al., 2011). However, components linking the receptor complexes and MAPK cascades are still largely unknown at present. The first flg22-activated MAPK cascade consist of MEKK1, MKK4/MKK5, and MPK3/MPK6 (Asai et al., 2002). This MEKK1-MKK4/MKK5-MPK3/MPK6 cascade is usually considered as a positive regulator of MAMP-triggered responses. However, genetic studies revealed unaltered MPK3/MPK6 activation in *mekk1* mutant plants upon flg22 elicitation, suggesting that MEKK1 is not upstream of MKK4/MKK5-MPK3/MPK6 (Suarez-Rodriguez et al., 2007). The second MAPK cascade downstream of FLS2 is composed of MEKK1, MKK1/MKK2, and MPK4 (Zhang et al., 2012). Based on both genetic and biochemical studies, the MEKK1-MKK1/MKK2-MPK4 cascade was identified as a negative regulator in plant immunity because constitutive defense responses and increased resistance to bacterial pathogens was observed in the mutants of this cascade (Berriri et al., 2012).

In addition to elf18 and flg22 recognized by EFR and FLS2 respectively, MPK3, MPK6, and MPK4 are also activated by the fungal MAMP chitin, the bacterial MAMP peptidoglycans (PGNs) and harpin proteins, and Nep1-like proteins (NLPs) from

oomycetes, suggesting that these MAPKs are the converging points of MAMP signaling (Yu et al., 2017).

The flg22-activated ROS burst is unchanged in two independent lines overexpressing a MAPK phosphatase inactivating MPK3 and MPK6, suggesting that MPK3/MPK6 cascade is not required for the ROS burst in MTI (Suarez-Rodriguez et al., 2007). Recently, A *mpk3 mpk6* double mutant displays similar MAMP-induced ROS burst levels as wildtype, providing supportive genetic evidences demonstrate that the ROS burst is independent of MPK3/MPK6 (Xu et al., 2014). There are also results showed that the flg22-induced ROS burst is independent of the MEKK1-MKK1/MKK2-MPK4 cascade (Zhang et al., 2012).

MAPK cascades controls transcription reprogramming in nucleus in MTI by regulates a series of transcription factors. WRKY gene family transcription factors are usually induced in response to diverse biotic stresses, suggesting their vital roles in plant defense. The MEKK1-MKK4/MKK5-MPK3/MPK6 induces expression of two WRKY transcription factors WRKY22 and WRKY29 in response to flg22 treatment (Asai et al., 2002). However, the mechanism by which WRKY22/WRKY29 are activated downstream of MPK3/MPK6 is still elusive. In addition, MPK3/MPK6 directly phosphorylates WRKY transcription factor WRKY33 to regulate the expression level of camalexin biosynthetic genes in defense against the necrotrophic fungus *Botrytis* (Lippok et al., 2007). Interestingly, WRKY33 could also directly target ABA biosynthetic genes to limit ABA biosynthesis and then suppress the negative regulation of ABA on plant resistance towards *Botrytis* (Liu et al., 2015). ERF family is another large plant-specific transcription

factor family involved in plant immunity. ERF transcription factor ERF104 is characterized as a MPK6 substrate in MAMP signaling, and the phosphorylation of ERF104 by MPK6 likely promotes protein stability (Bethke et al., 2009). Similarly, ERF6 is another ERF transcription factor phosphorylated by MPK3/MPK6 upon *Botrytis* infection (Meng et al., 2013). MPK3/MPK6 also regulate ERF6 activity at both the transcriptional and post-translational levels, because phosphorylation of ERF6 by MPK3/MPK6 also stabilizes ERF6 protein and ERF6 gene expression is also upregulated by MPK3/MPK6 activation (Meng et al., 2013). Recently, the Trihelix transcription factor ASR3 was characterized as another novel negative regulator in MTI and is rapidly phosphorylated by the MEKK1-MKK1/MKK2-MPK4 cascade upon MAMP treatment (Li et al., 2015). Phosphorylation of ASR3 by MPK4 seems not to affect its transcriptional repressor activity but indeed enhances its DNA binding activity.

1.3 Lipid metabolism in MTI responses

1.3.1 Membrane lipids composition dynamics and lipid-derivatives production

As membrane depolarization always lead to dynamic changes in lipids composition, production of lipid and lipid-derivatives are very common in the PRR response. Lipids play irreplaceable roles in MTI responses and those lipid or lipid derivatives function as signal transducers or serve as synthesis precursors in MTI (Couto and Zipfel, 2016).

Membrane lipid remodeling occurs in response to stresses such as freezing, dehydration and nutrition depletion, and contributes to the maintenance of membrane

properties affecting lipid dynamics, membrane integrity and membrane-bound protein functions. Signaling lipids include a wide range of lipid classes, are usually present in small quantities in tissues, and are quickly synthesized from pre-existing membrane lipids or biosynthetic intermediates of membrane lipids. There has not been a detailed profile of the membrane lipid remodeling in MTI, but some recent reports on MAMP-triggered lipid production are waking up the silent beautiful field (Couto and Zipfel, 2016).

1.3.2 Free Fatty Acid Production in MTI

Treatment of algae with LPS from Salmonella abortus equi and Marinobacter hydrocarbonoclasticus induce free myristic acid (C14:0), palmitic acid (C16:0), palmitoleic acid (C16:1), stearic acid (C18:0), and oleic acid (C18:1) at 30 min after treatment. In addition, free linoleic acid (C18:2), linolenic acid (C18:3), octadecatetraenoic acid (C18:4), arachidonic acid (C20:4), and eicosapentaenoic acid (C20:5) are induced at 60 min after treatment (Kupper, Gaquerel et al. 2006). However, the knowledge on whether and how these lipids regulates MTI responses awaits further investigation (Kupper et al., 2006).

1.3.3 Phosphatidic Acid Production in MTI

Phosphatidic acid (PA), an important intermediate in lipid biosynthesis, is also considered to be a key signaling molecule regulating various cellular activities and environmental responses. In plant immunity, PA is potentially involved in the regulation of ROS production and actin remodeling (Testerink and Munnik, 2011). Two PA

biosynthetic pathways exist in plants: the direct hydrolysis of phospholipids by phospholipase D (PLD) and the combined actions of phospholipase C (PLC) and diacylglycerol kinase (DGK) to phosphorylate diacylglycerol (DAG) to PA (Yu et al., 2017).

Transient accumulation of PA has been observed in tomato suspension cells when treated with flg22, xylanase and chitotetraose (van der Luit et al., 2000). A rapid and transient PA induction was also detected in chitosan-treated rice suspension cells, and exogenously applied PA and DAG induce ROS in the absence of elicitors (Yamaguchi et al., 2003). N-acetylchitooligosaccharide induces activation of PLC and PLD in rice suspension cells and accumulation of PA and DAG.

1.3.4 IP3, DGPP, G3P Production in MTI

Treatment of algae with LPS from *Salmonella abortus equi* and *Marinobacter hydrocarbonoclasticus* induce free myristic acid (C14:0), palmitic acid (C16:0), palmitoleic acid (C16:1), stearic acid (C18:0), and oleic acid (C18:1) at 30 min after treatment, and induce free linoleic acid (C18:2), linolenic acid (C18:3), octadecatetraenoic acid (C18:4), arachidonic acid (C20:4), and eicosapentaenoic acid (C20:5) at 60 min after treatment (Kupper et al., 2006). However, the knowledge on whether and how these membrane lipids regulates MTI responses awaits further investigation.

PLC cleave PIP2 into IP3 and DAG. IP3 can act as an important second messenger to trigger Ca^{2+} release from internal Ca^{2+} stores like the endoplasmic reticulum, Golgi body, or vacuole (Allen et al., 1995; Berridge, 1993).

Plants can phosphorylate PA to produce DGPP, which has been found in yeast but not in higher animals. DGPP concentration increases within minutes in response to pathogens (van Schooten et al., 2006).

The glycerolipid, Glycerol-3-phosphate (G3P), has been suggested as a novel regulator of plant defense signaling. The glycerol kinase (also designated as NHO1) and NAD-dependent G3P dehydrogenase (GPDH) are two key enzymes involved in the G3P biosynthesis. Under flg22 stimulation, the expression levels of NHO1(Ph) and GPDH(Ph) were up-regulated, G3P levels increased, and the contents of floridoside decreased (Lai et al., 2015).

Although it remains unknown how those lipids contribute to MTI, it is conceivable that lipid metabolism was associated with the MAMP-induced defense responses.

1.4 Hormone signaling crosstalk with MTI

Phytohormones salicylic acid (SA), jasmonic acid (JA), and ethylene (ET) are the major defense hormones *in planta*, constituting another important class of signaling molecules involved in both local and systemic induced responses (Broekaert et al., 2006; Browse, 2009; Vlot et al., 2009).

As is known to all, SA signaling is usually involved against biotrophic or hemibiotrophic phytophogens, while JA and ET signaling are generally necessary against necrotrophic phytophogens. MAMP perception usually triggers SA, JA, and ET productions in plant (Yu et al., 2017).

In Arabidopsis, SA production begins between 3-6 h after flg22 treatment and peaks around 9 h (Tsuda et al., 2008), while ET production starts around 1 h after flg22 treatment and peaks around 4 h (Liu and Zhang, 2004). Notably, there is no significant induction of JA production upon flg22 in Arabidopsis (Nomura et al., 2012). However, JA production is elicited in potato by Pep-13, an MAMP from Phytophthora species (Halim et al., 2009). Increased susceptibility observed in SA-deficient mutants *sid2* and *pad4* revealed that SA positively contributes to MAMP-triggered immunity against bacterial pathogens and absence of SA signaling results in altered expression level of MAMP-regulated genes (Tsuda et al., 2009). Interestingly, it is demonstrated that phosphorylation of ACS2 and ACS6 by MPK3 and MPK6 is a key step for ET production (Liu and Zhang, 2004).

Besides, some of the molecular mechanisms involved in MAMP control of phytohormone biosynthesis have been identified. Making use of *dde2 ein2 pad4 sid2* quadruple mutant, it is revealed that all single SA, JA, and ET signaling pathways positively contribute to MAMP-triggered immune response and those MTI responses strongly relies on synergistic interactions among crosstalk of these hormone signalings (Tsuda et al., 2009).

In addition to SA, JA and ET, other phytohormones, such as abscisic acid (ABA), brassinosteroids (BR), gibberellins (GA), cytokinin (CK), and auxin (IAA), were also shown to play roles in MAMP-triggered immunity (Boller and Felix, 2009). For example, BES1, the key transcription factor in brassinosteroid (BR) signaling, is characterized as a

positive regulator on plant resistance and MTI gene induction and is phosphorylated by the MAMP-activated MPK6 (Kang et al., 2015).

1.5 JA synthesis and JA signaling

Jasmonoyl-isoleucine (JA-Ile) is a lipid-derived phytohormone necessary for regulation of growth and developmental processes such as pollen development and senescence (Browse, 2009). JA-Ile is also essential for plant defense responses to insects, nematodes, and necrotrophic fungal and bacterial pathogens.

JA is derived from polyunsaturated linolenic acid (18:3) and hexadecatrienoic Acid (16:3), which are oxygenated by either 9-lipoxygenases (LOX1 and LOX5 in Arabidopsis) or 13-lipoxygenases (LOX2, LOX3, LOX4, and LOX6 in Arabidopsis) (Glazebrook, 2005). The immediate product of 13-LOX is 13-hydroperoxyoctadecatrienoic acid (13-HPOT) produced from its action on 18:3 and 11-hydroperoxy-hexadecatrienoic acid (13-HPHT) from 16:3. Both 13-HPOT and 13-HPHT serves as the substrates for allene oxide synthase (AOS). Then, allene oxide cyclase converts the AOS products into cis-(+)-12-oxo-phytodienoic acid (12-OPDA) or dinor-12-oxo-phytodienoic acid (dn-OPDA) (Stenzel et al., 2003). Both 12-OPDA and dn-OPDA are transported into the peroxisome and converted to cyclopentanones by OPDA reductase (OPR3) and finally lead to JA after three rounds of β-oxidation by acyl-CoA oxidase (ACX) enzymes (Stintzi and Browse, 2000). JA is transported to the cytoplasm where it can be converted to the active form, (+)-7-iso-jasmonoyl-L-isoleucine (JA-Ile),

which can bind to the receptor coronatine-insensitive 1 (COI1) in nucleus in Arabidopsis (Dave and Graham, 2012).

The JA receptor is a nucleus-localized complex consist of COI1 and jasmonate ZIM domain (JAZ) proteins. COI1 is an F-box protein that is part of the SCF (Skp1/Cullin/F-box) E3 ubiquitin ligase complex, and JAZ proteins directly interact with repress transcriptional activators MYC2, MYC3, and MYC4. JA-Ile is the bioactive form of this hormone and promotes formation of the COI1-JAZ interaction triggers ubiquitination of JAZ repressors leading to degradation through proteasome, which in turn activates several transcription factors that regulate expression of a series of genes (Dave and Graham, 2012).

Remarkably, the bacterium *Pseudomonas syringae* employs a toxin called coronatine (COR) to enhance virulence (Tsai et al., 2009; Xin and He, 2013). COR is a structural mimic of JA-Ile with even higher affinity towards CO1 than JA-Ile. By mimicking JA, COR helps to activate JA signaling and dampen plant resistance by reducing the plant immune responses against this bacterial pathogen. In addition, COR also prevents stomatal closure which facilitates the entering of *Pseudomonas syringae* into the plant (Arnaud and Hwang, 2015; Xin and He, 2013).

1.6 Oxylipin production in MTI

The lipoxygenase (LOX) pathway is the major producer of plant oxylipins (Fessler and Parks, 2011) and unlike their mammalian analogues, these fatty-acid derived hormone-like metabolites are poorly understood in plants. The most elusive group, in

terms of functional characterization, are 9-oxylipins derived from 9-LOX reactions. Recent evidence has implicated 9-oxylipins in MTI-mediated responses. In potato suspension cells treated with an elicitor obtained from Phytophthora infestans, expression of 9-LOX and activity was increased (Gobel et al., 2001). In agreement with these observations, a hydroxy-fatty acid oxylipin (9-HOD) and divinyl ether oxylipin (colneleic acid) increased in accumulation. Furthermore, increases in the level of a hydroxy-(9-HOT) and trihydroxy-fatty acid oxylipins (9,10,11-TriHOD, 9,12,13-TriHOD) were observed in potato leaves at 12 hours after treatment with P.s.t. DC3000 (Gobel et al., 2002). These reports suggest that 9-LOX pathway activation is a general response against diverse pathogens through recognition of pathogen-derived elicitors.

Not only are 9-oxylipins induced during plant responses to pathogens, but 9-oxylipins also instill greater resistance against impending pathogen attack through direct antimicrobial toxicity or through poorly characterized signaling activity. Accumulation of a keto-fatty acid (9-KOT) increased 2 days after infection with P.s.t. DC3000 and was the most effective in reducing disease progression when used as a pretreatment (Vicente et al., 2012).

One of 9-LOXs in Arabidopsis, LOX1, which is expressed in guard cells, is required for stomatal closure in response to flg22. PUFA, the LOX substrates, trigger stomatal closure. The LOX products, fatty acid hydroperoxides, or reactive electrophile oxylipins induce stomatal closure (Montillet et al., 2013). the flg22-mediated stomatal closure is conveyed by both LOX1 and the mitogen-activated protein kinases MPK3 and MPK6 and involves salicylic acid.

Recently, 9-HOT and 9-KOT were shown to promote callose formation by activating brassinosteroid signaling (Marcos et al., 2015). Concentrated culture filtrate from *Phytophthora infestans* induced a sharp increase of linoleic acid and linolenic acid in tobacco cells at 8 hours after treatment. In contrast, linoleic acid and linolenic acid decreased in potato cells. In potato cells, only colneleic acid increased slightly until 16 h (Saubeau et al., 2013). LPS from *Pectobacterium atrosepticum* significantly induce 9,10,11-THOD in potato cells at 16 hours after treatment (Saubeau et al., 2013).

It remains unknown whether and how any of these oxylipins specifically contribute to plant defense and to the selective regulation of a subset of MTI responses.

1.7 Lipase-like protein EDS1/PAD4/SAG101

The nucleocytoplasmic lipase-like protein enhanced disease susceptibility 1 (EDS1) controls both basal and induced resistance towards biotrophic pathogens and play a vital role in regulation of transcriptional reprogramming to limit pathogen colonization in Effector-triggered immunity (ETI) (Feys et al., 2005). Arabidopsis EDS1 can directly interact with two homologous signaling partners, phytoalexin-deficient 4 (PAD4) (Feys et al., 2001)and senescence-associated gene 101 (SAG101) (Feys et al., 2005) in nucleocytoplasmic and nuclear complexes. EDS1, PAD4 and SAG101 constitute a plant-specific family with N-terminal a/b hydrolase motif and a highly conserved C-terminal EDS1-PAD4 (EP) domain with no known homologies (Feys et al., 2001; Feys et al., 2005). Arabidopsis EDS1 associations with PAD4 or SAG101 in separate complexes which are indispensable for basal resistance and induced resistance (Feys et al., 2005). An

Arabidopsis EDS1-SAG101 heterodimer and a derived EDS1-PAD4 heterodimer structural model provide a molecular basis for actions of exclusive EDS1 heterodimers with each partner in plant innate immunity (Wagner et al., 2013). Moreover, a ternary SAG101-EDS1-PAD4 complex was also discovered, suggesting a potential regulation mechanism. It is also demonstrated that SAG101 contributes to basal resistance and ETI in the absence of PAD4, suggesting the important roles of EDS1 family proteins in plant innate immunity. Notably, it is reported that inactivated EDS1 does not affect oxylipin synthesis (Ochsenbein et al., 2006).

1.8 Objective and importance for the study

MTI has essential role in plant defense against different phytopathogens. A detailed characterization and signal transduction for MTI will help us improve crops with high yield and durable resistance.

We aim to identify novel regulators of plant immune gene expression by map-based cloning on *Arabidopsis* EMS mutants. Furthermore, we want to understand the mechanisms behind MTI by combining genetic, biochemical studies on these regulators.

2. GENETIC DISSECTION AND FUNCTIONAL CHARACTERIZATION OF *ARABIDOPSIS GENE GOVERNING IMMUNE GENE EXPRESSION* 5

2.1 Summary

Perception of microbe-associated molecular patterns (MAMPs) by pattern recognition receptors (PRRs) elicits MAMP-triggered immunity (MTI) and contributes to plant resistance to pathogen infection. To understand the mechanisms underlying MTI responses, we have performed a genetic screen for the Arabidopsis genes governing immune gene expression (*aggie*) using transgenic plants carrying a luciferase reporter under the control of the promoter of a MTI marker gene FRK1(*pFRK1::LUC*).

The dominant mutant *aggie5-1* showed the reduced expression of *pFRK1::LUC* reporter and endogenous MTI marker genes in response to the treatments by multiple MAMPs. The activation of evolutionarily conserved MAP kinase cascades constitutes a convergent step downstream of multiple PRR signaling. However, MAMP-induced MAPK activation remained unaltered in *aggie5-1*. MAMP perception triggers a rapid burst of reactive oxygen species (ROS), which was reduced in *aggie5-1*. The data suggest that AGGIE5 regulates a subset of MTI outputs. Consistent with the reduced MTI responses, the *aggie5-1* mutant showed increased susceptibility against a virulent bacterial pathogen *Pseudomonas syringae*.

Map-based cloning coupled with bulk population sequencing revealed that aggie5 carries a mutation in a putative GHSL lipase gene (AGGIE5) linked to the reduced luciferase activity. Overexpression of the mutant form of AGGIE5 (AGGIE5^{D618N}) in wild-type *pFRK1::LUC* plants reduced multiple MTI responses, mimicking the *aggie5-1*

mutant. Clearly, AGGIE5^{D618N} globally negatively regulates MTI responses in Arabidopsis.

AGGIE5 encodes a plant-specific protein possessing both NTPase motif and putative lipase motif and is conserved among different land plants. AGGIE5 is an active NTPase *in vitro* and play an indispensable positive role in MTI responses. Both functional NTPase catalytic motif and putative lipase motif are required for its full functionality in MTI. AGGIE5 localizes to peroxisome membrane and chloroplast outermembrane.

In this study, we characterized Aggie5 (*aggie5-1*) mutant and identified the amino acid change of Aspartic acid (D) at 618 to Asparagine (N) (D618N) in AGGIE5 disrupts AGGIE5 normal function in *aggie5-1*, and then globally, dominantly suppresses MAMP-induced immune gene expression in nucleus. Mutational analysis revealed that peroxisome/chloroplast-localized AGGIE5 plays a crucial role in regulating immune gene expression and induced defense response.

Our study discovered a novel component of MAMP-triggered immunity in response to multiple MAMPs and characterized an informative mutation for gaining better understanding MTI signaling.

2.2 Introduction

In order to dissect MTI pathway, our lab initiated a forward genetic screen in search of mutants with altered MTI response indicated by *pFRK1::LUC* activity. FRK1 is an early, specific responsive gene to multiple MAMPs. *pFRK1::LUC* was generated by fusing FRK1 promoter with a luciferase gene. Transgenic plant seeds carrying

pFRK1::LUC were subjected to mutagen ethyl methanesulfonate (EMS) treatment to generate random mutations. *pFRK1::LUC* activity was measured via a luminometer machine.

Analysis of the mutant *aggie1* revealed that RNA polymerase II C-terminal domain phosphatase-like 3 (CPL3) is a novel negative regulator of MTI. The characterization of this phosphatase led to the discovery of a phosphorylation circuit that regulates immune gene expression via direct modulating phosphorylation dynamics of RNA polymerase II C-terminal domain (CTD) together with MAP kinases and CTD kinases.

Analysis of the mtuant *aggie2*, another novel negative regulator of MTI was identified as poly(ADP-ribose) glycohydrolase (PARG). Poly(ADP-ribose) polymerase (PARP) transfers ADP-ribose moieties from NAD^+ to acceptor proteins to generate protein modification defined as PARylation. PARG is the enzyme to hydrolyze the covalently attached poly(ADP-ribose) polymers on the acceptor proteins. Through *aggie2* study, Poly(ADP-ribosyl)ation (PARylation) was identified as a post-translational modification that plays a critical role in plant immune gene expression and defense to pathogen attacks.

Compared to the extensive studies of protein post-translation modification in plasma membrane-localized and nucleus-localized proteins, the involvement and regulation of organelles in plant MTI signaling are relatively less understood (Li et al., 2014a).

2.3 Materials and methods

2.3.1 Plant materials and growth conditions

Arabidopsis accessions Col-0 and *pFRK1::LUC* (wild-type, WT), various mutants and transgenic plants used in this study were grown in soil (Metro Mix 366, LP5) in a growth room at 23°C, 60% relative humidity, 70 μE $m^{-2}s^{-1}$ light with a 12-hr light/12-hr dark photoperiod. The sets of confirmed *Arabidopsis* T-DNA insertion lines (CS27941, CS27943 and CS27944) were obtained from the *Arabidopsis* Biological Resource Center (ABRC) and confirmed by PCR using primers listed in the table. Seedlings were grown on agar plates containing ½ Murashige and Skoog medium (½MS) with 0.5% sucrose, 0.8% agar and 2.5 mM MES at pH 5.7, in a growth chamber at 23°C or 30°C, 70 μE $m^{-2}s^{-1}$ light with a 12-hr light/12-hr dark photoperiod.

2.3.2 Plasmid construction and generation of transgenic plants

The *AGGIE5* gene were amplified from Col-0 or *aggie5-1* cDNA with primers containing BamHI-XbaI or XbaI at N terminus and StuI at C terminus (Table S5) and ligated into a plant protoplast expression vector *pHBT* with a *CaMV 35S* promoter at N-terminus and HA epitope-tag at C-terminus. The point mutations of $AGGIE5^{S235A}$ and $AGGIE5^{G717A}$ were generated by site-directed mutagenesis with primers listed in Table S5. To construct the pCAMBIA2300 and pCB302 binary vector containing AGGIE5 for *Agrobacterium*-mediated transformation assay in *Arabidopsis thaliana*, the AGGIE5 fragment was released from the *pHBT* vector digested with BamHI or XbaI and StuI and

ligated into the pCAMBIA2300 and pCB302 binary vector. All the clones were confirmed by sequencing. Arabidopsis transgenic plants were generated using *Agrobacterium*-mediated transformation by the floral-dip method.

2.3.3 *Arabidopsis* protoplast and *Nicotiana benthamiana* transient assays

For *Arabidopsis* protoplast transient expression, protoplasts from WT mutant were transfected with HA/FLAG/MYC-tagged genes in the *pHBT* vector and incubated for 12 hr. Proteins were isolated with 2 x SDS loading buffer and subjected to immunoblot analysis with anti-HA antibody. For *N. benthamiana* transient expression, *Agrobacterium tumefaciens* strain GV3101 containing *pCB302* vector was cultured in LB medium at 28ºC for overnight. Bacteria were harvested by centrifugation and re-suspended with buffer (10 mM MES, pH5.7, 10 mM $MgCl_2$, 200 μM acetosyringone) at OD_{600}=0.75. Leaves of four-week-old soil-grown *N. benthamiana* were hand-infiltrated using a needleless syringe with *Agrobacterium* cultures. Leaf samples were collected 36 hr after infiltration for protein isolation and immunoblot analysis.

2.3.4 Map-based cloning

Seeds containing the *pFRK1::LUC* transgenic seeds were treated with 0.4% EMS for 8 hours. M2 plants were screened for aggie mutants with the high or low luciferase activity based upon P.s.t. DC3000 *hrcC* infection. The F2 populations for mapping the aggie5 mutations were derived from genetic crossing between the *aggie5-1* mutant in the

Col-0 background to WT plants in the Ler background. Bulked segregation analysis was performed on pools of about 50 plants with INDEL markers between Col-0 and Ler.

2.3.5 Disease assay

P.s.t. DC3000, P.s.t. DC3000 *hrcC*, P.s.t. DC3000 AvrRps4 strains were grown overnight at 28°C in the King's medium B (KB) containing rifamycin and kanamycin (each at 50 µg ·ml-1). Psm strain was grown overnight at 28°C in the KB medium containing rifamycin (50 µg ·ml-1). Bacteria were pelleted by centrifugation, washed, and diluted to the desired density (OD=0.01 for HR, $5x10^{-4}$ cfu/ml for disease assay). The leaves were hand-inoculated with bacteria using a needleless syringe, and collected at the indicated time (0dpi, 3dpi) for bacterial counting. To measure bacterial growth, two leaf discs were ground in 100 µl water and serial dilutions were plated on TSA (1% Bacto tryptone, 1% sucrose, 0.1% glutamic acid, 1.5% agar) medium with appropriate antibiotics. Bacterial colony forming units (cfus) were determined after incubation at 28°C. At least three independent experiments were performed for all experiments. A one-way ANOVA analysis was performed with SPSS software with (SPSS Inc., Chicago).

2.3.6 MAPK activation assay

To detect MAPK activity, 10-day-old WT, aggie4 and aggie5 seedlings grown on ½ MS medium were transferred to water, incubated overnight and then treated with 100 nM flg22 or water for indicated time points (0, 15, 45min) and frozen in liquid nitrogen. The seedlings were homogenized in an extraction buffer (20 mM Tris-HCl, pH7.5, 100

mM NaCl, 1 mM EDTA, 10% Glycerol, 1% Triton X-100). Supernatant after centrifugation was transferred into a new tube. Equal amount of total proteins was electrophoresed on 10% SDS–PAGE. A α-pERK antibody (Cell Signaling) was used to detect phosphorylation status of MPK3 and MPK6 with an immunoblot. For different treatments, the seedlings were treated with 100 nM flg22 for indicated length of time.

2.3.7 ROS production assay

Leaves from 4 to 5-week-old soil-grown Arabidopsis plants were punched into leaf discs with the diameter of 5 mm and then cut three times with a razor blade into leaf strips. Leaf strips were incubated in 100 µl ddH2O overnight with gentle shaking to eliminate the wounding effect. Then, water was replaced with 100 µl reaction solution containing 50 µM luminol, 10 µg/ml horseradish peroxidase (Sigma-Aldrich) supplemented with or without 100 nM flg22. Luminescence was measured with a luminometer (Perkin Elmer, 2030 Multilabel Reader, Victor X3) with a setting of 1 min as the interval for a period of 40 min. Detected values of ROS production were indicated as means of Relative Light Units (RLU).

2.3.8 RNA Isolation and qRT-PCR Analysis

Total RNA from Ten-d-old seedlings was extracted by TRIzol reagent (Invitrogen) and quantified with NanoDrop (Thermo Scientific). RNA was then reverse transcribed to synthesize first-strand cDNA with M-MuLV Reverse Transcriptase and oligo(dT) primer following RNase-free DNase I (New England Biolabs) treatment. qRT-PCR analysis was

performed using iTaq SYBR green Supermix (Bio-Rad) with an ABI GeneAmp PCR System 9700 following standard protocol. The expression of each gene was normalized to the expression of UBQ10.

2.3.9 RNA-seq and Data Analysis

Two independent repeats were performed for RNA-seq analysis. For each repeat, equal amounts of RNA from two biological replicates was pooled for RNA-seq library construction. RNA-seq library preparation and sequencing were performed on an Illumina HiSequation 2500 platform with 100-nucleotide single-end reads at Texas AgriLife Genomics and Bioinformatics Service (College Station, TX). Approximately 15 million reads were obtained for each sample, which corresponds to 30× coverage of the Arabidopsis transcriptome. RNA-seq reads with low sequencing quality or reads with sequencing adaptors were filtered from the raw data. The resulting clean reads were then aligned to the Arabidopsis reference genome (TAIR10) using TopHat (Trapnell et al., 2009) with default parameters. A GFF (general feature format) formatted gene model annotation file was provided for reads alignment. Following the alignments, Cuffdiff (Trapnell et al., 2010) was used to calculate the number of fragments per kilobase of exon per million fragments mapped and to find the significant differential gene expression. Genes with expression fold change $\geqslant$ 2 and P value < 0.05 were considered as significantly different between samples with and without flg22 treatment. The differentially expressed genes were chosen for the hierarchical clustering analysis. A clustering heat map was generated using the Mev software (Howe et al., 2011). GO term

enrichment in each gene list was identified using GO Term Finder (Boyle et al., 2004) with the latest Arabidopsis GO term annotations. The data are sent to the PANTHER Classification System which contains up to date GO annotation data for Arabidopsis and other plant species. The cutoff for significant enrichment is P value < 0.01 and calculation false discovery rate < 0.5. The fold enrichment was calculated based on the frequency of genes annotated to the term compared with their frequency in the genome.

2.3.10 Subcellular Localization

Agrobacterium strain GV3010 containing pCAMBIA2300-35S::YFP-AGGIE5, p CAMBIA2300-35S::YFP-AGGIE5 and vector was cultured at 28°C overnight. Bacteria were harvested by centrifugation and resuspended with buffer (10 mM MES, pH 5.7, 10 mM MgCl2, and 200 μM acetosyringone) at OD600 = 0.75. Leaves of 3-week-old soil-grown *N. benthamiana* were infiltrated with Agrobacterium cultures. Fluorescence signals were detected 2 dpi. Arabidopsis transgenic plants expressing YFP-AGGIE5 were generated by Agrobacterium-mediated floral dipping transformation. For transient protoplast expression, protoplasts were co-transfected with YFP-AGGIE5, YFP-AGGIE5^{D618N} or vector and a peroxisome-localized red fluorescence protein (RFP-SKL), and signals were observed 12 h after transfection. Fluorescence images were taken with confocal laser microscope systems and images were processed using NIS-Elements microscope imaging software. The excitation laser of 537 and 561 nm was used for imaging YFP and RFP signals, respectively.

2.3.11 Co-immunoprecipitation (co-IP) assay

For protoplast-based co-IP assay, protoplasts were transfected with a pair of constructs (empty vector as control, 100 μg DNA for 500 μl protoplasts at the density of 2 x 10^5/ml for each sample) and incubated at room temperature for 10 hr. After treatment of flg22 with indicated concentration and time points, protoplasts were collected by centrifugation and lysed in 300 μl co-IP buffer (150 mM NaCl, 50 mM Tris-HCl, pH7.5, 5 mM EDTA, 0.5% Triton, 1 × protease inhibitor cocktail, before use, adding 2.5 μl 0.4 M DTT, 2 μl 1M NaF and 2 μl 1M Na3VO3 for 1 ml IP buffer) by vortexing. After centrifugation at 10,000×g for 10 min at 4°C, 30 μl of supernatant was collected for input control and 7 μl a-FLAG-agarose beads were added into the remaining supernatant and incubated at 4 °C for 1.5 hr. Beads were collected and washed three times with washing buffer (150 mM NaCl, 50 mM Tris-HCl, pH7.5, 5 mM EDTA, 0.5%Triton) and once with 50 mM Tris-HCl, pH7.5. Immunoprecipitates were analyzed by WB with indicated antibodies.

2.3.12 Recombinant protein isolation

Fusion proteins were produced from E. coli BL21 strain at 16°C using LB medium with 0.25 mM isopropyl -D-1-thiogalactopyranoside (IPTG). Glutathione Stransferase (GST) fusion proteins were purified with Pierce glutathione agarose (Thermo Scientific), and maltose binding protein (MBP) fusion proteins were purified using amylose resin (New England Biolabs) according to the standard protocol from companies.

2.3.13 *In vitro* GTPase and ATPase assay

Recombinant GST-AGGIE5 and truncated or mutated constructs were assayed for GTPase activity and ATPase activity in the presence and absence of MESG and PNP. GTPase activity was measured in solution by determining the amount of inorganic phosphate released by GTP or ATP hydrolysis using the EnzChek Phosphate Assay Kit (E6646; Molecular Probes).

In the presence of Pi, the substrate 2-amino-6-mercapto-7-methylpurine riboside (MESG) is converted enzymatically by purine nucleoside phosphorylase (PNP) to ribose 1-phosphate and 2-amino-6-mercapto-7-methylpurine. Enzymatic conversion of MESG results in a spectrophotometric shift in maximum absorbance from 330 nm for the substrate to 360 nm for the product.

In a 165 μL reaction, 0.8 nmol each of the purified protein component GST-AGGIE5^{EN}, GST-AGGIE5$^{EN,\ D618N}$, GST-AGGIE5$^{EN,\ G717A}$, GST-AGGIE5^{N} or GST protein or a substrate control that lacked protein components and MESG, PNP were incubated in reaction buffer at 22 °C for 10 mins. Then 400 uM GTP or 400 uM ATP are added and mixed well; in a parallel control assay, buffer was added instead of substrate. The absorbance of each sample was immediately measured at 360 nm with UV light after 30 mins incubation. Furthermore, a standard curve of inorganic phosphate was linear between 0 and 80 nmol of Pi and was used to determine the amount of Pi released in each assay. Throughout the duration of the assay, the amount of GTP or ATP hydrolyzed increased linearly.

2.4 Results

2.4.1 The *aggie5-1* mutant displays compromised immune gene expression

To mine novel components involved in regulating plant immune gene expression, a genetic screen of the EMS mutagenized *pFRK1::LUC* transgenic plants were carried out. One mutant termed as *aggie5-1* was isolated and displayed reduced FRK1 promoter activity upon flg22 treatment compared to its parental line, *pFRK1::LUC* (WT) (Fig. 2.1A). In addition to flg22, bacterial elicitors elf18, LPS, PGN and fungal elicitors chitin also triggered reduced FRK1 promoter activity in the *aggie5-1* compared to WT plants (Fig. 2.1B), indicating that *aggie5-1* functions as a convergent component downstream of multiple MAMP receptors. Consistently, the *aggie5-1* mutant exhibited the reduced FRK1 promoter activity in response to the non-pathogenic bacterium *Pseudomonas syringae* pv. *tomato* (P.s.t.) DC3000 *hrcC* which was defected in type III secretion system and failed to secret type III effectors into plant cells (Fig. 2.1C). The responses elicited by P.s.t. DC3000 *hrcC* were considered as MAMP-triggered immune responses which could be suppressed by multiple effectors secreted from the virulent pathogenic bacterium P.s.t. DC3000. The reduced luciferase activity in the *aggie5-1* mutant was observed over a 72-hr time course period upon flg22 treatment (Fig. 2.1D), excluding the possibility that the MTI induced immune gene induction was delayed in *aggie5-1*.

We further detected endogenous FRK1 expression in flg22-treated seedlings of WT and *aggie5-1* mutant with quantitative reverse transcription-polymerase chain reaction (qRT-PCR) analysis. The expression of the MTI marker gene FRK1 was

significantly elevated in the WT *pFRK1::LUC* transgenic plants compared to that of *aggie5-1* mutant at 60 min after flg22 treatment (Fig. 2.1E). Similarly, MYB15, WRKY30 and several other early MAMP marker genes expression was also reduced in the *aggie5-1* mutant (Fig. 2.1E). Taken together, the results indicate that *aggie5-1* negatively regulates the expression of certain flg22-induced genes.

In order to precisely position *aggie5-1* mutation in MTI signaling, we also detected two early events triggered by multiple MAMPs in WT and *aggie5-1* mutant, MAPK activation and ROS production. The flg22-induced MAPK activation detected by pERK antibody did not show significant and reproducible difference in WT and *aggie5-1* seedlings (Fig. 2.2A), suggesting that *aggie5-1* acts either independently or downstream of MAPK cascade. The flg22-induced ROS burst appeared to be significantly suppressed in the *aggie5-1* mutant compared to that in WT plants (Fig. 2.2B), suggesting that *aggie5-1* mutant may act upstream of ROS burst or dampen flg22-induced ROS burst by cross-talking with components regulating ROS signaling. We observed reproducible disease alternation in the *aggie5-1* mutant compared to WT plants in response to Psm infection by hand-infiltration (Fig. 2.2C). Consistently, in disease assays with P.s.t. DC3000 hand-infiltration, we also observed that *aggie5-1* was more susceptible than WT plants. Especially, the flg22-triggered protection was partially disrupted in *aggie5-1* mutant, which provided strong evidence that supports *aggie5-1* carries a mutation or mutations negatively regulating MTI (Fig. 2.2E). Besides, the *aggie5-1* mutant showed unaltered resistance to an avirulent pathogenic strain P.s.t. DC3000 carrying effector AvrRps4,

indicating the mutations harbored in *aggie5-1* specifically impact on MTI but not ETI (Fig. 2.2D).

2.4.2 Bulk sequencing reveals candidate SNPs of semi-dominant mutant *aggie5-1*

To isolate the causative mutation in *aggie5-1*, we first backcrossed *aggie5-1* (in the Col-0 accession background) with the WT *pFRK1::LUC* transgenic plants and performed genetics analysis. The *pFRK1::LUC* activity in BCF1 and the segregation radio in BCF2 population suggests *aggie5-1* is a semi-dominant mutant (Fig. 2.3A). Then we crossed *aggie5-1* (in the Col-0 accession background) with the Ler accession and mapped *aggie5-1* to a 2 Megabase pair (Mb) region between markers HG8CH3 and nga126 on Chromosome 3 by classical mapping approach (Fig. 2.3B). However, we found difficulties in further fine-mapping. Refer to well-developed mapping-by-sequencing method, we built two DNA pool based on phenotypes of F2 individual plants and then performed Illumina whole genome sequencing of *aggie5-1* phenotype pool and WT *pFRK1::LUC* transgenic plants phenotype pool. In this case that *aggie5-1* is a semi-dominant mutant, the sequencing results was aligned to reference genome Ler. We looked for the candidates of causative mutation in the SNP depletion region (Fig. 2.3C). The analysis of bulk sequencing also supports the causative mutation locates at the north arm of Chr3 (Fig. 2.3C). The comparative sequence analysis totally identified 9 mutations within this 2 Mb region (Fig. 2.3D, Table 2.1). Among them, a G to A mutation at the position 1852 bp of At3g07400 is the mutation showing highest frequency in *aggie5-1* phenotype pool but second lowest frequency in WT phenotype pool (Table. 2.1).

2.4.3 AGGIE5^{D618N} compromises flg22-triggered ROS production, transcriptome reprogramming and resistance

According to the annotation in TAIR, *Aggie5-1*(AGGIE5) encodes a putative class 3 lipase (Fig. 2.4A). The mutation was further confirmed by Sanger sequencing of the genomic DNA of At3g07400. At3g07400 encodes AGGIE5 and the mutation in the *aggie5-1* mutant causes an amino acid change of Aspartic acid (D) at 618 to Asparagine (N) (D618N) (Fig. 2.4B). The D618 in AGGIE5 resides in a conserved region in the middle with unknown function. Notably, this residue is relatively invariable in different species of Family Brassicaceae, suggesting the essential role of this residue in AGGIE5 functions. To confirm that the D618N lesion in AtAGGIE5 is the causative mutation in *aggie5-1*, we transformed a construct carrying AtAGGIE5 cDNA fused with a GFP epitope tag under the control of 35S promoter (p35S::AtAGGIE5^{D618N}-GFP) into *pFRK1::LUC* plants, to test whether transgenic plants expressing AtAGGIE5^{D618N}-GFP could phenocopy *aggie5-1* mutant or not. Three homozygous T3 transgenic lines were chosen for the assays. All lines phenocopied *aggie5-1* level of *pFRK1::LUC* activity upon *hrcC* treatment quantified by a luminometer (Fig. 2.4C), confirming that the reduced FRK1 promoter activity in *aggie5-1* is caused by the mutation in AtAGGIE5. Notably, three homozygous T3 transgenic lines expressing AtAGGIE5-GFP could not phenocopied *aggie5-1* level of *pFRK1::LUC* activity upon *hrcC* treatment, excluding the possibility that AGGIE5 itself worked as a negative regulator in controlling of *pFRK1::LUC* activity (Fig. 2.4C). Besides, we further detected endogenous FRK1 expression in flg22-treated

seedlings of WT, p35S::AtAGGIE5^{D618N}-GFP and p35S::AtAGGIE5-GFP transgenic plants with qRT-PCR analysis. The FRK1 expression was significantly reduced in p35S::AtAGGIE5^{D618N}-GFP transgenic plants compared to that of WT and p35S::AtAGGIE5-GFP transgenic plants at 60 min after flg22 treatment (Fig. 2.4D). Similarly, the expression of several other early MAMP marker genes, including MYB15 and At2g17740 was also reduced in the p35S::AtAGGIE5^{D618N}-GFP transgenic plants (Fig. 2.4D). Taken together, the results indicate that AGGIE5^{D618N} negatively regulates the expression of certain flg22-induced genes and MAMP-triggered immunity.

We also isolated T-DNA insertion line of AtAGGIE5, *aggie5-2* (CS825036) and *aggie5-3* (CS842133) (Fig. 2.4A) and examined flg22-induced immune gene activation. Like the *aggie5-1* mutant, *aggie5-2* displayed the elevated susceptibility to virulence strain P.s.t. DC3000 compared to WT Col-0 plants (Fig. 2.5A). However, the *aggie5-2* mutant showed unaltered resistance to an avirulent pathogenic strain P.s.t. DC3000 carrying effector AvrRps4, indicating AGGIE5 is not required for ETI response in Arabidopsis (Fig. 2.5B). We found that *aggie5-2* and *aggie5-3* displays increased susceptibility towards non-pathogenic strain P.s.t. DC3000 *hrcC* (Fig. 2.5C), although the ROS burst are unaltered in *aggie5-2* mutant, which is different from *aggie5-1* mutant (Fig. 2.5D). Overexpression of AGGIE5 in *aggie5-2* mutant could successfully restore this phenotype, while overexpession of AGGIE5^{D618N} fail to render plants the ability to defend against this non-pathogenic plant (Fig. 2.5C). These results indicate AGGIE5 play a vital and positive role in plant innate immunity and D618N appears a loss-of-function mutation. Interestingly, *aggie5-2* and *aggie5-3* also partially lost flg22-triggered protection

compared to WT Col-0 plants (Fig. 2.5E). Consistent with the flg22 protection assay, the flg22-triggered primary root growth inhibition was partially recovered in the *aggie5-2* (Fig. 2.5F). Apparently, overexpression of AGGIE5 alone was sufficient to restore flg22-triggered inhibition of hypocotyl growth in *aggie5-2* to WT level (Fig. 2.5F), indicating the knockout of AGGIE5 is the causative mutation in *aggie5-2*. The recovery could not be restored by overexpression of AGGIE5^{D618N} (Fig. 2.5F), which also phenocopies the suppressed flg22-triggered primary root growth inhibition in both *aggie5-1* mutant and phenocoping line p35S::AtAGGIE5-GFP transgenic plants (Fig. 2.4D). Taken together, the results indicate that AGGIE5 plays a positive role in immune gene regulation and plant immunity.

2.4.4 AGGIE5 is a putative GHSL lipase and possesses intact lipase motif and NTPase motif

Although there are no paralogs of AGGIE5 in Arabidopsis thaliana genome, orthologs of AGGIE5 could be found in Moss, Rice, Maize, Tomato, Potato, Soybean and other land plants (Fig. 2.6A). Notably, orthologs of AGGIE5 could not be found in genomes in other kingdoms. Interestingly, this plant-specific protein possesses a putative lipase motif and a putative NTPase motif, according to prediction at NCBI Conserved Domain Search (https://www.ncbi.nlm.nih.gov/Structure/cdd/wrpsb.cgi). Despite low sequence homology between AGGIE5 and its most similar protein identified from TAIR blast 2.2.8 (https://www.arabidopsis.org/Blast/) (Fig. 2.6B), we defined 3 domains in AGGIE5 protein except N-terminus and C-terminus, which are Lipase-like domain, EP-

like domain and NTPase-like domain, referring to gene structure of EDS1 as reported (Fig. 2.4A).

The Arabidopsis genome encodes at least 20 GHSL lipases (Fig. 2.7A), each of which contains an evolutionarily conserved GHSL catalytic motif GHSLG. GHSL lipases represent a subfamily of lipolytic enzymes, which like other members of the lipase and esterase families that possess a conserved catalytic triad Ser(S)… Asp(D)…His(H). However, in contrast to most lipases that contain the esterase box GxSxG, GHSL lipases exhibit a specific GHSL motif GHSLG. GHSL lipases have also been found in various plant species including Arabidopsis, rice and maize, and they have been implicated in plant development, morphogenesis and the defense response. Because the putative lipase catalytic motif, GHSLG box, is highly evolutionarily conserved in AGGIE5 and its orthologs (Fig. 2.7B), it is expected that AGGIE5 is a functional lipase.

Besides, AGGIE5 can be recognized as a putative GTPase by 4 to 5 highly conserved sequence motifs in its NTPase-like domain (Fig. 2.8B). In general, GTPases have several motifs recognizable at the sequence and structural levels. These include the G1-G2-G3-G4-G5 motifs and the highly mobile switch I and switch II regions. These motifs coordinate the binding of guanine nucleotides (G motifs) and the positioning of Mg^{2+} and water for efficient hydrolysis. A traditional GTPase usually consist of G1, G2, G3 and G4 motifs at least. Clearly, G1-G2-G3-G4 motifs are highly conserved in orthologs of AGGIE5 in different organisms (Fig. 2.8B). The G5 motif, present in some GTPases, is poorly defined in AGGIE5 and is not depicted. It is reported that G5 is dispensable in some GTPases, which is not required for GTPase function in some cases.

Interestingly, AGGIE5 is only one Arabidopsis lipase possesses a putative NTPase domain, which is homologous to Era-like subfamily GTPase that generally function in RNA/ribosome binding in bacteria (Fig. 2.8A). Although the full-length protein shows low similarity to the GTPases in subfamily Era, the NTPase motif show high similarity among the motifs of Era GTPases in Arabidopsis.

2.4.5 The ATP/GTP-hydrolyzing activity of AGGIE5 *in vitro*

Interestingly, there are two predicted transmembrane (TM) motifs in AGGIE5, a TM surrounding conserved GHSL motif and a TM motif at the C terminus (Fig. 2.9F), so recombinant GST-AGGIE5 protein could not be successfully isolated. However, recombinant GST-AGGIE5^{EN} protein which contain the EP-like domain and NTPase-like domain was isolated to test its NTPase activity against ATP or GTP.

NTPase is a nucleoside-triphosphatase, which is an enzyme that catalyzes the chemical reaction: NTP + H_2O → NDP + phosphate. Indeed, GST-AGGIE5^{EN} is an active NTPase catalyzing hydrolase of ATP/GTP to generate ADP/GDP and phosphate, respectively (Fig. 2.9A and Fig. 2.9C). The two substrates of AGGIE5 are NTP and H_2O, whereas its two products are NDP and phosphate: ATP + H_2O → ADP + phosphate; GTP + H_2O → GDP + phosphate. Aggie mutant forms of AGGIE5^{EN}, AGGIE5$^{EN, D618N}$, was also tested for its activity. The D618N substitution clearly does not affect AGGIE5 NTPase activity *in vitro* (Fig. 2.9A and Fig. 2.9C). Next, we further truncate the AGGIE5^{EN} and isolated recombinant GST-AGGIE5^{N}, which only contain intact predicted NTPase motif. From the results, we could conclude that the AGGIE5^{N} possesses in vitro

NTPase activity, indicating that the EP-like domain of AGGIE5 appears is not required for its NTPase activity in vitro (Fig. 2.9B and Fig. 2.9D). However, that's just an in vitro NTPase activity test. We could not rule out the possibility that how the full-length AGGIE5 regulates its NTPase by folding and other approaches. It should be noted that AGGIE5 is the only one active NTPase which possesses putative lipase motif in Arabidopsis.

2.4.6 Intact lipase motif and NTPase motif are required for functionality of AGGIE5 in regulation of defense responses

How post-translational modification regulates AGGIE5 NTPase activity and putative lipase activity remains largely unknown in plants. Some study in other ATPase has suggested phosphorylation of ATPase could directly regulate ATPase activation and function. To understand how the NTPase activity of AGGIE5 contributes to its function in plant defense, transgenic plants expressing AGGIE5^{G717A} in *aggie5-2* background were generated. T2 homozygous lines maintain comparable expression level of AGGIE5s were subjected to hand-infiltration of P.s.t. DC3000. According to the symptom and quantified bacteria growth speed, it could be concluded that the disruption of conserved NTPase motif leads to increased susceptibility towards virulent bacterial pathogen (Fig. 2.10A). Although the lipase activity of AGGIE5 have not been verified experimentally, we take the same approach to mutate the catalytic residue in lipase motif. T2 homozygous lines of transgenic plants expressing AGGIE5S235A that maintain comparable expression level of AGGIE5s were also subjected to hand-infiltration of P.s.t. DC3000 (Fig. 2.10A). The

disease assay results revealed that the conserved lipase motif of AGGIE5 were required for plant resistance as well, suggesting AGGIE5 is a functional esterase *in vivo*. To further examine the requirement of S234A or G717A, we infected the set of plants with non-pathogenic strain P.s.t. DC3000 *hrcC* (Fig. 2.10B). All transformants expressing AGGIE5^{703G} or AGGIE5^{G717A} do not exhibit resistance as WT, indicating failed complementation of P.s.t. resistance (Fig. 2.10B). Therefore, catalytic residues of AGGIE5 in both lipase and NTPase motifs appear to underlie AGGIE5 function in plant innate immunity. Moreover, T2 homozygous lines of transgenic plants expressing AGGIE5^{D618N} that maintain comparable expression level of AGGIE5s were also susceptible, supporting the founding D618N mutation negatively regulates plant defense responses to P.s.t. DC3000 (Fig. 2.10C). Interestingly, neither S235A nor G717A mutation further enhance susceptibility in AGGIE5^{D618N} background, suggesting the negative role of AGGIE5^{D618N} does not require both lipase and NTPase motifs (Fig. 2.10C). Therefore, it is speculated that the D618N mutation in AGGIE5 is a loss-of-function mutation.

2.4.7 AGGIE5 localizes to peroxisome membrane and chloroplast outermembrane

Consistent with its potential function as a class 3 lipase annotated by TAIR and its two putative transmembrane motifs (Fig. 2.9F), fluorescence signals derived from yellow fluorescent protein (YFP) fusion of AGGIE5 (YFP-AGGIE5) were observed only in the peroxisomes and chloroplast outermembranes in both *Nicotiana benthamiana* transient assays (Fig. 2.11B) and Arabidopsis protoplast transient assay (Fig. 2.12A). The set of pictures from Z scanning stacks clearly shows though YFP-AGGIE5 has chloroplasts

membrane localization, but it does have brighter signal surrounding the peroxisomes (Fig. 2.12F). Clearly, in *Nicotiana benthamiana* transient assays, the dot-like fluorescence signals from both YFP-AGGIE5 and AGGIE5-YFP were observed only in the peroxisomes but not in the endosomes (Fig. 2.11A and Fig. 2.12B). The fluorescence signals from YFP-AGGIE5^{D618N} were exactly consistent with observation with YFP-AGGIE5 and only localized to the peroxisomes (Fig. 2.11C), so it is very possible that D618N mutation does not affection subcellular localization of AGGIE5. Similarly, stable Arabidopsis transgenic plants carrying YFP-AGGIE5 under the control of the Cauliflower mosaic virus 35S promoter showed strong fluorescence signals in the peroxisomes and chloroplast outermembranes (Fig. 2.11D). Especially, in stable Arabidopsis transgenic plants, we observed strong fluorescence signals from YFP-AGGIE5 in dot-like organelle which should be peroxisomes, indicating AGGIE5 preferentially localize to peroxisomes (Fig. 2.12C). In the transgenic plants stably expressing YFP-AGGIE5, the peroxisomes stay closely to chloroplasts. Since stomatal cells have more chloroplasts than cortical cells, images clearly showed those bright peroxisomes also accumulate in stomatal cells. Clearly, the signal on the peroxisomes is much higher than the signal on the membrane of chloroplasts (Fig. 2.12C). The main localization of YFP-AGGIE5 in transgenic plant is peroxisome membranes (Fig. 2.12E), suggesting AGGIE5 mainly function in some pathways happened in peroxisome. Besides, when we observed RFP-SKL, it was found that peroxisomes prefer to locate closely to chloroplasts, even were trapped by chloroplasts. Clearly, the moving peroxisomes have tails. It looks like those moving

peroxisomes were trapped by chloroplasts (Fig. 2.12B). However, the localization on chloroplast membranes also indicates its function in chloroplast (Fig. 2.12D).

2.4.8 AGGIE5^{D618N} globally regulates flg22-induced immune genes

To further identify the AGGIE5-regulated flg22-induced genes, we performed RNA sequencing (RNA-seq) analysis with 10-d-old seedlings of wild-type, *aggie5-1*, and p35S::AtAGGIE5^{D618N}-FLAG transgenic line with or without 100 nM flg22 treatment for 60 min. Samples from three independent biological repeats were collected and RNAs from two repeats were pooled for RNA-seq. The correlation coefficient (R) for the expression profiles of all transcripts between the wild type and *aggie5-1*, and between the wild type and p35S::AtAGGIE5^{D618N}-FLAG without flg22 treatment was close to linear (0.99), suggesting that AGGIE5 does not affect general gene transcription (Fig. 2.13A). Among 25,862 detectable transcripts, 122 genes showed differential expression (fold change $\geqslant$ 2, P value < 0.05), with 85 showing enhanced and 37 reduced expression in the *aggie5-1* mutant compared with wild-type plants without treatment (Supplemental Data Set 1A). Compared with no treatment, flg22 treatment induced 790, 209, and 678 genes (fold change $\geqslant$ 2, P value < 0.05) in the wild type, *aggie5-1*, and p35S::AtAGGIE5^{D618N}-FLAG transgenic line, respectively, with 184 genes induced in all three genotypes (Fig. 2.13B; Supplemental Data Set 1B, 1C, 1D). Hierarchical clustering analysis with all detected transcripts in any of the three genotypes suggested that the *aggie5-1* mutant displayed an overall compromised flg22 response, whereas p35S::AtAGGIE5^{D618N}-FLAG transgenic line displayed a similar response as *aggie5-1* mutant, compared with wild-type plants (Fig.

2.13C). We further analyzed the differential flg22-induced genes in the wild type and the *aggie5-1* mutant and p35S::AtAGGIE5^{D618N}-FLAG phenocopying line, which were defined as AGGIE5^{D618N}-dependent flg22-induced genes and classified them into four groups: Group I, 693 genes as AGGIE5^{D618N}-supprressed flg22-induced genes (genes induced in the wild type but not in *aggie5-1* and p35S::AtAGGIE5^{D618N}-FLAG phenocopying line); Group II, 338 genes as AGGIE5^{D618N}-attenuated flg22-induced genes (genes induced in both the wild type and *aggie5-1* or p35S::AtAGGIE5^{D618N}-FLAG phenocopying line with at least 1.5-fold higher induction in the wild type than *aggie5-1* and p35S::AtAGGIE5^{D618N}-FLAG phenocopying line, respectively); Group III, 8 genes as AGGIE5^{D618N}-potentiated flg22-induced genes (genes induced in both the wild type and *aggie5-1* and p35S::AtAGGIE5^{D618N}-FLAG phenocopying line with at least 1.5-fold higher induction in *aggie5-1* or p35S::AtAGGIE5^{D618N}-FLAG phenocopying line than the wild type, respectively); and Group IV, 63 genes as AGGIE5^{D618N}-required flg22-induced genes (genes induced in *aggie5-1* and p35S::AtAGGIE5^{D618N}-FLAG phenocopying line but not in the wild type) (Fig. 2.13D; Supplemental Data Set 1E, 1F, 1G, 1H). Importantly, enrichment analysis of Gene Ontology (GO) categories indicates that genes associated with response to chitin, response to bacterium, secondary metabolic process, immune system process, and response to biotic stimulus were significantly enriched (P value < 0.01) among Group I and II genes (Fig. 2.13E;). This observation is consistent with the idea that AGGIE5^{D618N} regulates a large subset of flg22-regulated genes through playing a role as class 3 lipase in secondary metabolic process. Taken together, the global gene

expression data suggest that AGGIE5^{D618N} functions as a negative regulator in MTI transcription reprogramming.

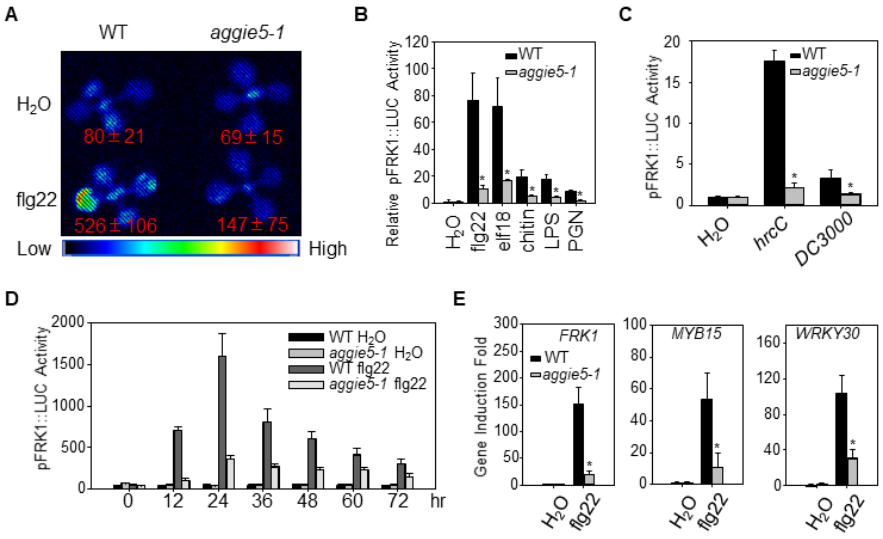

Figure 2.1 Reduced pFRK1::LUC expression and MAMP-triggered immune gene expression in *aggie5-1* mutant.

A. Luciferase activity from ten-day-old *pFRK1::LUC* (WT) and *aggie5-1* seedlings treated with or without 10 nM flg22 for 12 hr. The photograph was taken with an EMCCD camera. The *pFRK1::LUC* transgenic plants (WT) and *aggie5-1* mutant were included in the assay. The number below indicates quantified signal intensity shown as means ± se from 12 seedlings. **B.** The *pFRK1::LUC* activity in response to different MAMPs. Ten-day-old seedlings were treated with 100 nM elf18, 50 µg/ml chitin, 1 µM LPS, or 500 ng/ml PGN for 12 hr. The *pFRK1::LUC* transgenic plants (WT) and *aggie5-1* mutant were included in the assay. The data are shown as means ± se from at least 12 seedlings for each treatment. **C**. The *pFRK1::LUC* activity triggered by different bacteria. Four-week-old soil-grown plants were hand-inoculated with different bacteria at the concentration of OD_{600} = 0.5. The *pFRK1::LUC* transgenic plants (WT) and *aggie5-1* mutant were included in the assay. The data are shown as means ± se from at least 12 leaves for each treatment at 24 hr post-inoculation (hpi). **D**. Time-course of *pFRK1::LUC* activity in response to 100 nM flg22 treatment. The *pFRK1::LUC* transgenic plants (WT) and *aggie5-1* mutant were included in the assay. The data are shown as means ± se from at least 20 seedlings for each time point. **E**. Endogenous MAMP-induced marker gene expression. Ten-day-old seedlings were treated with 100 nM flg22 for 60 min for qRT-PCR analysis. The *pFRK1::LUC* transgenic plants (WT) and *aggie5-1* mutant were included in the assay. The data are shown as means ± se from three biological repeats with Student's *t*-test. * indicates $p<0.05$ and ** indicates $p<0.01$ when compared to WT. The above experiments were repeated 3 times with similar results.

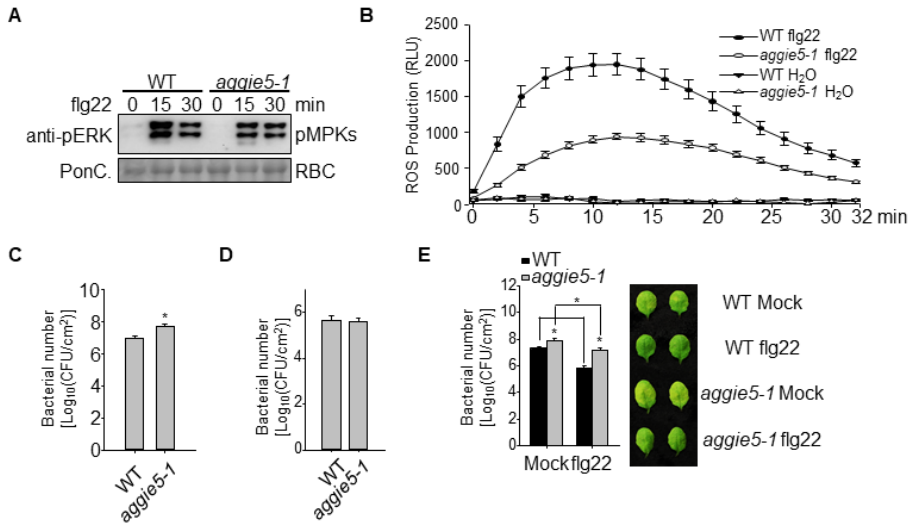

Figure 2.2 Compromised MAMP-triggered resistance in *aggie5-1* mutant.

A. Flg22-induced phosphorylation of MPK3/4/6 is not changed in *aggie5-1*. Ten-days-old seedling were treated with or without 100 nM flg22 treatment for indicated time points. MAPK activation was analyzed with an α-pERK antibody (top panel), and protein loading was shown by Coomassie Brilliant Blue (CBB) staining for RuBisCO (RBC) (bottom panel). The *pFRK1::LUC* transgenic plants (WT) and *aggie5-1* mutant were included in the assay. **B.** Flg22-triggered ROS production is reduced in *aggie5-1*. Leaf discs were treated with 100 nM flg22, and the ROS production was measured with a plate reader over 40 min (2400 seconds). The *pFRK1::LUC* transgenic plants (WT) and *aggie5-1* mutant were included in the assay. The data are shown as means ± standard errors from 20 leaf discs for flg22 treatment. **C.** Disease resistance to *P.s.t. DC3000* infection in compromised in *aggie5-1*. Four-week-old plants were hand-inoculated with *P.s.t. DC3000* at 5×10 cfu/ml. The *pFRK1::LUC* transgenic plants (WT) and *aggie5-1* mutant were included in the assay. The *in planta* bacterial growth was measured at 3 days-post inoculation (dpi). The data are shown as means ± standard errors. **D.** Disease resistance to *P.s.t. DC3000* carrying effector AvrRps4 infection in not altered in *aggie5-1*. Four-week-old plants were hand-inoculated with *P.s.t. DC3000* carrying effector AvrRps4 at 5×10 cfu/ml. The *pFRK1::LUC* transgenic plants (WT) and *aggie5-1* mutant were included in the assay. The *in planta* bacterial growth was measured at 3 days-post inoculation (dpi). The data are shown as means ± standard errors. **E.** Flg22-mediated protection against *P.s.t. DC3000* infection is partially compromised in *aggie5-1*. Four-week-old plants were hand-inoculated with H_2O or 100 nM flg22 24 hours before inoculation of *P.s.t. DC3000* at 5×10 cfu/ml. The *pFRK1::LUC* transgenic plants (WT) and *aggie5-1* mutant were included in the assay. The *in planta* bacterial growth was measured at 3 days-post inoculation (dpi). The data are shown as means ± standard errors. The above experiments were repeated 3 times with similar results.

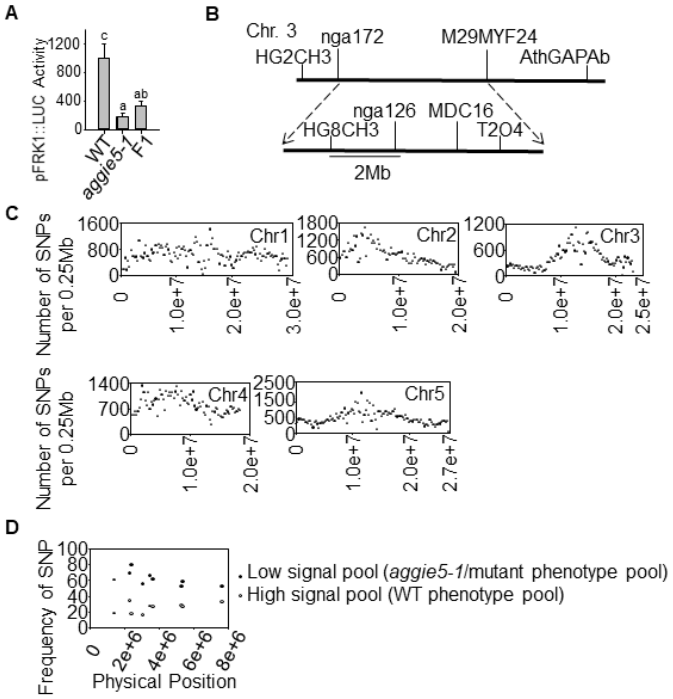

Figure 2.3 The *aggie5-1* was mapped to Arabidopsis chromosome 3.

A. Causal mutation in *aggie5-1* is semi-dominant. The F1 plants crossed from *aggie5-1* and the *pFRK1::LUC* transgenic plants (WT) showed *pFRK1::LUC* activity similar to *aggie5-1* upon infiltration of *P.s.t. DC3000 hrcC*. The different letters indicate statistically significant differences from WT within the same time point according to two-way ANOVA followed by Tukey test ($p<0.05$). **B.** Map-based cloning of *aggie5-1*. F1 plants were obtained by outcrossing *aggie5-1* (in Col-0 background) with another WT Landsberg *erecta* (Ler). After one generation of self-crossing, F2 plants were subjected to screen of homozygotes, which displayed unaltered *P.s.t. DC3000 hrcC*-elicited *pFRK1::LUC* activity. The causal mutation was mapped to a region between genetic marker HG8CH3 and nga126 on *Arabidopsis* chromosome 3. **C.** SNP density map of WT-phenotype pool (high signal pool) of F2 of cross between Ler (♀) and *aggie5-1* (♂), Landsberg *erecta*-0 (Ler-0) as reference. F1 plants were obtained by outcrossing *aggie5-1* (in Col-0 background) with another WT Ler. After one generation of self-crossing, F2 plants were subjected to screen of homozygotes, which displayed unaltered *P.s.t. DC3000 hrcC*-elicited *pFRK1::LUC* activity. Genomic DNA of 52 plants that show unaltered *pFRK1::LUC* activity were mixed as WT-phenotype (high signal pool) and genomic DNA of 47 plants that show compromised *pFRK1::LUC* activity were mixed as mutant-phenotype pool (low signal pool). Two pools of DNA were subjected to whole genome sequencing respectively. The SNP to Ler genome were analysis for mapping causal mutation in *aggie5-1*. **D.** Distribution of SNPs at chromosome 3 0-7.5Mb of *AGGIE5* in mutant-phenotype pool (low signal pool) or wild-type phenotype (high signal pool) of F2 of cross between Ler(♀) and *AGGIE5*(♂).

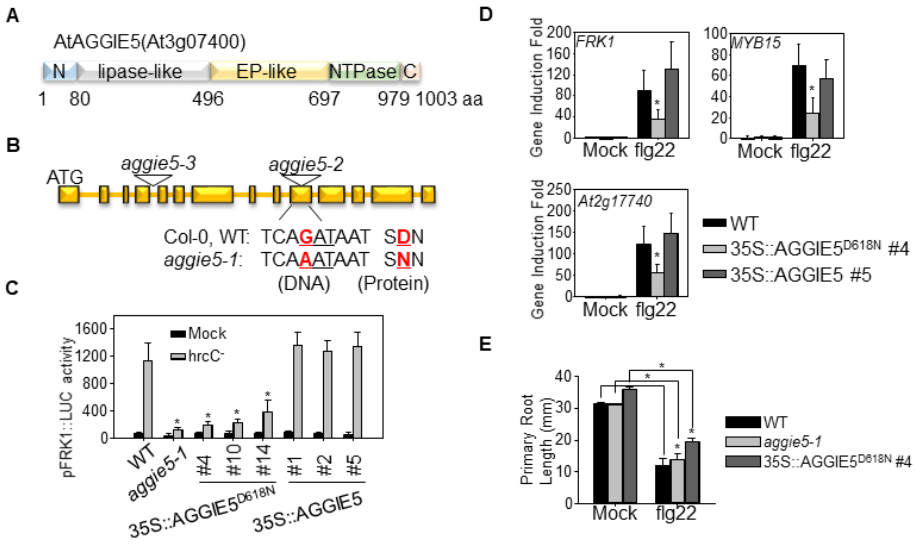

Figure 2.4 *Aggie5-1* encodes AtAGGIE5.

A. AGGIE5 encodes a protein with putative lipase and NTPase motifs. The structure of AGGIE5 labeled with the putative protein motifs is shown on top, and the amino acid sequence with the starting and ending positions for each motif is shown below. N, N-terminal; Lipase-like, lipase-like domain; EP-like, EP-like domain; NTPase, NTPase domain; C, C-terminal. **B**. Aspartic acid 618 (D618; red) in AtAGGIE5 was mutated to Asparagine (N) in *aggie5-1*. *aggie5-2* and *aggie5-3*, two T-DNA mutants. **C**. Transgenic plants overexpressing AtAGGIE5^{EN} but not transgenic plants overexpressing AtAGGIE5 phenocopy *aggie5-1* mutant. Leaves of 4-week-old soil-grown plants were treated with or without *P.s.t. DC3000 hrcC* for 16 hr. The *pFRK1::LUC* transgenic plants (WT), *aggie5-1* mutant and three independent homozygous lines of p35S*::AtAGGIE5-GFP*, p35S*::AtAGGIE5*^{D618N}*-GFP* transgenic plants in WT background were included in the assay. The data are shown as means ± se from at least 10 plants. The protein expression of the transgene was detected with an α-FLAG Western blot. **D.** Reduced immune gene expression in p35S*::AtAGGIE5*^{D618N}*-GFP* transgenic plants. Ten-day-old seedlings were treated with 100 nM flg22 for 60 min for qRT-PCR analysis. The *pFRK1::LUC* transgenic plants (WT), one homozygous lines of p35S*::AtAGGIE5-GFP*, p35S*::AtAGGIE5*^{D618N}*-GFP* transgenic plants in WT background were included in the assay. The data are shown as means ± se from three biological repeats with Student's *t*-test. * indicates $p<0.05$ when compared to WT. **E.** AGGIE5 is required for disease resistance to *P.s.t. DC3000* infection. AtAGGIE5 complements *aggie5-2* mutant phenotype, while AGGIE5^{D618N} could not complement *aggie5-2* mutant phenotype. Four-week-old plants were hand-inoculated with *P.s.t. DC3000* at 5×10 cfu/ml. Col-0 (WT), *aggie5-2* and *aggie5-3* mutants and two independent homozygous lines of p35S*::AtAGGIE5-FLAG*, p35S*::AtAGGIE5*^{D618N}*-FLAG* transgenic plants in *aggie5-2* background were included in the assay. The *in planta* bacterial growth was measured at 3 days-post inoculation (dpi). The data are shown as means ± standard errors. The above experiments were repeated 3 times with similar results.

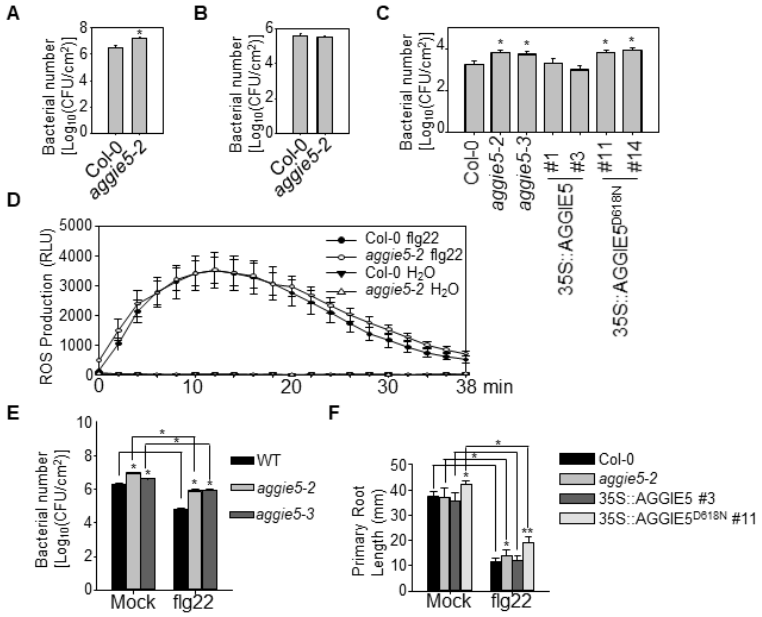

Figure 2.5 AGGIE5 plays a positive role in defense against bacterial infection and MAMP-triggered immune response.

A. AGGIE5 is required for disease resistance to *P.s.t. DC3000* infection. Four-week-old plants were hand-inoculated with *P.s.t. DC3000* at 5×10 cfu/ml. The *in planta* bacterial growth was measured at 3 days-post inoculation (dpi). Col-0 (WT) and *aggie5-2* mutant were included in the assay. The data are shown as means ± standard errors. **B.** AGGIE5 is not required for disease resistance to *P.s.t. DC3000 AvrRps4* infection. Four-week-old plants were hand-inoculated with *P.s.t. DC3000 AvrRps4* at 5×10 cfu/ml. The *in planta* bacterial growth was measured at 3 days-post inoculation (dpi). Col-0 (WT) and *aggie5-2* mutant were included in the assay. The data are shown as means ± standard errors. **C.** AGGIE5 is required for flg22-mediated protection against *P.s.t. DC3000* infection. Four-week-old plants were hand-inoculated with H_2O or 100 nM flg22 24 hours before inoculation of *P.s.t. DC3000* at 5×10 cfu/ml. Col-0 (WT), *aggie5-2* and *aggie5-3* mutant were included in the assay. The *in planta* bacterial growth was measured at 3 days-post inoculation (dpi). The data are shown as means ± standard errors. **D.** Flg22-triggered growth inhibition is partially rescued in aggie5-2, and AGGIE5 but not AGGIE5^{EN} complements *aggie5-2*. Four-day-old seedlings were treated with 200 nM flg22 or H_2O for 6 days in ½ MS liquid medium. Col-0 (WT), *aggie5-2* mutant and homozygous lines of p35S*::AtAGGIE5-FLAG*, p35S*::AtAGGIE5*^{D618N}*-FLAG* transgenic plants in *aggie5-2* background were included in the assay. The data are shown as means ± se from three biological repeats with Student's *t*-test. * indicates $p<0.05$ when compared to WT. **E.** AGGIE5^{D618N} partially rescues flg22-triggered growth inhibition. Four-day-old seedlings were treated with 200 nM flg22 or H_2O for 6 days in ½ MS liquid medium. The *pFRK1::LUC* transgenic plants (WT), *aggie5-1* mutant and homozygous lines of p35S*::AtAGGIE5*^{D618N}*-GFP* transgenic plants in WT background were included in the assay. The data are shown as means ± se from three biological repeats with Student's *t*-test. * indicates $p<0.05$ when compared to WT. **F.** AGGIE5 is not required for flg22-triggered ROS production. Leaf discs from Col-0 (WT), *aggie5-2* were treated with 100 nM flg22, and the ROS production was measured with a plate reader over 40 min (2400 seconds). The data are shown as means ± standard errors from 20 leaf discs for flg22 treatment. The above experiments were repeated 3 times with similar results.

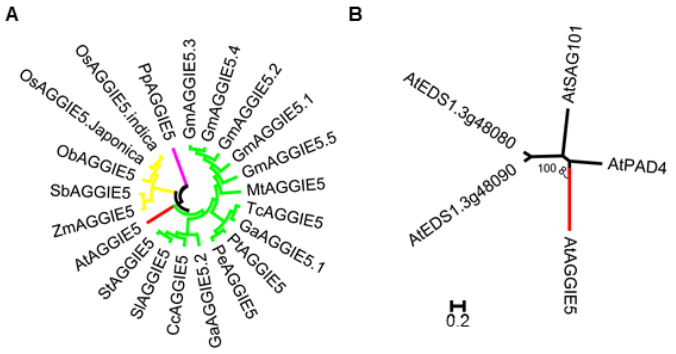

Figure 2.6 AGGIE5 is a plant-specific gene.

A. Phylogenetic clustering of putative *At*AGGIE5 orthologs in a cladogram. A subset of orthologous sequences was used. The evolutionary history was inferred using the Neighbor-joining method. The percentage of replicate trees in which the associated taxa clustered together in the bootstrap test (2000 replicates) are shown next to the branches. The evolutionary distances were computed using the Poisson correction method and are in the units of the number of amino acid substitutions per site. The analysis involved 21 amino acid sequences. All positions containing gaps and missing data were eliminated. Evolutionary analyses were conducted in MEGA6.06. The green branches consist of AGGIE5 homologs in dicot plants, the yellow branches consist of AGGIE5 homologs in monocot plants, the purple branches consist of AGGIE5 homolog in moss. The red branch indicates the AGGIE5 in Arabidopsis thaliana. **B**. The evolutionary history was inferred using the Neighbor-joining method. The percentage of replicate trees in which the associated taxa clustered together in the bootstrap test (2000 replicates) are shown next to the branches. The tree is drawn to scale, with branch lengths in the same units as those of the evolutionary distances used to infer the phylogenic tree. The evolutionary distances were computed using the Poisson correction method and are in the units of the number of amino acid substitutions per site. The analysis involved amino acid sequences of AGGIE5, EDS1-80, EDS1-90, PAD4 and SAG101. All positions containing gaps and missing data were eliminated. Evolutionary analyses were conducted in MEGA6.06.

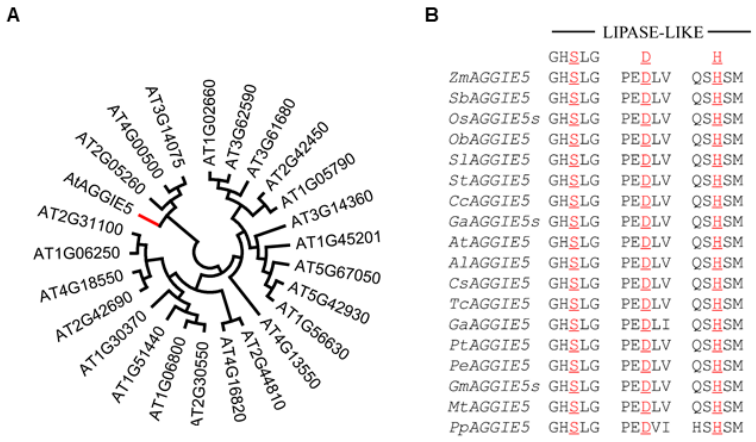

Figure 2.7 AGGIE5 encodes a putative GHSL lipase.

A. Phylogenetic clustering of AtAGGIE5 and 24 Arabidopsis putative GHSL lipases in a cladogram. A subset of all sequences was used. The evolutionary history was inferred using the Neighbor-joining method. The percentage of replicate trees in which the associated taxa clustered together in the bootstrap test (2000 replicates) are shown next to the branches. The tree is drawn to scale, with branch lengths in the same units as those of the evolutionary distances used to infer the phylogenic tree. The evolutionary distances were computed using the Poisson correction method and are in the units of the number of amino acid substitutions per site. The analysis involved 21 amino acid sequences. All positions containing gaps and missing data were eliminated. Evolutionary analyses were conducted in MEGA6.06. The green branches consist of AGGIE5 homologs in dicot plants, the yellow branches consist of AGGIE5 homologs in monocot plants, the purple branch consist of AGGIE5 homolog in moss. The red branch indicates the AGGIE5 in Arabidopsis thaliana. **B.** Conservation of lipase catalytic triad residues in AGGIE5 orthologs. Sequences were aligned, and positions corresponding to the catalytic S-D-H of α/β hydrolases, including the characteristic lipase GxSxG motif, are shown. GaAGGIE5s represents GaAGGIE5.1 and GaAGGIE5.2, whose motif are identical; OsAGGIE5s represents OsAGGIE5.Janpanica and OsAGGIE5.Indica, whose motif are identical; GmAGGIE5s represents GmAGGIE5.1, GmAGGIE5.2, GmAGGIE5.3, GmAGGIE5.4 and GaAGGIE5.5, whose motif are identical.

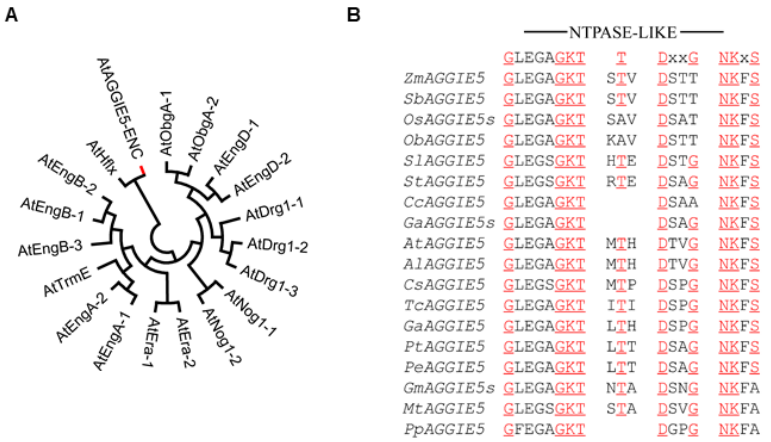

Figure 2.8 AGGIE5 possesses a putative NTPase domain.

A. Phylogenetic clustering of AtAGGIE5^{ENC} (aa498-1003) and 18 Arabidopsis Era subfamily GTPase in a cladogram. A subset of all sequences was used. The evolutionary history was inferred using the Neighbor-joining method. The percentage of replicate trees in which the associated taxa clustered together in the bootstrap test (2000 replicates) are shown next to the branches. The evolutionary distances were computed using the Poisson correction method and are in the units of the number of amino acid substitutions per site. The analysis involved 19 amino acid sequences. All positions containing gaps and missing data were eliminated. Evolutionary analyses were conducted in MEGA6.06. The red branch indicates the AGGIE5. **B.** Conservation of NTPase catalytic residues in AGGIE5 orthologs. Sequences were aligned, and positions corresponding to the G1-G4 (GxxxxGKT…T…DxxG…NKxS) moitf of NTPase are shown. GaAGGIE5s represents GaAGGIE5.1 and GaAGGIE5.2, whose motif are identical; OsAGGIE5s represents OsAGGIE5.Janpanica and OsAGGIE5.Indica, whose motif are identical; GmAGGIE5s represents GmAGGIE5.1, GmAGGIE5.2, GmAGGIE5.3, GmAGGIE5.4 and GaAGGIE5.5, whose motif are identical.

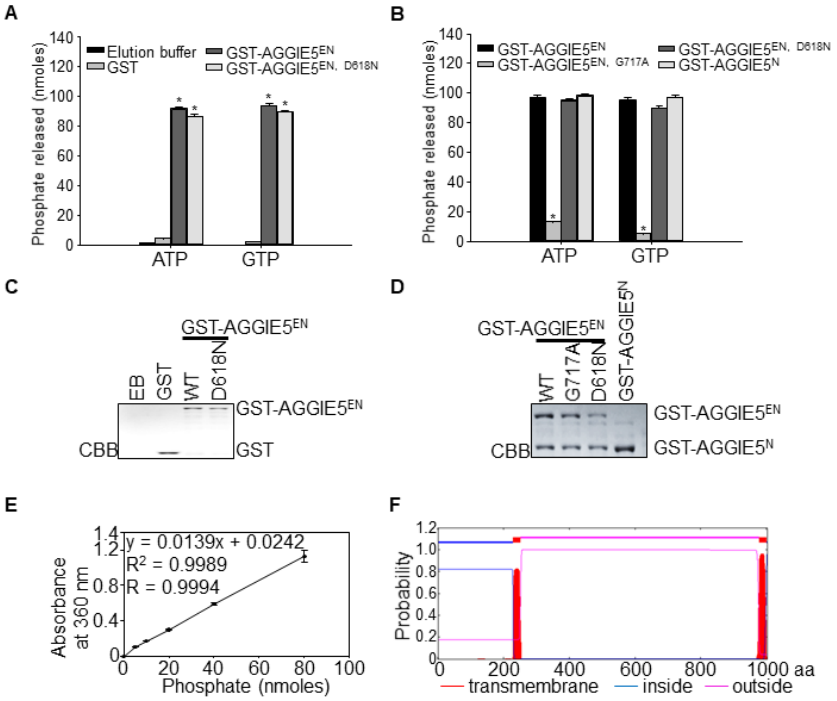

Figure 2.9 AGGIE5 is a functional NTPase whose activity is not affected by D618N mutation.

A. AGGIE5^{EN} and AGGIE5$^{EN, D618N}$ hydrolases ATP and GTP *in vitro*. *In vitro* NTPase assay was performed by incubating control, GST, GST-AGGIE5^{EN} or GST-AGGIE5$^{EN, D618N}$ fusion protein with ATP or GTP in reaction buffer plus MESG and PNP. **B.** EP-like domain is not required for *in vitro* NTPase activity of AGGIE5. *In vitro* NTPase assay was performed by incubating GST-AGGIE5^{EN}, GST-AGGIE5$^{EN. G717A}$, GST-AGGIE5$^{EN. D618N}$ or GST-AGGIE5^{N} fusion protein with ATP or GTP in reaction buffer plus MESG and PNP. **C.** Protein loading control in (A) was shown by CBB (bottom panel). **D.** Protein loading control in (B) was shown by CBB (bottom panel). **E.** Standard curve for i*n vitro* NTPase assay in (A) and (B). **F.** AGGIE5 contains two predicted transmembrane motifs. The first one is surrounding the putative lipase motif, and the second one is close to the C-terminal. The prediction is conducted in TMHMM2.0. Red indicates transmembrane motif. Blue indicates inside domains. Purple indicates outside domain.

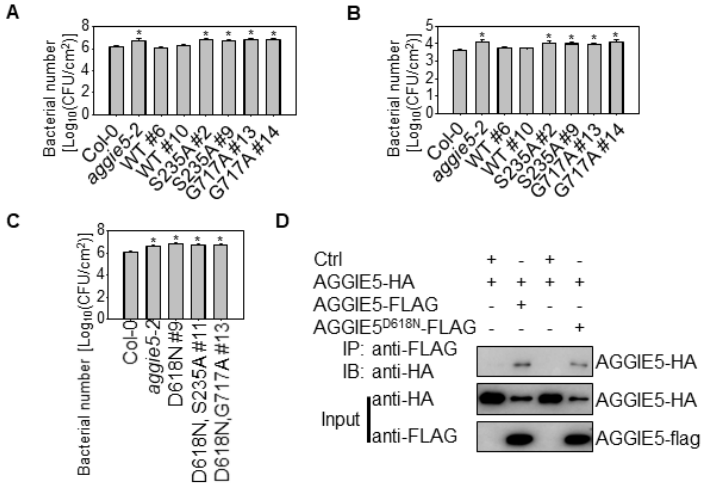

Figure 2.10 Intact lipase motif and NTPase motif are required for functionality of AGGIE5 in innate immunity.

A. Both NTPase activity and putative lipase activity positively regulate AGGIE5 function in disease resistance to *P.s.t. DC3000* infection. Col-0 (WT), *aggie5-2* mutant, two independent homozygous lines of pAGGIE5::*AGGIE5*-FLAG, pAGGIE5::*AGGIE5*^{S235A}-FLAG and pAGGIE5::*AGGIE5*^{G717A}-FLAG transgenic plants in *aggie5-2* background were hand-inoculated with *P.s.t. DC3000* at 5×10 cfu/ml. The *in planta* bacterial growth was measured at 3 days-post inoculation. **B**. Both NTPase activity and putative lipase activity positively regulate AGGIE5 function in disease resistance to *P.s.t. DC3000 hrcC* infection. Col-0 (WT), *aggie5-2* mutant, two independent homozygous lines of pAGGIE5::*AGGIE5*-FLAG, pAGGIE5::*AGGIE5*^{S235A}-FLAG and pAGGIE5::*AGGIE5*^{G717A}-FLAG transgenic plants in *aggie5-2* background were hand-inoculated with *P.s.t. DC3000 hrcC* at 5×10 cfu/ml. The *in planta* bacterial growth was measured at 3 days-post inoculation. **C**. Both NTPase activity and putative lipase activity are not required for AGGIE5^{D618N} function in disease resistance to *P.s.t. DC3000* infection. Col-0 (WT), *aggie5-2* mutant, homozygous lines of pAGGIE5::*AGGIE5*^{D618N}-FLAG, pAGGIE5::*AGGIE5*$^{D618N,\ S235A}$-FLAG and pAGGIE5::*AGGIE5*$^{D618N,\ G717A}$-FLAG transgenic plants in *aggie5-2* background were hand-inoculated with *P.s.t. DC3000* at 5×10 cfu/ml. The *in planta* bacterial growth was measured at 3 days-post inoculation. **D**. Multimerization of AGGIE5. Protoplasts were co-transfected with AGGIE5-HA and AGGIE5-FLAG/AGGIE5^{D618N}-FLAG or an empty vector control (Ctrl). co-IP was performed with a-FLAG antibody (IP: a-FLAG), and the proteins were analyzed using immunoblots with a-HA antibody (IB: a-HA). The above experiments were repeated 3 times with similar results.

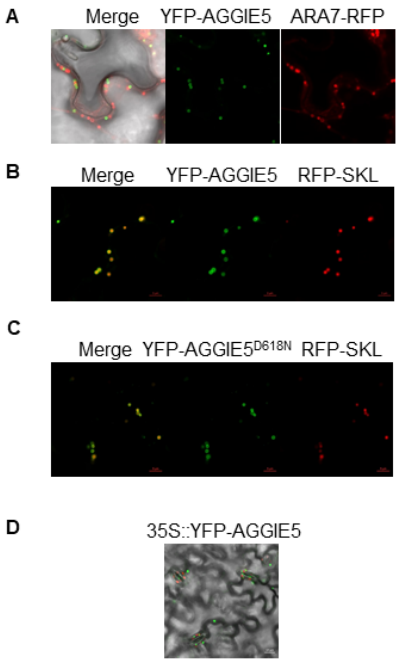

Figure 2.11 AGGIE5 localizes to peroxisome.

A. Transiently expressed YFP-AGGIE5 does not overlapped with early/late endosome marker (ARA7-RFP) in tobacco epidermal cells. **B.** Transiently expressed YFP-AGGIE5 localize to peroxisome in tobacco epidermal cells. Transiently expressed YFP-AGGIE5 overlapped with peroxisome marker (RFP-SKL) in tobacco epidermal cells. **C.** Transiently expressed YFP-AGGIE5^{D618N} localize to peroxisome in tobacco epidermal cells. Transiently expressed YFP-AGGIE5^{D618N} overlapped with peroxisome marker (RFP-SKL) in tobacco epidermal cells. **D.** Epidermal cells of Arabidopsis transgenic plants constitutively expressed p35S::YFP-AGGIE5. All these experiments are done by Kai Tao.

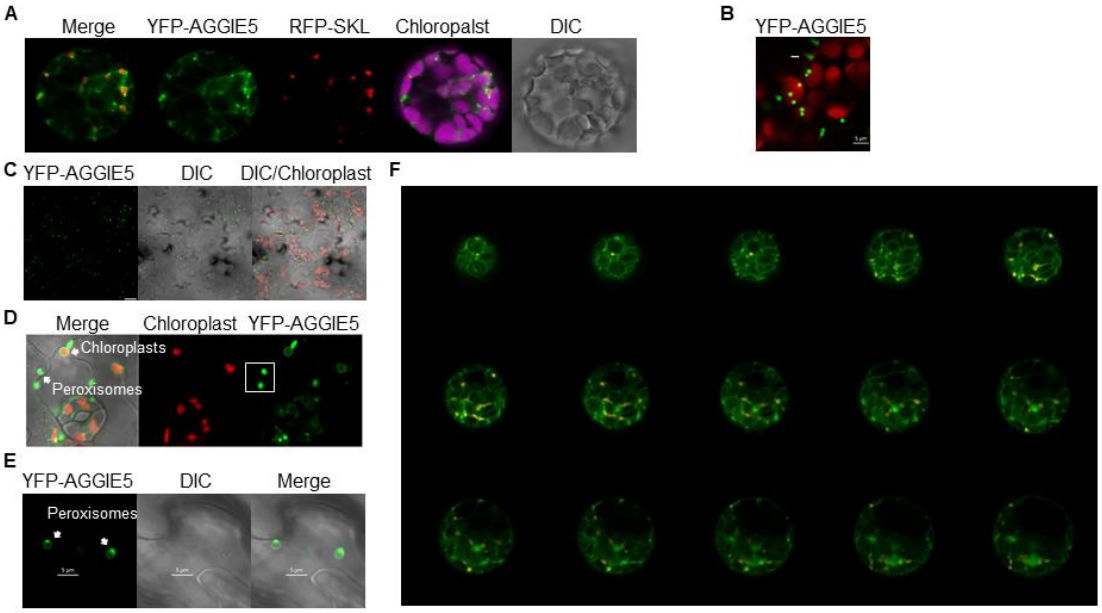

Figure 2.12 AGGIE5 localizes to peroxisome and outer membrane of chloroplast.

A. Transiently expressed YFP-AGGIE5 co-localize with peroxisome and chloroplast in Arabidopsis protoplast. Transiently expressed YFP-AGGIE5 overlapped with peroxisome marker (RFP-SKL) in Arabidopsis protoplast. Purple indicates auto-fluorescence signal from Chloroplast. **B.** Some peroxisomes transiently expressing YFP-AGGIE5 were trapping to chloroplast in Arabidopsis protoplast. Red indicates auto-fluorescence signal from Chloroplast. **C.** Fluorescence signal of YFP in constitutively expressed p35S::YFP-AGGIE5 transgenic lines. Red indicates auto-fluorescence signal from Chloroplast. **D.** Zoom-in of (C). **E.** Zoom- in of (D). **F.** Z-stack picture of (A). All these photos are done by Kai Tao. YFP-AGGIE5 transgenic plants are generated by Chenglong Liu.

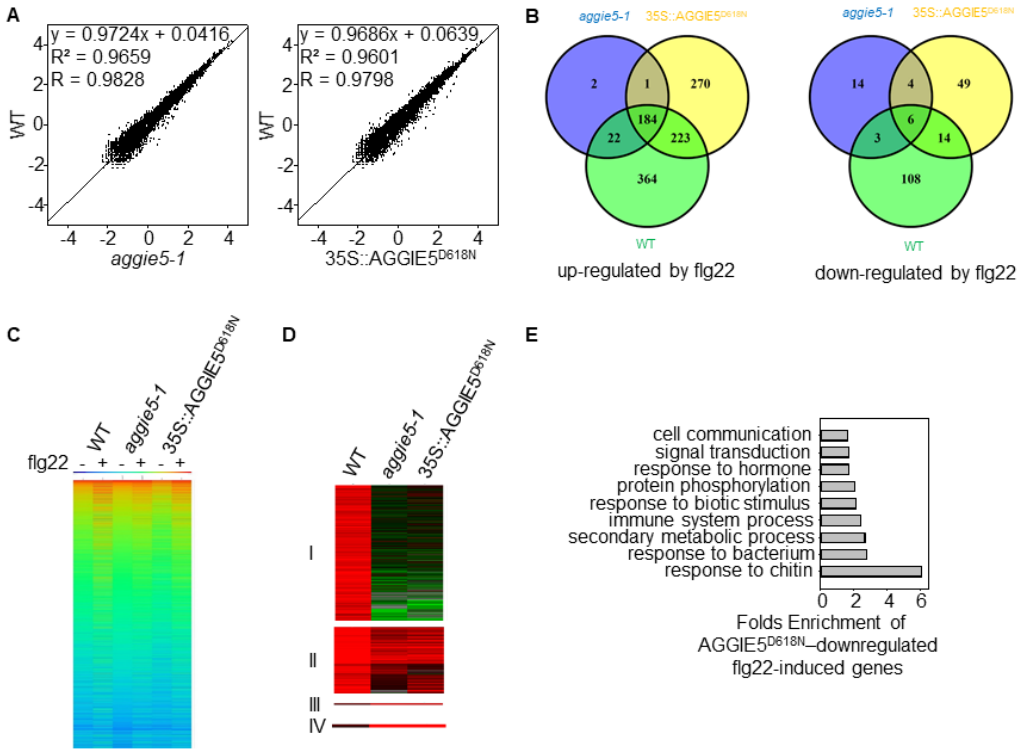

Figure 2.13 AGGIE5^{D618N} globally regulates flg22-induced gene expression.

A. Scatter plots of whole-genome transcript fragments per kilobase of transcript per million mapped reads (FPKM) in *pFRK1::LUC* (WT) versus *aggie5-1* mutant (left) or 35S::AGGIE5^{D618N} transgenic plants (right). Gene expression levels were detected in ten-d-old seedlings without treatment. The y axis indicates gene expression in the wild type, and the x axis indicates gene expression in *aggie5-1* mutant or p35S::AGGIE5^{D618N} transgenic plants. **B.** Venn diagram of flg22-induced genes (fold change >2 and P value < 0.05; 60 min after 100 nM flg22 treatment) in WT, *aggie5-1* mutant, or p35S::AGGIE5^{D618N} transgenic plants. **C.** Heat map of flg22-induced genes in WT, *aggie5-1*, or p35S::AGGIE5^{D618N} transgenic plants. The original FPKM values were subjected to data adjustment by normalized genes/rows and hierarchical clustering was generated with the average linkage method using MeV4.9. Red color indicates relatively high expression, and blue indicates relatively low expression. **D.** Clustering display of AGGIE5^{D618N}-dependent flg22 upregulated genes in WT, *aggie5-1*, and p35S::AGGIE5^{D618N} mutant plants. The four clusters are defined in the text. The flg22 induction fold of individual genes with the log2-transformed values was used for hierarchical clustering analysis with the average linkage method using MeV4.9. Red color indicates upregulation and green indicates downregulation with flg22 treatment. The gene list for this analysis is shown in Supplemental Data Set 1E, 1F, 1G, 1H. **E.** Enrichment of genes with GO terms related to defense response for Group I and II genes in **(D)**. The fold enrichment was calculated based on the frequency of genes annotated to the term compared with their frequency in the genome.

Table 2.1 Position, mutation and frequency of SNPs at chromosome 3 0-7.5Mb of AGGIE5 in mutant phenotype pool (low signal pool) or WT phenotype (high signal pool) of F2 of cross between Ler(♀) and aggie5-1(♂).

			Low Pool			High Pool			
Position	WT	*aggie5-1*	Count	Coverage	Frequency	Count	Coverage	Frequency	AGI Number
1372534	G	A	11	18	61.1	3	16	18.8	AT3G04950
2248153	G	A	7	10	70.0	8	23	34.8	AT3G07100
2370795	G	A	12	15	80.0	2	11	18.2	AT3G07400
3007245	C	T	10	18	55.6	3	18	16.7	AT3G09800
3416878	G	A	10	15	66.7	7	25	28.0	AT3G10915
3604451	G	A	10	16	62.5	4	15	26.7	AT3G11440
5269196	G	A	11	21	52.4	7	24	29.2	AT3G15550
5325394	-	T	10	17	58.8	3	11	27.3	AT3G15720
7602961	A	C	9	17	52.9	3	9	33.3	AT3G21580

Table 2.2 Cloning primers used in study in chapter 2.

Gene	Forward Primer	Reverse Primer
AGGIE5	GCTCTAGACGGGATCCATGGAGTCGATACAGAGC	GAAGGCCTGGGTTTTCGTAAAGCGG
AGGIE5-EN	CGGGATCCATGTCTATGAAGTCCTATAGGTC	AAGGCCTACCATCTACGACACGGTC
AGGIE5-N	CGGGATCCATGTTCTCGTCTGTTGATTCG	AAGGCCTACCATCTACGACACGGTC
pAGGIE5	CCGCTCGAGCCCTGTGTCTTAAAATACCTC	GCTCTAGATACTACAACCTTTGGTCAATACC

Note: The restriction enzyme sites are underlined.

Table 2.3 Genotyping primers used in study in chapter 2.

Gene	Forward Primer	Reverse Primer
aggie5-2	ATCGGTACGAGCTTCTTTTCC	TTCAGGACGGACAAACTTGTC
aggie5-3	CCTCTAGGGGGACAAGTTTTG	ATTGTTTGCATCCTTTGTTGG

Note: The T-DNA left and right border primers were selected accordingly to each mutant. For SAIL lines (*aggie5-2*), LB (GCCTTTTCAGAAATGGATAAATAGCCTTGCTTCC); for WiscDsLox lines (*aggie5-3*), LB (CGTCCGCAATGTGTTATTAAGTTG) was used respectively.

Table 2.4 qRT-PCR primers used in study in chapter 2.

Gene	Forward Primer	Reverse Primer
FRK1	ATCTTCGCTTGGAGCTTCTC	TGCAGCGCAAGGACTAGAG
WRKY30	GCAGCTTGAGAGCAAGAATG	AGCCAAATTTCCAAGAGGAT
MYB15	CTTGGCAATAGATGGTCAGC	TGAGTGTGCCATACGTTCTTG
At2g17740	TGCTCCATCTCTCTTTGTGC	ATGCGTTGCTGAAGAAGAGG
UBQ10	AGATCCAGGACAAGGAAGGTATTC	CGCAGGACCAAGTGAAGAGTAG

Table 2.5 Point-mutation primers used in study in chapter 2.

Gene	Forward Primer	Reverse Primer
AGGIE5-S235A	GTATTATGTGGACACGCACTTGGTGGAGCTGTAG	CTACAGCTCCACCAAGTGCGTGTCCACATAATAC
AGGIE5-G717A	GGGCTTGAGGGTGCTGCTAAAACCTCTCTATTCC	GGAATAGAGAGGTTTTAGCAGCACCCTCAAGCCC
AGGIE5-T612A	GGAATCTTTCCCTACA**GCA**CCTGCTTATTCTTCAG	CTGAAGAATAAGCAGG**TGC**TGTAGGGAAAGATTCC
AGGIE5-T612E	GGAATCTTTCCCTACA**GAA**CCTGCTTATTCTTCAG	CTGAAGAATAAGCAGG**TTC**TGTAGGGAAAGATTCC

Note: The restriction enzyme sites are underlined, and the point mutation sites are underlined and in bold.

2.5 Discussion

Although it is clear that AGGIE5 positively regulates plant defense responses towards bacterial pathogens, it is still illusive that what is the molecular function of AGGIE5, a plant-specific protein possessing both lipase motif and NTPase motif. The structural similarity of EDS1 to α/β hydrolases and conservation of critical residues in EDS1 and PAD4 orthologs prompted us to investigate whether AGGIE5 hydrolase activity is required for disease resistance. According to the bioinformatic analysis, the S (S235 in AGGIE5) in the lipase motif (GxSxG) is required for all of the lipases known and the G (G717 in AGGIE5) in the NTPase motif (GxxxxGKT) is also indispensable for its hydrolytic activity. AGGIE5 is not a soluble protein whose lipase motif is embedded within one predicted transmembrane motif, it is hard to attest the putative lipase motif is catalytically active or inactive. However, GHSLG motif is highly conserved in AGGIE5 orthologs, indicating esterase activity of AGGIE5 is maintained in plant genomes with evolution. The requirement of G717 had been verified experimentally in *in vitro* NTPase assay. Then, we tested whether the AGGIE5 predicted catalytic triad is required for resistance in Arabidopsis to the semi-biotrophic bacteria pathogen. We made stable transformants of *aggie5-2* mutant with a construct containing wild-type (WT) AGGIE5 under its respective native promoters as a positive control. On the other hand, we did point mutation to generate these two putative loss-of-function alleles of AGGIE5: the AGGIE5 variant with Ser exchanged to Ala (denoted AGGIE5^{S235A}) and the AGGIE5 variant with Gly exchanged to Ala (denoted AGGIE^{G717A}). T2 generation homozygous transgenic plants expressing comparable level of AGGIE5s were tested for Pst resistance.

Complementation lines expressing WT AGGIE5 were resistant, and those expressing AGGIE5^{S235A} AGGIE5^{G717A} were susceptible to Pst. From the results of complementation assay on disease resistance by introducing these two putative loss-of-function alleles into *aggie5-2* knockout mutant, we could conclude that the functionality of AGGIE5 require both intact lipase and NTPase motifs.

G1 is the P loop (for phosphate binding) motif GxxxxGKS/T, originally termed the Walker A motif. G2 has only a Thr almost totally conserved, and G3 is DxxG. G4, the N/TKxD motif, is the major determinant of guanine base–binding specificity, and G5 is only weakly conserved. Because ATP-binding proteins also contain the G1-G2-G3 motifs, the absence of the G4 or G5 motif has led to some misassignments. The Asp of DxxG, also called the Walker B motif, makes a water-mediated contact to the Mg^{2+} ion, which is critically required for tight nucleotide binding and GTP hydrolysis in most G proteins. D can be replaced by E, and it does not necessarily make contact to the nucleotide. Gly is also not universally conserved. Specificity for guanine is caused by the Asp side chain of N/TKxD (G4), which usually forms a bifurcated H bond with guanine, occasionally substituted by Glu. Most G proteins have an alanine residue in the G5 motif that forms a main-chain interaction with the O6 oxygen of guanine. AGGIE5 is an active NTPase which is able to hydrolyze both ATP and GTP *in vitro* as least, this is most likely due to a modified G4 motif. In contrast to most GTPases that contain a conserved G4 motif N/TKxD, NTPase motif of AGGIE5 exhibits a variable G4 motif NKFA/S, in which the Aspartic acid is usually replaced by Alanine and seldomly replaced by Serine. As reported, the GTPases maintain N/TKxD motif specially hydrolyze GTP, whereas the protein

without conserved D usually lose specificity towards substrates and could hydrolyze GTP, ATP, CTP or TTP. The variant G4 motif in AGGIE5 lead to the loss of specificity of substrate. Especially, the most closed homolog of AGGIE5 NTPase domain is HflX, which is a protein which has been reported to bind and hydrolyze GTP and ATP, although HflX still maintain the conserved N/TKxD motif. Some ancestral G proteins lost or switched nucleotide specificity, so we must be careful about judging the nucleotide specificity from the sequence. In this way, biochemical experiments are required. Our biochemical experiments clearly show the predicted GTPase-like domain of AGGIE5 has almost no nucleotide specificity, justifying its reference as an NTPase.

Many members of the GHSL lipases family are biochemically not well characterized, and no other membrane-localized lipase activity analysis methods are available as originally proposed. Additionally, AGGIE5 also consists of two putative transmembrane motifs, a relatively long N-terminus and a relatively short C-terminus. Localization study indicates AGGIE5 localizes to peroxisome and chloroplast, where are the major sites of phytohormone synthesis and secondary metabolism in plant cell. It is still difficult to assess the function of the lipase motif as well as the transmembrane domain due to the unavailable of purified AGGIE5 full length protein, but future functional analysis will be applicable.

Another interesting founding is that either AGGIE5 or AGGIE5^{D618N} could dimerized with each other in protoplasts, as the observes positive results in co-immunoprecipitation assay (Fig. 2.10D). It appears that AGGIE5 could form dimer with either AGGIE5 or AGGIE5^{D618N}. Because the genetic analysis supports AGGIE5^{D618N} is

a semi-dominant allele, it is very possible that D618N is a loss-of-function mutation but disrupts the function of the homodimer/heterodimer of AGGIE5. In this way, AGGIE5^{D618N} behaves as a dominant-negative mutation in genetic perspective, which biologically play a negative role in regulation of MTI. However, more experimental data are needed to verify this hypothesized model.

In all, AGGIE5 gene encodes a plant-specific protein of unknown function. Based on AGGIE5D618N negatively regulates plant defense responses in MTI, we hypothesized that AGGIE5 arises from moss and evolve essential functions in land plants in regulating plant innate immunity.

3. PHOSPHORYLATION OF AGGIE5 BY MPK7 REGULATES PLANT INNATE IMMUNITY

3.1 Summary

We found flg22 treatment contributes to rapid phosphorylation of AGGIE5 at threonine 612 via MPK7, a group C mitogen-activated protein kinase that was characterized as a positive regulator of MTI responses. Importantly, in mutational analysis of the AGGIE5, all the T-DNA knockout mutants *aggie5-2*, *aggie5-3* and CRISPR/Cas9-edited knockout mutants *mpk7-1*, *mpk7-2* show reduced disease resistance to virulent bacterial pathogen infection and transgenic plants expressing the wild-type or phospho-mimetic form of AGGIE5 rescue MTI responses. These results revealed that group C MAPK MPK7 positively regulates MTI responses in Arabidopsis by phosphorylating the substrate AGGIE5. Our work first reports that AGGIE5 interacts with another novel MTI signaling transducer MPK7. More importantly, phosphorylation of AGGIE5 at Thr-612 by MPK7 was blocked by the mutation D618N therefore negatively regulating plant immunity. Our study reveals a direct link between PRR activated protein kinases and peroxisome/chloroplast-localized protein and provides novel insight of the activation of signal messengers in plant innate immunity.

3.2 Introduction

In plant, mitogen-activated protein kinase (MAPK) cascades generally transduce extracellular stimuli into intracellular responses. These stimuli include the perception of microbe-associated molecular patterns (MAMPs) by plasma membrane-localized pattern

recognition receptors (PRR). In Arabidopsis, several MAPK cascade components have been characterized as important signal transducers in MTI and defense hormone signalings. In a few cases, MAPK cascade components have been directly linked to the transcription of target genes or to the synthesis of phytohormone.

The Arabidopsis genome encodes 60 MAP3Ks, 10 MAP2Ks, and 20 MAPKs, suggesting that there is some level of specificity and redundancy. An MAPK cascade downstream of FLS2 consisting of two MAP2Ks (MKK4 and MKK5) and two MAPKs (MPK3 and MPK6) were characterized as positive regulators of MTI responses. Another MAPK cascade downstream of FLS2 consisting of two MAP2Ks (MKK1 and MKK2) and one MAPK (MPK4) were originally reported as a negative regulator of plant innate immunity, because extreme high levels of salicylic acid and constitutively expresses pathogenesis-related (PR) genes was detected in the *mpk4* mutant which has a severely dwarfed growth phenotype (Petersen et al., 2000).

Arabidopsis MAPKs have either a Thr-Glu-Tyr (TEY) activation motif, similar to the mammalian MAPKs ERK subfamily, or a Thr-Asp-Tyr (TDY) activation motif, which is unique to Arabidopsis MAPKs. Based on sequence similarities, Arabidopsis TEY MAPKs can be classified into three groups (group A, B, and C), whereas the TDY MAPKs constitute a more distant group (group D). The group A MPKs MPK4/MPK11 and the group B MPKs MPK3/MPK6 are the most intensively studied plant MAPKs in MAMP-triggered immunity. MPK3, MPK4, and MPK6 are all obviously activated by multiple MAMPs. Activated MPKs phosphorylates their substrate proteins including transcription factors, protein kinases, or hormone biosynthesis enzymes and triggers a number of

effective induced defense responses. However, it is still elusive whether group C MPK kinases are involved in MAMP-triggered immunity.

3.3 Materials and methods

3.3.1 Recombinant protein isolation and i*n vitro* kinase assays

Fusion proteins were produced from E. coli BL21 strain at 16°C using LB medium with 0.25 mM isopropyl-D-1-thiogalactopyranoside (IPTG). Glutathione Stransferase (GST) fusion proteins were purified with Pierce glutathione agarose (Thermo Scientific), and maltose binding protein (MBP) fusion proteins were purified using amylose resin (New England Biolabs) according to the standard protocol from companies.

The *In vitro* kinase assays were performed with 0.5 μg of kinase proteins and 5 μg of substrate proteins in 30 μl kinase reaction buffer (10 mM Tris-HCl, pH7.5, 5 mM MgCl2, 2.5 mM EDTA, 50 mM NaCl, 0.5 mM DTT, 50 μM ATP and 1 μCi [γ 32P]ATP). After gentle shaking at room temperature for 2 hr, samples were denatured with 4 x SDS loading buffer and separated by 10% SDS-PAGE gel. Phosphorylation was analyzed by autoradiography.

3.3.2 Yeast two-hybrid screen

The cDNA library constructed in a modified pGADT7 vector (Clontech) was described before (Lu et al., 2011b). The AGGIE5^{EN} was cloned into a DNA-binding domain fusion vector pBridge (Clontech) and transformed into yeast first. The cDNA

library was then transformed into the yeast containing pBridge-AGGIE5^{EN} and transformants were screened in the synthetic defined media (SD) without Trp, Leu, His, Ade (SD-T-L-H-A) and SD-T-L-H + 1 mM 3-Amino-1,2,4-triazole (3AT). No colonies grew in the medium SD-T-L-H-A and the biggest colonies in SD-T-L-H+3AT were further confirmed in SD-T-L-H+3AT medium and subjected to plasmid isolation and sequencing.

3.3.3 *In vitro* GST pull-down assay

MBP fusion protein isolation was described in previous chapters. For GST-agarose beads, GST-AGGIE5 or GST protein isolation was performed as described before and the agarose beads were obtained after elution and washed with PBS for three times. MBP-MPK7 or MBP protein (2 μg) were pre-incubated with 10ul prewashed glutathione agarose in 300ul pull-down incubation buffer (20 mM Tris-HCl, pH 7.5, 100 mM NaCl, 0.1mM EDTA, and 0.2% Triton X-100) for 30 min at 4°C. 5ul GST or GST-AGGIE5 agarose beads were pre-incubated with 20 μg BSA in 300ul incubation buffer for 30 min at 4 °C.

Then the supernatant containing MBP-MPK7/MBP was mixed with the preincubated GST/GST-AGGIE5 agarose beads for 1hr at 4°C. The agarose beads were precipitated and washed three times in pull-down washing buffer (20 mM Tris-HCl, pH 7.5, 300 mM NaCl, 0.1 mM EDTA, and 0.5% Triton X-100). The pull-down proteins were analyzed by WB with an α-HA antibody.

3.3.4 CRISPR/Cas9 edition

The CRISPR/Cas9 edition targets in the MPK7 was predicted on the website http://chopchop.cbu.uib.no/.

Choose The target sequence was chosen with the ranking of low off-targets rate, high editing efficiency, closer to the start codon or in the first several exons and containing restriction enzyme cutting sites covering the third nucleotide in front of PAM sequence NGG. The reverse complement primer was designed and annealed to get the double stranded DNA fragment. The CRISPR-cas9 vector pHEE401E was linearized with Bsa I and ligase the annealed fragment into it. The clone was screened by colony PCR with primers gDNA1-RP and U6-26P-F and confirmed by Sanger sequencing using U6-26P-F as the sequencing primer.

The vector was transformed into Agrobacterium and then dipped for Arabidopsis transformation.

The T0 seeds of transgenic plants was screened on ½ MS plates supplemented with Hygromycin. Transfer Hyg-resistant plants to soil and grow for another 2~3 weeks. Genomic DNA from individual line was isolated and served as PCR template to amplify 451 bp fragment covering the edited site with specific primers. The PCR products was digested with the restriction enzyme to screen for the edited lines. The edited sequence by confirmed by sanger sequencing and the target gene from individual lines take good care of the plants with homozygous editing, harvest seeds to get the T2 plants. Notably, as the Cas9 protein is still there, the editing continues.

3.3.5 Plasmid construction and generation of transgenic plants

The MPK7 gene were amplified from Col-0 cDNA with primers containing NcoI at N terminus and StuI at C terminus and ligated into a plant protoplast expression vector pHBT with a CaMV 35S promoter at N-terminus and HA epitope-tag at C-terminus. The point mutations of $MPK7^{Y113C}$, $AGGIE5^{T612A}$ and $AGGIE5^{T612E}$ were generated by site-directed mutagenesis with primers listed in Table S5. To construct the pCAMBIA2300 and pCB302 binary vector containing AGGIE5 or MPK7 for Agrobacterium-mediated transformation assay in Arabidopsis thaliana, the AGGIE5 or MPK7 fragment was released from the pHBT vector digested with BamHI and StuI and ligated into the pCAMBIA2300 and pCB302 binary vector. All the clones were confirmed by sequencing. Arabidopsis transgenic plants were generated using Agrobacterium-mediated transformation by the floral-dip method.

3.4 Results

3.4.1 AGGIE5 interacts with and is phosphorylated by a group C MAPK, MPK7

AGGIE5 is a peroxisome/chloroplast-localized protein and appears to function upstream of transcription reprogramming in MTI signaling. However, there are no any publications on functional reports about AGGIE5. Aiming to elucidate it molecular function in MTI, we carried out two yeast-two-hybrid screens with using either pBK-AGGIE5 or pBK-$AGGIE5^{EN}$ as baits, looking for its interacting proteins. In screen with pBK-AGGIE5, few proteins were pulled out. Possibly AGGIE5 possesses two TM motifs

so that pBK-AGGIE5 does not fit this pBK/pAD system. However, 17 putative interactors were identified in the screen of about 180,000 transformants with the soluble part of AGGIE5, AGGIE5^{EN}. Interestingly, among total 27 positive pAD-clones got from screen with the bait pAD-AGGIE5^{EN}, three different individual pAD-clones encodes the N terminus of the Mitogen-Activated Protein Kinase 7 (MPK7) were repeatedly identified. The Arabidopsis genome encodes 20 MPK genes, MPK3/4/6/11 has been characterized as the vital regulators in MTI signaling (Fig. 3.1C). However, it is unknown whether the plant-specific group 3 of MPKs are involved in MTI responses. In addition to MPK7, there are another 3 members in group 3 of MPKs, which are MPK1, MPK2 and MPK14. The strong interaction between MPK7 and AGGIE5^{EN} were confirmed by yeast-two-hybrid, while weak interaction between MPK1/2 and AGGIE5^{EN} were also observed (Fig. 3.1A). Notably, two well-known positive regulators, MPK3 and MPK6 could not interact with AGGIE5 in yeast (Fig. 3.1B). In addition, MPK7 coimmunoprecipitated with AGGIE5 when coexpressed in protoplasts, indicating the intact protein of AGGIE5 also can associates with MPK7 *in vivo* (Fig. 3.2A and Fig. 3.2B). Then, a transgenic plant expressing both p35S::MPK7-HA and p35S::AGGIE5-FLAG were built to test whether MPK7 indeed interacts with AGGIE5 full length protein *in planta*. Following immunoprecipitation with the α-FLAG antibody, the MPK7-HA detected by the α-HA antibody was observed in AGGIE5-FLAG transgenic plants but not in the control transgenic plants (Fig. 3.1C). The coimmunoprecipitation (co-IP) in this transgenic plant with α-FLAG or α-HA antibody indicated that MPK7 associated with AGGIE5 *in planta* (Fig. 3.1C). In addition, to test whether MPK7 directly interacts with AGGIE5, an *in vitro*

pull-down assay was performed with glutathione S-transferase (GST)-tagged AGGIE5^{EN} immobilized on glutathione Sepharose beads as bait against MBP-MPK7 fusion protein with an HA epitope tag. Apparently, MBP-MPK7 could be pulled down by AGGIE5^{EN}, AGGIE5$^{EN,\ D618N}$ and AGGIE5^{N}, but not by GST alone (Fig. 3.1D). It appears that the D618N mutation did not affect MPK7 and AGGIE5 interaction (Fig. 3.1D). Taken together, the data point to MPK7 is a protein can directly interact with AGGIE5. We further examined the signaling events that potentially related with MPK7-AGGIE5 interaction, which suggests that AGGIE5 may function as a direct target of MPK7 in immune signaling. Refer to previous reports about activated form of MPK3, MPK4 and MPK6, we mutated Y113 into C in the MPK7 to generate a putative activated MPK7. The MPK7-FLAG and MPK7^{Y113C}-FLAG were expressed in protoplasts, and immunoprecipitated for an in vitro kinase assay using common MPK substrate myelin basic protein (MBP) as a substrate. Importantly, MPK7^{Y113C}-FLAG strongly phosphorylated MBP *in vitro* (Fig. 3.3A). Thus, MPK7^{Y113C} could serve as an activated kinase for *in vitro* kinase assay and was named as MPK7^{ac}. The FLAG-tagged MPK7 and MPK7^{ac} were respectively expressed in protoplasts, and immunoprecipitated for an *in vitro* kinase assay using glutathione S-transferase (GST)-tagged AGGIE5^{EN} as a substrate. Clearly, MPK7^{ac} strongly phosphorylated AGGIE5^{EN} *in vitro* (Fig. 3.3B). Most importantly, in the *in vitro* kinase assays with polyhistidine (His)-tagged MPK7^{ac}, His-MPK7^{ac} can only phosphorylates AGGIE5^{EN} but not AGGIE5$^{EN,\ D618N}$ (Fig. 3.3D). Considering that in *in vitro* pull-down assay MBP-MPK7 could be pulled down by both AGGIE5^{EN} and AGGIE5$^{EN,\ D618N}$, these founding suggests the D618N mutation could

disrupts some certain phosphorylation happened within EN domains of AGGIE5. Because the consensus extracellular signal-regulated kinase (ERK) type MAPK phosphorylation site is PxT/SP, we looked for the PxT/SP motif by bioinformatic analysis (Fig. 3.3C). Only one canonical MPK phosphorylation site (S/TxP), Thr-612 residue, was found in the EN domain of AGGIE5. We then investigated whether MPK7 phosphorylates AGGIE5 at Thr-612. In mutational analysis, MPK7 was unable to phosphorylate AGGIE5^{T612A} as expected. These data suggest that activated MPK7 directly phosphorylates AGGIE5^{EN} on the Thr-612 residue. Interestingly, Thr-612 is highly conserved in different organisms in family *Brassicaceae*, suggesting the important role played by AGGIE5 in family *Brassicaceae*. Strikingly, the D618N mutation also abolished the phosphorylation on AGGIE5^{EN} by MPK7 (Fig. 3.3C). This founding points to that the D618N mutation restrains the phosphorylation on Thr-612 of AGGIE5 by MPK7 or other kinases. It is reported that the MPK7 expressed in protoplasts could be activated by treatment with exogenous H_2O_2, and immunoprecipitated for an *in vitro* kinase assay using MBP as a substrate. Considering that AGGIE5 is a key positive regulator in MTI responses, we hypothesized that MPK7 could also phosphorylate Thr-612 after triggered by the MAMP flg22. Here, we developed a time-course *in vitro* phosphorylation assay with transiently expressed MPK7 tagged with a FLAG epitope at the C-terminus in Arabidopsis protoplasts treated with flg22. Strikingly, the phosphorylation activity of immunoprecipitated MPK7 toward MBP was increased with flg22 treatment from 0min to 15min and started reducing after 15min, so the conclusion could be drawn that flg22 indeed slightly activated MPK7 (Fig. 3.4A). Apparently, the flg22-mediated enhancement

of MPK7 activity was not due to the increase of protein expression after treatment (Fig. 3.4A). In H_2O_2 singling, MKK3 is the double kinase upstream of MPK7. *In vitro* kinase activity of MPK7-FLAG was largely increased when coexpressed with MYC-tagged $MKK3^{EE}$, which is reported as an activation form of MKK3. Interestingly, the $MKK3^{EE}$-mediated kinase activity is comparable to the kinase activity elicited by flg22 coexpressed with MYC-tagged MKK3 (Fig. 3.4B). The data demonstrate that MPK7 possesses phosphorylation activity *in vivo* and MPK7-mediated protein phosphorylation could be regulated by flg22 signaling in addition to H_2O_2, indicating that the flg22 activate MPK7 through MKK3-MPK7 cascade as well as H_2O_2 signaling. Consistently, in the *in vitro* phosphorylation assay with transiently expressed MPK7 tagged with a FLAG epitope at the C-terminus in Arabidopsis protoplasts treated with flg22, flg22-elicited MPK7-FLAG could successfully phosphorylate AGGIE5 but not $AGGIE5^{T612A}$ or $AGGIE5^{D618N}$. This data demonstrates that AGGIE5 could be phosphorylated after treatment with flg22 and the D618N mutation could block this phosphorylation. Taken together, the data lead to a model that AGGIE5 directly interacts with MPK7 and is phosphorylated by MPK7 mainly on the Thr-612 residue upon flg22 perception. This model is supported by MPK7-FLAG coexpressed with MYC-MKK3 in protoplasts, activated by flg22 and immunoprecipitated for an in vitro kinase assay using common $AGGIE5^{EN}$ as the substrate. Consistently, MPK7 was able to phosphorylate the $AGGIE5^{EN}$, but neither $AGGIE5^{EN,\ D618N}$ nor $AGGIE5^{EN,\ T612A}$. Notably, phosphorylation of $AGGIE5^{EN}$ by MPK7 was totally abolished in the $AGGIE5^{EN,\ D618N}$ and $AGGIE5^{EN,\ T612A}$ mutants, providing genetic evidence of the involvement of MPK7 in negative regulation of $AGGIE5^{D618N}$ in MTI.

3.4.2 MPK7 indispensably plays a positive role in disease resistance to bacterial pathogens

Since *mpk7* T-DNA mutants are not available in all Arabidopsis seed stocks, we initially generated two MPK7 knockout mutants *mpk7-1* and *mpk7-2* by CRISPR-CAS9. Both *mpk7-1* and *mpk7-2* carries a single T insertion resulted in early stop codon (Supplement Figure 1). Genotyping confirmed that *mpk7-1* and *mpk7-2* are two knockout mutants. Accordingly, the *mpk7-1* mutant was mainly used for further studies. *mpk7-1* and *mpk7-2* mutants displayed an elevated susceptibility towards virulent bacteria P.s.t. DC3000 (Fig. 3.5A), although the flg22 triggered protection seems unaltered in both *mpk7-1* and *mpk7-2* (Fig. 3.5E). In addition, the *mpk7-1* mutant was more susceptible to P.s.t. DC3000 *hrcC* than were wild-type plants (Fig. 3.5B). Whereas, both *mpk7-1* and *mpk7-2* mutants displayed unaltered MAPK activation and ROS burst to flg22 treatment (Fig. 3.5C and Fig. 3.5D). To confirm the positive role played by MPK7 in plant immunity, we also introduced FLAG epitope-tagged MPK7^{ac} under the control of 35S promoter into the Col-0. Three independent transgenic lines with similar detectable MPK7^{ac} expression does show elevated resistance to pathogenic strain P.s.t. DC3000 (Fig. 3.6D), even though the resistance to non-pathogenic strain DC3000 *hrcC* are almost unaltered (Fig. 3.6E). Although MPK7^{ac} does not affect MAPK activation (Fig. 3.6A), all of three independent transgenic lines show elevated expression level of FRK1 and WRKY30 than that of WT without any MAMP treatment (Fig. 3.6B) and increased expression level of some SA-responsive genes, such as PAD4, PAL1 and PR1 (Fig. 3.6C). It suggests that activation of

MPK7 positively regulates induction of a set of MTI and SA signaling genes. Together, these results suggest that MPK7 positively regulates immune gene expression and disease resistance to virulent bacterial pathogens and non-pathogenic strains. However, flg22-induced ROS burst and activation of MPK3/4/6 did not show a detectable difference in wild-type and *mpk7-1* plants, suggesting that MPK7 functions either downstream or independently of canonical MAPK activation and ROS production in FLS2 signaling.

3.4.3 Phosphorylation at T612 is critical to functionality of AGGIE5 in Arabidopsis immunity

Considering the involvement of AGGIE5 and AGGIE5^{D618N} in MAMP-triggered immunity and AGGIE5^{D618N} block the phosphorylation at Thr-612 of AGGIE5 by MPK7, we tried to assess how the phosphorylation event at Thr-612 regulates plant resistance and regulate AGGIE5 function. We introduced AGGIE5^{T612E}-FLAG and AGGIE5^{T612A}-FLAG under the control of its native promoter into *aggie5-2* mutant. Two transgenic lines of each transformants show comparable expression level of AGGIE5 are used for disease assay with DC3000 and *hrcC* (Fig. 3.7A and (Fig. 3.7B). Quantified by in planta bacterial multiplication, the increased susceptibility in *aggie5-2* could be repeatedly restored by the ectopic expression of AGGIE5^{T612E}-FLAG but not AGGIE5^{T612A}-FLAG. These results lead us to hypothesize that phosphorylation at T612 is required for the positive role played by AGGIE5 in controlling disease resistance and that the negative role played by AGGIE5^{D618N} may be from the disruption of the phosphorylation at Thr-612.

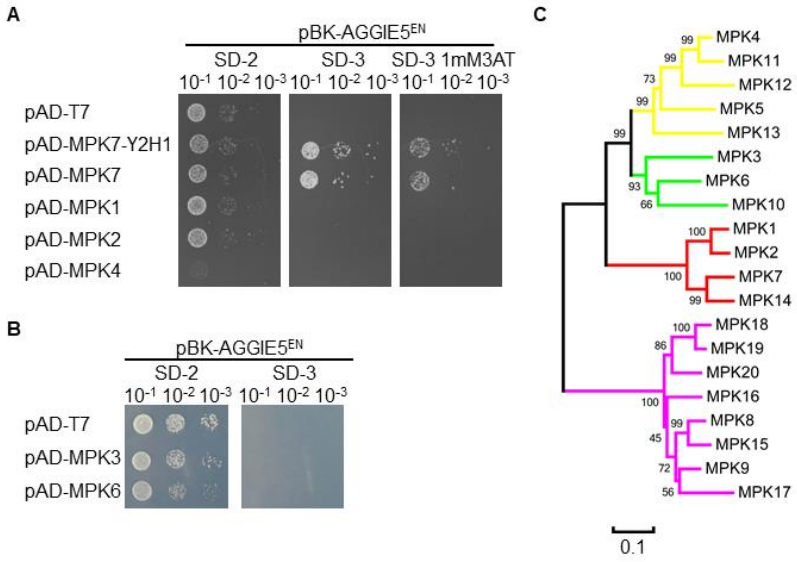

Figure 3.1 AGGIE5 interacts with a group C Mitogen-activated protein kinase MPK7 in yeast.

A. AGGIE5 interacts with MPK7 in yeast two-hybrid assay. pBK-AGGIE5^{EN} and different construct in pAD vectors were co-transformed into yeast. Transformants grown on SD-L-T plate were tested on SD-L-T, SD-L-T-H, SD-L-T-H plus 1mM 3AT plate with series dilutions. Y2H: truncation from yeast two-hybrid screen. **B.** AGGIE5 does not interacts with MPK3 or MPK6 in yeast two-hybrid assay. pBK-AGGIE5^{EN} and different construct in pAD vectors were co-transformed into yeast. Transformants grown on SD-L-T plate were tested on SD-L-T, SD-L-T-H, SD-L-T-H plus 1mM 3AT plate with series dilutions. **C.** MPK7 is a group C Mitogen-activated protein kinase. The evolutionary history was inferred using the Neighbor-joining method. The percentage of replicate trees in which the associated taxa clustered together in the bootstrap test (2000 replicates) are shown next to the branches. The tree is drawn to scale, with branch lengths in the same units as those of the evolutionary distances used to infer the phylogenic tree. The evolutionary distances were computed using the Poisson correction method and are in the units of the number of amino acid substitutions per site. The analysis involved amino acid sequences of 20 Arabidopsis MPKs. All positions containing gaps and missing data were eliminated. Evolutionary analyses were conducted in MEGA6.06. The green branches consist of group A MPKs, the yellow branches consist of group B MPKs, the red branches consist of group C MPKs, and the purple branches consist of group D MPKs.

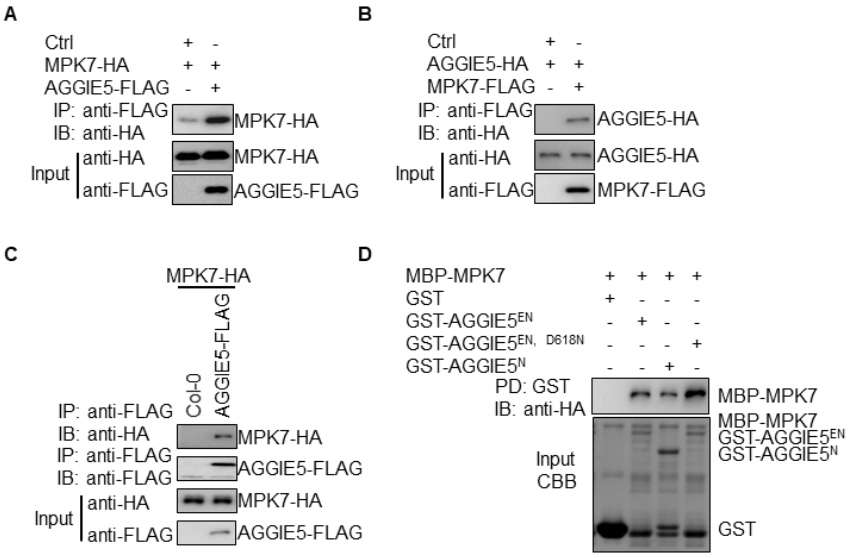

Figure 3.2 AGGIE5 interacts with a group C Mitogen-activated protein kinase MPK7.

A. AGGIE5 interacts with MPK7 in Co-IP assay. Protoplasts were co-expressed with MPK7-HA and AGGIE5-FLAG or Ctrl. The Co-IP assay was carried out with α-FLAG-Agarose and interacting proteins were examed by WB with α-HA. **B**. AGGIE5 interacts with MPK7 in Co-IP assay. Protoplasts were co-expressed with AGGIE5-HA and MPK7-FLAG or Ctrl. The Co-IP assay was carried out with α-FLAG-Agarose and interacting proteins were examed by WB with α-HA. **C**. AGGIE5 interacts with MPK7 in transgenic plants. Transgenic plants expressing p35S::AGGIE5-FLAG and p35S::MPK7-HA were used for Co-IP assay. The Co-IP assay was carried out with α-FLAG-Agarose and interacting proteins were examed by WB with α-HA. **D**. AGGIE5 interacts with MPK7 by in vitro pull-down assay. GST or GST-AGGIE5 immobilized on glutathione sepharose beads was incubated with MBP-MPK7 proteins. Washed beads were subjected to WB with α-HA or α-GST (top two panels). Input proteins were shown by CBB (bottom panel).

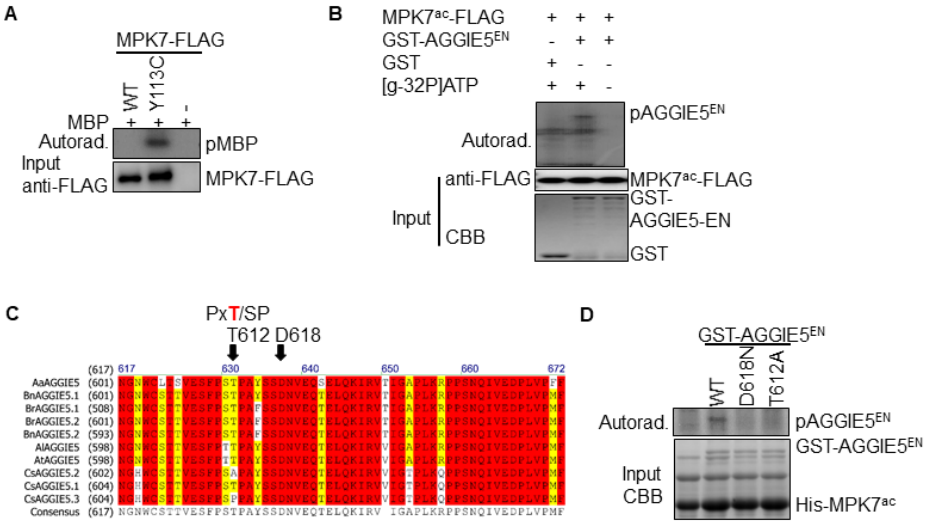

Figure 3.3 MPK7 phosphorylates AGGIE5 *in vitro*.

A. MPK7^{ac} phosphorylates MBP *in vitro*. *In vitro* kinase assay was performed by incubating MBP protein with MPK7-FLAG, MPK7^{ac}-FLAG or control in kinase buffer. Phosphorylation was detected by autoradiography (top panel). Protein loading control was shown by CBB (bottom panel). **B.** MPK7^{ac} phosphorylates AGGIE5^{EN} *in vitro*. *In vitro* kinase assay was performed by incubating MPK7^{ac}-FLAG fusion protein with GST or GST-AGGIE5^{EN} in kinase buffer. Phosphorylation was detected by autoradiography (top panel). Protein loading control was shown by CBB (bottom panel). **C.** The putative canonical MAPK phosphorylation site Thr612 is conserved in AGGIE5 orthologs in Family *Brassicaceae*. The Alignment is conducted in DNAMAN. **D.** MPK7^{ac} phosphorylates AGGIE5^{EN} *in vitro*. *In vitro* kinase assay was performed by incubating His-MPK7^{ac} fusion protein with control, GST-AGGIE5^{EN}, GST-AGGIE5$^{EN, D618N}$, GST-AGGIE5$^{EN, T612A}$ in kinase buffer. Phosphorylation was detected by autoradiography (top panel). Protein loading control was shown by CBB (bottom panel).

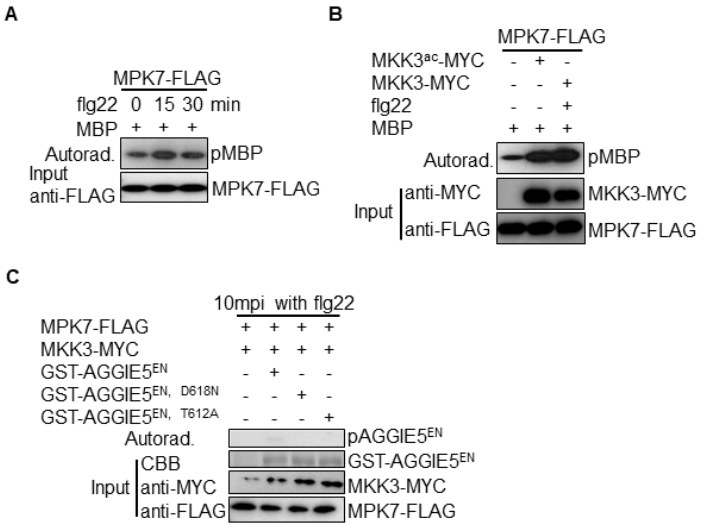

Figure 3.4 MAMP flg22 elicits the group C MPK MPK7 *in vivo*.

A. MAMP flg22-elicited MPK7 phosphorylates MBP *in vitro*. *In vitro* kinase assay was performed by incubating MBP protein with MPK7-FLAG in kinase buffer. Phosphorylation was detected by autoradiography (top panel). Protein loading control was shown by CBB (bottom panel). **B.** MAMP flg22-elicited MPK7 phosphorylates MBP *in vitro*. *In vitro* kinase assay was performed by incubating MBP protein with MPK7-FLAG in kinase buffer. Phosphorylation was detected by autoradiography (top panel). Protein loading control was shown by CBB (bottom panel). **C.** MAMP flg22-elicited MPK7 phosphorylates AGGIE5^{EN} *in vitro*. *In vitro* kinase assay was performed by incubating GST-AGGIE5^{EN}, GST-AGGIE5$^{EN, D618N}$, GST-AGGIE5$^{EN, T612A}$ protein with MPK7-FLAG in kinase buffer. Phosphorylation was detected by autoradiography (top panel). Protein loading control was shown by CBB (bottom panel).

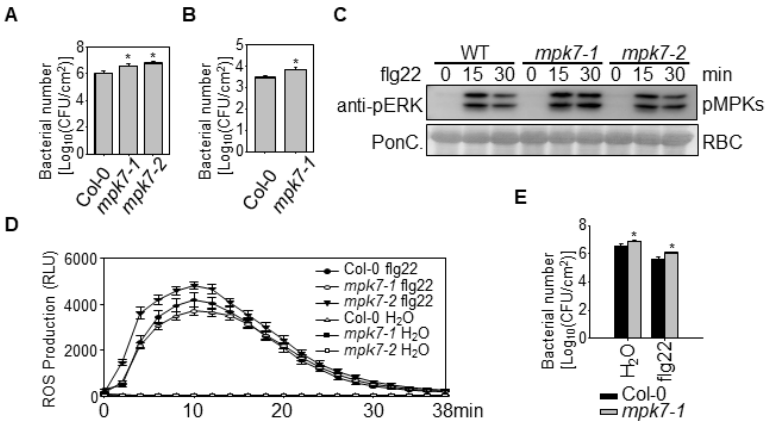

Figure 3.5 The group C MAPK MPK7 positively regulates plant resistance to bacterial pathogens.

A. MPK7 is required for disease resistance to *P.s.t. DC3000* infection. Four-week-old plants were hand-inoculated with *P.s.t. DC3000* at 5×10 cfu/ml. The *in planta* bacterial growth was measured at 3 days-post inoculation (dpi). Col-0 (WT), *mpk7-1* and *mpk7-2* mutant were included in the assay. The data are shown as means ± standard errors. **B.** MPK7 is required for disease resistance to *P.s.t. DC3000 hrcC* infection. Four-week-old plants were hand-inoculated with *P.s.t. DC3000 hrcC* at 5×10 cfu/ml. Col-0 (WT) and *mpk7-1* mutant were included in the assay. The *in planta* bacterial growth was measured at 3 days-post inoculation (dpi). The data are shown as means ± standard errors. **C.** flg22-induced phosphorylation of MPK3/4/6 is not changed in *mpk7-1* and *mpk7-2*. Ten-days-old seedling from Col-0 (WT), *mpk7-1* or *mpk7-2* plants were treated with or without 100 nM flg22 treatment for indicated time points. MAPK activation was analyzed with an α-pERK antibody (top panel), and protein loading was shown by Coomassie Brilliant Blue (CBB) staining for RuBisCO (RBC) (bottom panel). **D.** MPK7 is not required for flg22-triggered ROS production. Leaf discs from Col-0 (WT), *mpk7-1* and *mpk7-2* were treated with 100 nM flg22, and the ROS production was measured with a plate reader over 40 min (2400 seconds). The data are shown as means ± standard errors from 20 leaf discs for flg22 treatment. **E.** MPK7 is partially required for flg22-mediated protection against *P.s.t. DC3000* infection. Four-week-old plants were hand-inoculated with H_2O or 100 nM flg22 24 hours before inoculation of *P.s.t. DC3000* at 5×10 cfu/ml. Col-0 (WT) and *mpk7-1* mutant were included in the assay. The *in planta* bacterial growth was measured at 3 days-post inoculation (dpi). The data are shown as means ± standard errors. The above experiments were repeated 3 times with similar results.

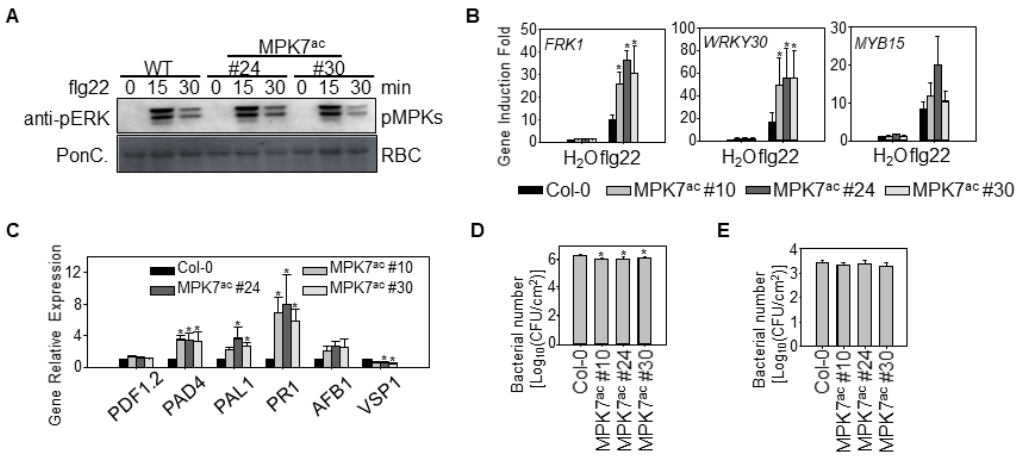

Figure 3.6 Overexpression of MPK7^{ac} enhances plant immune gene expression and resistance to bacterial pathogens.

A. Flg22-induced phosphorylation of MPK3/4/6 is not changed in two homozygous transgenic plants which overexpressing MPK7^{ac}-FLAG. Ten-days-old seedling from Col-0 (WT), two independent homozygous lines of p35S::MPK7^{ac}-FLAG transgenic plants in *Col-0* background were treated with or without 100 nM flg22 treatment for indicated time points. MAPK activation was analyzed with an α-pERK antibody (top panel), and protein loading was shown by Coomassie Brilliant Blue (CBB) staining for RuBisCO (RBC) (bottom panel). **B.** Elevated immune gene expression in p35S::MPK7^{ac}-FLAG transgenic plants. Ten-day-old seedlings seedling from Col-0 (WT), three independent homozygous lines of p35S::MPK7^{ac}-FLAG transgenic plants in *Col-0* background were treated with 100 nM flg22 for 60 min for qRT-PCR analysis. The data are shown as means ± se from three biological repeats with Student's *t*-test. * indicates $p<0.05$ when compared to WT. **C.** Altered phytohormone responsive gene expression in p35S::MPK7^{ac}-FLAG transgenic plants. Ten-days-old seedling from Col-0 (WT), three independent homozygous lines of p35S::MPK7^{ac}-FLAG transgenic plants in *Col-0* background without treatment were used for qRT-PCR analysis. The data are shown as means ± se from three biological repeats with Student's *t*-test. * indicates $p<0.05$ when compared to WT. **D.** MPK7^{ac} promotes disease resistance to *P.s.t. DC3000* infection. Four-week-old plants were hand-inoculated with *P.s.t. DC3000* at 5×10 cfu/ml. Col-0 (WT), two independent homozygous lines of p35S::MPK7^{ac}-FLAG transgenic plants in *Col-0* background were included in the assay. The *in planta* bacterial growth was measured at 3 days-post inoculation (dpi). The data are shown as means ± standard errors. **E.** MPK7^{ac} could not promote disease resistance to *P.s.t. DC3000 hrcC* infection. Four-week-old plants were hand-inoculated with *P.s.t. DC3000 hrcC* at 5×10 cfu/ml. Col-0 (WT), two independent homozygous lines of p35S::MPK7^{ac}-FLAG transgenic plants in *Col-0* background were included in the assay. The *in planta* bacterial growth was measured at 3 days-post inoculation (dpi). The data are shown as means ± standard errors. The above experiments were repeated 3 times with similar results.

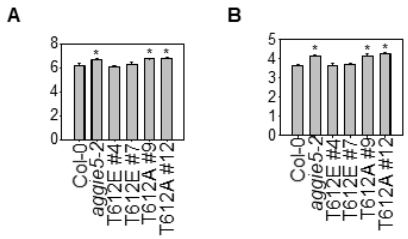

Figure 3.7 Phosphorylation at T612 is required for AGGIE5 function in innate immunity.

A. Phosphorylation at T612 positively regulates AGGIE5 function in disease resistance to *P.s.t. DC3000* infection. Col-0 (WT), *aggie5-2* mutant, two independent homozygous lines of pAGGIE5::AGGIE5-FLAG, pAGGIE5::AGGIE5^{T612E}-FLAG and pAGGIE5::AGGIE5^{T612A}-FLAG transgenic plants were hand-inoculated with *P.s.t. DC3000* at 5×10 cfu/ml. The *in planta* bacterial growth was measured at 3 days-post inoculation. **B**. Phosphorylation at T612 positively regulates AGGIE5 function in disease resistance to *P.s.t. DC3000 hrcC* infection. Col-0 (WT), *aggie5-2* mutant, two independent homozygous lines of pAGGIE5::AGGIE5-FLAG, pAGGIE5::AGGIE5^{T612E}-FLAG and pAGGIE5::AGGIE5^{T612A}-FLAG transgenic plants were hand-inoculated with *P.s.t. DC3000 hrcC* at 5×10 cfu/ml. The *in planta* bacterial growth was measured at 3 days-post inoculation. The above experiments were repeated 3 times with similar results.

Table 3.1 Cloning primers used in study in chapter 3.

Gene	Forward Primer	Reverse Primer
MPK7	CATGCCATGGCGATGTTAGTTGAG	AAGGCCTGGCATTTGAGATTTCAGC
MPK7-CRISPR-target1/2-BS	ATATATGGTCTCTATTGTTAAACTTCTTAGGCATGTGGTT	ATTATTGGTCTCTAAACTTGAAACTGGATCTATTAGCCAA
MPK7-CRISPR-target1/2	GTTAAACTTCTTAGGCATGTGGTTTTAGAGCTAGAAATAGC	CTTGAAACTGGATCTATTAGCCAATCTCTTAGTCGACTCTAC

Note: The restriction enzyme sites are underlined.

Table 3.2 Genotyping primers used in study in chapter 3.

Gene	Forward Primer	Reverse Primer
mpk7-crispr	*CATGCATGCGATGTTAGTTGAG*	*AACTGGCATTTGAGATTTCAGC*

Table 3.3 qRT-PCR primers used in study in chapter 3.

Gene	Forward Primer	Reverse Primer
FRK1	ATCTTCGCTTGGAGCTTCTC	TGCAGCGCAAGGACTAGAG
WRKY30	GCAGCTTGAGAGCAAGAATG	AGCCAAATTTCCAAGAGGAT
MYB15	CTTGGCAATAGATGGTCAGC	TGAGTGTGCCATACGTTCTTG
At2g17740	TGCTCCATCTCTCTTTGTGC	ATGCGTTGCTGAAGAAGAGG
UBQ10	AGATCCAGGACAAGGAAGGTATTC	CGCAGGACCAAGTGAAGAGTAG

Table 3.4 Point-mutation primers used in study in chapter 3.

Gene	Forward Primer	Reverse Primer
MPK7-Y113C	GGATGTTTATTTGGTT**TGT**GAGCTAATGGATACTG	CAGTATCCATTAGCTC**ACA**AACCAAATAAACATCC
MPK7-T191E, Y193E	GTAATGAACAGTTCATG**GAA**GAG**GAA**GTGGTTACACGTTGG	CCAACGTGTAACCAC**TTC**CTC**TTC**CATGAACTGTTCATTAC

Note: The point mutation sites are underlined and in bold.

3.5 Discussion

In the present study, a Y2H screen was carried out to look for the interacting protein of AGGIE5 and a group C MAPK MPK7 was successfully identified. Combining biochemical and genetic analysis, we found MPK7 phosphorylates AGGIE5 at Thr-612. This provides one of the first evidence that $MPK7^{Y113C}$ is an active kinase possesses phosphorylation activity both *in vivo* and *in vitro*. There are 20 MAPKs in the Arabidopsis genome and some of them have been characterized as vital regulators of MTI (Bueso et al., 2014; Zhang et al., 2015; Zhang et al., 2005). How many of substrates of MPK7 and whether other MPKs including group C MAPK or group D MAPK are involved in MTI will be interesting questions to address in the future.

An Y2H interaction assay as well as an *in vitro* pull-down assay suggested MPK7 directly interacts with AGGIE5. Although likely via the EP-like domain and NTPase-like domain, it remains unknown which part of AGGIE5 interacts with MPK7. Future structural studies could provide more insight of the interaction interface between MPK7 and AGGIE5.

Consistent with the interaction between MPK7 and AGGIE5, $AGGIE5^{EN}$ was phosphorylated by MPK7 *in vitro*. While the impact of MPK7 phosphorylation on AGGIE5 remains unclear, we speculate this phosphorylation might not be involved in AGGIE5 stability control as AGGIE5 protein level is unaltered when co-expressing MPK7. Considering that D618N mutation block phosphorylation on Thr-612 by MPK7, it seems that phosphorylation might also not affect localization of AGGIE5 because AGGIE5 and $AGGIE5^{EN}$ show similar pattern. One hypothesis is that this phosphorylation

is important for the enzymatic activity of AGGIE5 *in planta*, although the D618 is in the defined EP-like domain, relative far away from the putative lipase motif and NTPase motif. Another hypothesis is that this phosphorylation is important for interaction between peroxisome and chloroplast. We observed some peroxisomes are trapping to chloroplast. In transgenic plants, YFP-AGGIE5 preferentially localize to peroxisome membrane, but the subcellular dynamics of AGGIE5 *in planta* upon invasion of pathogen is still unknown and worthy further test. Confocal microscopy analysis with double transgenic plant expressing different fluorescent protein tagged MPK7 and AGGIE5 could potentially provide more detailed insight of the membrane protein AGGIE5 and interacting kinase MPK7 localization and interaction dynamics.

Our study is the first study in plants demonstrating that MPK7 directly regulates MAMP-triggered resistance and immune gene expression and discovered AGGIE5 as the first reported substrate of MPK7. Combined biochemical and genetic analysis, our study identified a novel group C MAPK MPK7 positively regulating AGGIE5 function and the phosphorylation of AGGIE5 positively regulate plant innate immunity. Strikingly, the D618N mutation block phosphorylation of AGGIE5 at Thr-612 by MPK7, providing informative evidence explaining the negative role of AGGIE5^{D618N} in plant innate immunity.

4. AGGIE5 AND MPK7 COORDINATE FINE-TUNING OF PLANT IMMUNE GENE EXPRESSION BY REGULATING MAMP-INDUCED DN-OPDA INDUCTION

4.1 Summary

Oxylipin profiling by liquid chromatography-tandem mass spectrometry (LC-MS/MS) revealed that P.s.t. DC3000 *hrcC* induced a series of oxylipins. Interestingly, as shown in *aggie5-1* mutant and phenocoping line, AGGIE5^{D618N} positively regulates dn-OPDA early induction. In addition, both *mpk7-1* and *aggie5-2* mutants displayed a higher content of dn-OPDA, 12-OPDA, OPC4-0, JA, JA-Ile compared with WT, indicating AGGIE5-MPK7 negatively regulates oxylipin early induction in MTI response. Taken together, the the data point to dn-OPDA whose MAMP-induced early induction are positively regulated by AGGIE5^{D618N} and negatively regulated by AGGIE5-MPK7.

Interestingly, AGGIE5^{D618N} positively regulates early induction of dn-OPDA and other oxylipins. As the point mutation AGGIE5^{D618N} blocked phosphorylation of AGGIE5 at Thr-612 and MPK7 negatively regulates MAMP-induced oxylipin early induction, the conclusion could be drawn that phosphorylation at Thr-612 was required for AGGIE5 to suppress MAMP-induced oxylipin induction.

Strikingly, oxylipin profiling from *aggie5* and *mpk7* mutants revealed that dinor-12-oxo-phytodienoic acid (dn-OPDA) is the most significant oxylipin regulated by MPK7-AGGIE5. Furthermore, WT plants pretreated with dn-OPDA show reduced immune expression and disease resistance to virulent bacterial pathogen infection. Moreover, biological and genetic study with the application of dn-OPDA on *opr3* and *coi1*

mutants demonstrate that dn-OPDA-mediated suppression were OPR3-independent and partially COI1-dependent, providing evidence showing the role of dn-OPDA in Arabidopsis immunity towards bacterial pathogens and indicting dn-OPDA may function as an important signal facilitating fine-tune of defense responses *in planta*.

Recently, it was discovered that the JA-Ile receptor COI1 is functionally conserved between the bryophyte *Marchantia polymorpha* and the eudicot *Arabidopsis thaliana* but COI1 responds to different ligands in each species during independent evolution. Remarkably, the ligand of *Marchantia* MpCOI1 as two isomeric forms of the JA-Ile precursor dinor-OPDA (dinor-cis-OPDA and dinor-iso-OPDA). Most interestingly, AtCOI1 functionally complements Mpcoi1 mutation and confers JA-Ile responsiveness and that a single residue substitution in MpCOI1 is responsible for the evolutionary switch in ligand specificity. Those founding revealed that the ancestral bioactive jasmonate and clarify its biosynthetic pathway, demonstrate the functional conservation of this signaling pathway and show that JA-Ile and COI1 emergence in vascular plants required co-evolution of hormone biosynthetic complexity and receptor specificity.

4.2 Introduction

Genetic and pharmacological studies demonstrated that plant-derived lipids, especially their oxidized products called oxylipins, govern the outcome of the host-fungal pathogen interactions (Farmer et al., 2003; Stintzi et al., 2001). More and more study points out that oxylipins are a newly emerging group of signals that serve defense roles or promote virulence.

In plants, a series of unsaturated fatty acids are oxygenated to produce plant hormones that are involved in senescence, flower development, and the response to insect pathogens. JA synthesis initiates in chloroplasts with release of the membrane fatty acids, such as α-linolenic or hexadecatrienoic acids. Oxygenation by 13-lipoxygenases and dehydration–cyclization by the enzymes AOS (allene oxide synthase) and AOC lead (allene oxide cyclase) to production of 12-oxo-phytodienoic acid (12-OPDA) and dinor-12-oxo phytodienoic acid (dn-OPDA). OPDA is transported into the peroxisome, where it is reduced by OPDA-reductase 3 (OPR3) and undergoes three beta-oxidation cycles to produce jasmonic acid (JA). Cytoplasmic JAR1 (Jasmonate-amido synthetase 1) conjugates JA to Ile, giving rise to the bioactive hormone (+)-7-iso-JA-L-Ile4,5 (Browse, 2009; Kachroo and Kachroo, 2009). Notably, dn-OPDA can also be incorporated into glycerolipids and galactolipids by conjugation. These lipids contain 12-OPDA or dn-OPDA are defined as arabidopsides (Andersson et al., 2006; Dave and Graham, 2012; Hartley et al., 2015; Hisamatsu et al., 2006; Kourtchenko et al., 2007; Lin et al., 2016; Mosblech et al., 2009; Nakajyo et al., 2011; Nakajyo et al., 2006; Nilsson et al., 2016; Pedras and To, 2017; Schafer et al., 2011; Xiao et al., 2010; Zhao et al., 2012).

In potato plants displayed systemic resistance by infiltration with *Pseudomonas syringae pv. maculicola*, accumulation of OPDA were detected in both infiltrated leaves and non-treated leaves of infected plants. In contrast, accumulation of JA was only found in infiltrated leaves (Landgraf et al., 2002). Moreover, 12-oxo-phytodienoic acid is increased in elicitor-treated moss tissues. Interestingly, it is demonstrated that OPDA

involve in N-Acyl-Homoserine Lactone primed resistance against *P.s.t. DC3000* (Schenk et al., 2014).

In a study of transcription profiling with *opr3-1* mutant, treating *opr3-1* plants with exogenous OPDA induces several genes and disclosed two distinct downstream signal pathways, one through COI1, the other bypass COI1, revealing that the OPDA regulates gene expression in concert with JA to fine-tune the expression of defense genes. Another genome-wide transcriptome analysis of Arabidopsis revealed that approximately 150 genes involved in the stress response and signal transduction responded to the application of 12-OPDA (Taki et al., 2005). Interestingly, this transcription reprogramming depended on TGA transcription factors TGA2, TGA5, and TGA6 (Mueller et al., 2008), consistence with the genes upregulated by SA or induced by some phytopathogens. In recent years, although JA-dependent responses and JA signaling has made considerable progress, knowledge of the regulation of OPDA-dependent plant responses and OPDA signaling is just emerging.

4.3 Materials and methods

4.3.1 Extraction of oxylipins and phytohormones in Arabidopsis

P.s.t DC3000 *hrcC* (at 5×10 cfu/ml) was hand-inoculated with needleless springe all over the four-week-old adult plants of Col-0, *aggie5-2*, *mpk7-1* and WT (*pFRK1::LUC*), *aggie5-1*, p35S::AGGIE5^{D618N} #4. Leave tissues were collected at 0, 3,

24 hpi and stored at -80C. Eight independent biological replicates were measured per time point. Leave tissues were ground in liquid nitrogen prior hormone measurements.

4.3.2 LC-MS/MS Analysis

The internal reference standard added for the quantitative analysis was the deuterated 9-hydroxy-10E,12Z-octadecadienoic acid (9-HODEd4, MW 300.5 g mol–1), at a final 2 μM concentration. Briefly, 20 mg of lyophilised matrix were vortex-mixed with 1 ml of extraction mixture (Hex:iPrOH, 3:2, v/v, with 0.0025% w/v of butylated hydroxytoluene). The clear upper phase was collected and added with 0.5 ml of a saline solution of 6.7% potassium sulphate. The Hex upper layer was transferred into a clear tube and dried under N2, reconstituted in 200 μl of MeOH and loaded onto the HPLC injector for oxylipin quantitative analysis. The concentration of oxylipins in the final volume of 200 μl was reported as μM. The equipment, chromatographic column and analysis software were all from Agilent Technologies (Santa Clara, CA, USA). Samples were analyzed by liquid chromatography (HPLC 1200 series rapid resolution; Agilent Technologies, Santa Clara, CA, USA) coupled to a mass spectrometer (G6410A series triple quadrupole, QqQ; Agilent Technologies) equipped with electrospray ionization (ESI). The acquisition was in negative-ion mode. Chromatographic separation was performed with a Zorbax ECLIPSE XDB-C18 rapid resolution HT 4.6 × 50 mm 1.8 μm p.s. column (Agilent Technologies). The mobile phases consisted of A: water/ACN 97:3 v/v containing 0.1% HCOOH, and B: ACN/iPrOH 90:10 v/v. The elution programme was as follows: 0–2 min 20% B, 2–4 min 35% B, 4–6 min 40%B, 6–7 min 42%B. 7–9 min

48% B, 9–15 min 65% B, 15–17 min 75% B, 17–18,5 min 85% B, 18,5–19,5 min 95% B, 19,5–24 min 95% B, 24–26 min 99% B, 26–30 min 99% B, 30–34 min 20% B. The flow rate was as follows: 0–24 min at 0.6 ml min^{-1}, 24–30 min at 1 ml min^{-1}, 30–34 min at 0.6 ml min^{-1}. The column was thermostated at 40°C. The injection volume was 10 µl. The injector needle was washed with the mobile phase in the wash port at the end of each HPLC run. Nitrogen was used as the nebulising and desolvation gas. The temperature and flow of the drying gas were 350°C and 10 l min^{-1}, respectively, with a nebulization pressure of 20 psi. The capillary and cone voltage were 4000 V. Experiments in MRM in negative ion mode [M-H]2 were performed. The fragmentor voltage (F) and collision energies (CE) were optimised for each oxylipin. The MRM transitions were obtained by flow injection of authentic standard. MRM data were processed using Mass Hunter Quantitative software (B.03.02 version, Agilent Technologies, Santa Clara, CA, USA).

4.3.3 Application of dn-OPDA

The dinor-12-oxo phytodienoic acid (OPDA) is from CAYMAN chemical company. OPDA is dissolved in 3% DMSO and stored at 4C. In treatment with dn-OPDA, ten-day-old seedlings cultured on ½ MS solid medium are transferred into ½ MS liquid medium plus dn-OPDA (in 3% DMSO), the seedlings transferred into the liquid MS medium plus 3% DMSO served as control. Four-week-old plants were hand-inoculated with dn-OPDA (in 3% DMSO) 6 hours before inoculation with corresponding pathogens, the plants inoculated with 3% DMSO served as control.

4.3.4 Application of 2,4-DB

The 4-(2,4-Dichlorophenoxy)butyric acid is from Sigma-Aldrich. 2,4-DB is dissolved in ethonol and stored at 4C. In treatment with 2,4-DB, ten-day-old seedlings were cultured on ½ MS solid medium plus 2,4-DB, the seedlings cultured on ½ MS solid medium served as control.

4.4 Results

4.4.1 MAMP-induced early dn-OPDA induction are negatively regulated by AGGIE5-MPK7

The biosynthesis of jasmonic acid (JA), the most important and well-studied oxylipin in plant, is initiated in chloroplasts, where linolenic acid is converted to OPDA by a series of enzymatic reactions. OPDA is then transported to peroxisome, where OPDA is reduced by OPR3, followed by three rounds of β-oxidation to form JA. JA is finally transported to the cytosol to form bioactive JA, such as JA-Ile. Since AGGIE5 localizes to both peroxisome and chloroplast membranes, we assessed whether AGGIE5 regulates basal or MAMP-induced oxylipin synthesis.

As AGGIE5^{D618N} have been shown to negatively regulate immune genes expression and MAMP-triggered protection, we tested the role of on AGGIE5^{D618N} in oxylipin production during P.s.t. DC3000 *hrcC* infection of Arabidopsis leave. Mutant lines were inoculated and a series of oxylipins were profiled by liquid chromatography-tandem mass spectrometry (LC-MS/MS). The oxylipin profiling identified by LC-MS/MS revealed that several oxylipins, such as 10-OPEA, 12,13-EpOD, 13-HOD, 13-HOT, 13-

KOD, 13-OH-12-KOD, 13-OH-12-KOM, 9, 12,13-THOM, 9-HOD, 9-HOT, 9-KOD and 9-KOT were induced by infiltration with Mock, supporting the founding that oxylipins were induced after physical damage. A series of oxylipins, such as 13-HOD, 13-HOT, 9-HOD, 9-HOT and 9-KOD were further induced by infiltration with P.s.t. DC3000 *hrcC* that was used as elicitors to trigger robust MTI responses in Col-0 and WT *pFRK1::LUC* plants (Fig. 4.1 and Fig. 4.3). However, those transient induced oxylipins were not further accumulated in the late stage of MTI (Fig. 4.2, and Fig. 4.4), suggesting they may function as primary signal transducer or secondary signal elicitor in subcellular signal network in plant cell. Remarkably, the content of most JA-related oxylipins including 12-OH-JA, 12-OH-JA-Ile, JA, JA-Ile, OPC4, 12-OPDA and dn-OPDA were increased steadily at 3 hpi. Interestingly, AGGIE5^{D618N} caused increased accumulation of dn-OPDA and reduced accumulation of SA at 3 hpi (Fig. 4.1 and Fig. 4.5). The mis-regulation of several oxylipins induction in the infected *aggie5-1* mutant and p35S::AtAGGIE5^{D618N} transgenic plants echoed the defection of phosphorylation of AGGIE5 by MPK7 in *in vitro* assay, which supports the hypothesis that MPK7 and AGGIE5 also contribute to oxylipin reprogramming against P.s.t. DC3000 *hrcC*. So, we also tested the involvement of AGGIE5 and MPK7 in oxylipin production during P.s.t. DC3000 *hrcC* infection with the same approach. To test this hypothesis, knock-out mutants of MPK7 and AGGIE5 were also infected with P.s.t. DC3000 *hrcC* and subjected to the robust and sensitive targeted analysis platform for oxylipins via LC-MS/MS. Both *mpk7-1* and *aggie5-2* mutants displayed a higher content of dn-OPDA, 12-OPDA, OPC4-0, JA, JA-Ile compared with WT at 3 hpi (Fig. 4.3 and Fig. 4.6). Remarkably, the dn-OPDA is the most significant

differentially-regulated oxylipin in *aggie5-1*, *aggie5-2* and *mpk7-1* mutants at 3 hpi, suggesting a major role of AGGIE5-MPK7 in the biosynthesis of dn-OPDA in early MTI response. Notably, the enhanced accumulation of dn-OPDA was more evident in *aggie5-1* at 24 dpi, although content of dn-OPDA was unaltered in *aggie5-2* and *mpk7-1* at 24 dpi compared to that of WT plants. Taken together, these data suggest that AGGIE5 and MPK7 negatively regulate dn-OPDA biosynthesis pathway in early induced response in MTI. This finding confirmed the results of the previous study showing opposite roles played by AGGIE5^{D618N} and AGGIE5 in regulation of MTI.

4.4.2 AGGIE5^{D618N} enhances MeJA-mediated growth inhibition

MeJA-mediated responses are costly but benefit plants under invasion of pathogen and are often accompanied by significant growth inhibition. Previous oxylipin profiling study shows that MAMP-induced early dn-OPDA induction are positively regulated by AGGIE5^{D618N} and negatively regulated by AGGIE5-MPK7, we tried to test whether AGGIE5^{D618N} positively affects MeJA-mediated growth inhibition. As expected, *aggie5-1* and the transgenic lines expressing AGGIE5^{D618N} were much more sensitive to MeJA than the WT plants in the growth inhibition assay. In the presence of 50uM MeJA, there was approximately 50% reduction in fresh weight of wild type seedlings with respect to the seedlings grown on only MS. In contrast, the *aggie5*-1 mutant and p35S::AGGIE5^{D618N}-FLAG line showed 65% reduction in seedling weight compared to the WT plants (Fig. 4.8A). Clearly, the growth inhibition effect of MeJA was significantly enhanced in the mutant *aggie5-1* and phenocoping line in comparison with the WT. Also,

although *aggie5-1* showed only a slightly higher sensitivity to MeJA-mediated mediated inhibition of hypocotyl growth, under our experimental conditions, the AGGIE5^{D618N} transgenic overexpression plants was more sensitive to MeJA-mediated hypocotyl inhibition on MS medium. It is clear that AGGIE5^{D618N} enhances MeJA-mediated growth inhibition. The data revealed that AGGIE5^{D618N} positively regulates MeJA-mediated response and are consistent with that AGGIE5^{D618N} promotes dn-OPDA synthesis. However, the mechanism underlying this observation is still elusive. It should be noted that the MeJA-mediated growth inhibition is unaltered in *aggie5-2* and *aggie5-3* mutants, indicating AGGIE5 does not contribute to dn-OPDA synthesis without pathogens (Fig. 4.8B). These results contrast with those from MeJA-mediated growth inhibition assay that showed the plants expressing AGGIE5^{D618N} exhibited enhanced MeJA-mediated growth inhibition. It is possible that enhanced dn-OPDA induction by AGGIE5^{D618N} results in elevated content of JA compounds or that enhanced dn-OPDA induction by AGGIE5^{D618N} directly facilitates MeJA-mediated response.

4.4.3 AGGIE5^{D618N} enhances resistance to *Botrytis cinerea*

As reported, JA is an important defense hormone for Arabidopsis in resistance to necrotrophic plant pathogens or insects. To confirm AGGIE5^{D618N} positively regulates MeJA-mediated response, we tested the resistance of those mutants towards a significant necrotrophic plant pathogen, *Botrytis cinerea*. Apparently, detached leaves of *mpk7-1* and *mpk7-2* mutants displayed elevated resistance to *Botrytis*, suggesting MPK7 negatively regulates JA signaling (Fig. 4.9A). However, we only observed increased resistance in

aggie5-1 mutant but not in the *aggie5-2* and *aggie5-3* (Fig. 4.9B and Fig. 4.9C). It seems that AGGIE5 is not required for resistance to necrotrophic plant pathogens, although AGGIE5^{D618N} indeed positively resistance to *Botrytis cinereal* because the transgenic line expressing AGGIE5^{D618N} phenocopied *aggie5-1* mutant (Fig. 4.9B).

4.4.4 AGGIE5^{D618N} does not affect beta-oxidation in peroxisome

Beta-oxidation is the catabolic process by which fatty acid molecules are broken down, which is named as such because the beta carbon of the fatty acid undergoes oxidation to a carbonyl group. Fatty acid oxidation also occurs in peroxisomes when the fatty acid chains are too long to be handled by the mitochondria. In peroxisomes, the 4-(2,4-Dichlorophenoxy)butyric acid (2,4-DB) was converted into 2,4-D through beta-oxidation and the synthesized 2,4-D was able to inhibits growth at the tips of stems and roots. However, the seedlings of WT, *aggie5-1* and phenocoping line grown on the Murashige and Skoog medium (MS) supplemented with different concentration of 2,4-DB does grow as same as WT (Fig. 4.10), suggesting beta-oxidation is not affected by AGGIE5^{D618N}.

4.4.5 dn-OPDA suppresses immune genes induction upon flg22 and compromises disease resistance to virulent bacterial pathogens

Previous RNA-seq study clearly showed AGGIE5^{D618N} globally regulates flg22-induced immune genes, and oxylipin profiling study revealed dn-OPDA is the most

significant differentially regulated oxylipin in *aggie5-1*, *aggie5-2* and *mpk7-1* mutants in the early response in MTI. These founding led us to hypothesize enhanced dn-OPDA induction is the reason why the flg22-induced immune genes were suppressed in *aggie5-1*, *aggie5-2* and *mpk7-1* mutants. To assess this hypothesis, we first examined the effectiveness of dn-OPDA on disease resistance. In the disease assay, 10um, 100 uM, 200 uM dn-OPDA was applied to Arabidopsis leaves by hand-inoculation 6 hours before infiltration with virulence pathogen P.s.t. DC3000. Clearly, application of 100 uM dn-OPDA lead to decreased resistance, indicating that dn-OPDA contributes to negative regulation of plant defense against bacterial pathogen (Fig. 4.11A). We then tested expression levels of endogenous MTI marker genes in the WT Col-0 seedlings undergoing flg22 elicitation after 6 hours cultured in ½ MS liquid medium with or without 100 uM dn-OPDA with qRT-PCR analysis. The expression of the MTI marker gene FRK1 and WRKY30 were significantly elevated in the Col-0 pretreated with DMSO compared to that of seedlings pretreated with dn-OPDA for 6 hours at 60 min after flg22 treatment (Fig. 4.11B). The results indicate that application of dn-OPDA play a negative role in regulation of certain flg22-induced genes expression.

4.4.6 Attenuation of dn-OPDA on immune gene expression is OPR3-independent but partially COI1-dependent

Considering that JA plays a negative regulatory role in plant defense against bacterial pathogens and dn-OPDA could be converted into JA through JA synthesis pathway, it is difficult to conclude that dn-OPDA directly represses immune gene

induction in MTI. Because JA synthesis mutants have not been available, *opr3* mutants *opr3-1* and *opr3-3* were used for investigation of differentiate effectiveness of dn-OPDA. In the beginning, the uncertainty led us to test whether dn-OPDA may cause altered the expression of immune genes in *opr3-1* mutant. Similar to WT Col-0, the expression of the MTI marker gene FRK1 and WRKY30 were also reduced in the seedlings of *opr3-1* pretreated with dn-OPDA, although induction of MYB15 was not affected by dn-OPDA (Fig. 4.11B). However, it is reported the OPR3 transcript is detectable upon pathogen infection. Possibly OPR3 transcribes after treatment with P.s.t. DC3000 *hrcC*. So, we tested another mutant *opr3-3,* which was identified and claimed as a null mutant of OPR3. It is reported that the JA synthesis through dn-OPDA and 12-OPDA is largely blocked in *opr3-3* mutant. Consistent with results observed in *opr3-1,* the induction of the MTI marker gene FRK1 and WRKY30 was also suppressed by pretreatment with dn-OPDA in the *opr3-3* seedlings (Fig. 4.12A). Together, application of exogenous 100 uM dn-OPDA could efficiently suppress MTI marker genes expression in *opr3* mutants, suggesting OPR3 is not required for attenuation of dn-OPDA on MTI marker genes expression. In this study, we also investigated the COI1 dependency of dn-OPDA functionality in Arabidopsis innate immunity. Interestingly, we found that the suppression of the MTI marker gene FRK1 and WRKY30 after pretreatment with dn-OPDA was partially rescued in *coi1-30* knockout mutant (Fig. 4.12A), suggesting that dn-OPDA was implicated in the regulation of immune gene expression through COI1. The bacteria grew faster in WT plants pretreated with dn-OPDA compared with WT plants (Fig. 4.12B). Similarly, the attenuation of dn-OPDA on plant resistance to bacterial pathogen is almost fully

maintained in *opr3-3* mutant (Fig. 4.12B), consistent with the effect on immune gene expression (Fig. 4.12A). Notably, in *coi1-30* mutant, dn-OPDA could only weakly reduce the resistance (Fig. 4.12B), providing biological evidence supporting that dn-OPDA were implicated in the regulation of plant resistance through COI1. Therefore, the attenuation of dn-OPDA on MTI marker genes expression is OPR3-independent but partially COI1-dependent. In oxylipin profiling study, *aggie5-1* was characterized as a mutant showing enhanced dn-OPDA induction upon MAMP treatment. We further test the effectiveness of dn-OPDA in *aggie5-1* background. It appears that dn-OPDA could not suppress plant disease in *aggie5-1* as effectively as in WT, since the dn-OPDA is probably already saturated in *aggie5-1*. In all, these defects including reduced immune gene induction and increased susceptibility were caused by application of exogenous dn-OPDA. These data provide evidence supports that MAMP-induced dn-OPDA biogenesis is required for fine-tune of transcription reprogramming and induced resistance in MTI.

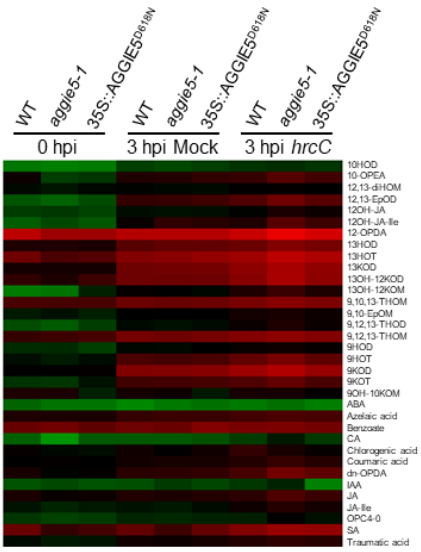

Figure 4.1 AGGIE5^{D618N} regulates hrcC-induced early oxylipin reprogramming.

Heat map of *hrcC*-induced oxylipin reprogramming in *pFRK1::LUC* (WT), *aggie5-1* or 35S::AGGIE5^{D618N} transgenic plants. Four-week-old plants were hand-inoculated with *P.s.t. DC3000 hrcC* at 5×10 cfu/ml. The leaves were collected at 3 hours-post inoculation (hpi). The *pFRK1::LUC* transgenic plants (WT), *aggie5-1* mutant and homozygous lines of p35S*::AtAGGIE5*^{D618N}*-GFP* transgenic plants in WT background were included in the assay. The original content values were subjected to data adjustment by normalized genes/rows and hierarchical clustering was generated with the average linkage method using MeV4.9. Red color indicates relatively high concentration, and green indicates relatively low concentration.

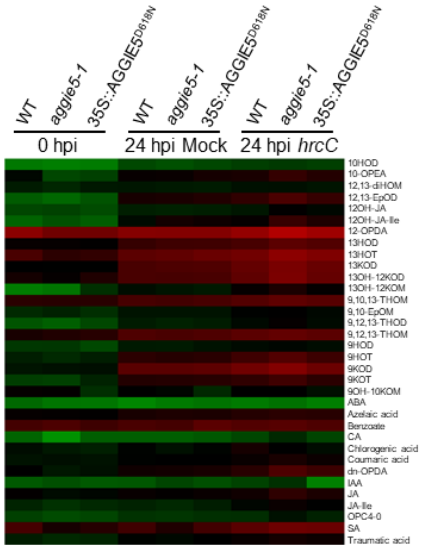

Figure 4.2 AGGIE5^{D618N} regulates hrcC-induced late oxylipin reprogramming.

Heat map of *hrcC*-induced oxylipin reprogramming in *pFRK1::LUC* (WT), *aggie5-1* or 35S::AGGIE5^{D618N} transgenic plants. Four-week-old plants were hand-inoculated with *P.s.t. DC3000 hrcC* at 5×10 cfu/ml. The leaves were collected at 24 hours-post inoculation (hpi). The *pFRK1::LUC* transgenic plants (WT), *aggie5-1* mutant and homozygous lines of p35S*::AtAGGIE5*^{D618N}*-GFP* transgenic plants in WT background were included in the assay. The original content values were subjected to data adjustment by normalized genes/rows and hierarchical clustering was generated with the average linkage method using MeV4.9. Red color indicates relatively high concentration, and green indicates relatively low concentration.

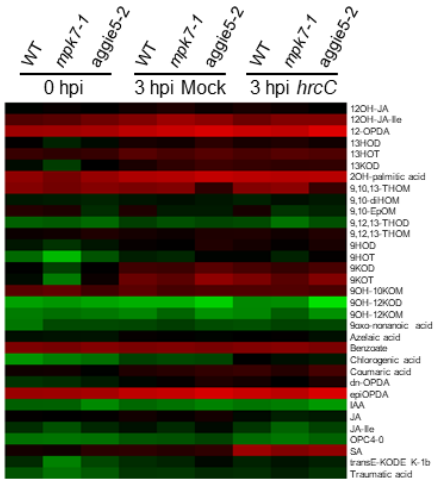

Figure 4.3 AGGIE5 and MPK7 regulates hrcC-induced early oxylipin reprogramming.

Heat map of *hrcC*-induced oxylipin reprogramming in Col-0 (WT), *mpk7-1* or *aggie5-2*. Four-week-old plants were hand-inoculated with *P.s.t. DC3000 hrcC* at 5×10 cfu/ml. The leaves were collected at 3 hours-post inoculation (hpi). The *Col-0* (WT), *mpk7-1* and *aggie5-2* mutant were included in the assay. The original content values were subjected to data adjustment by normalized genes/rows and hierarchical clustering was generated with the average linkage method using MeV4.9. Red color indicates relatively high concentration, and green indicates relatively low concentration.

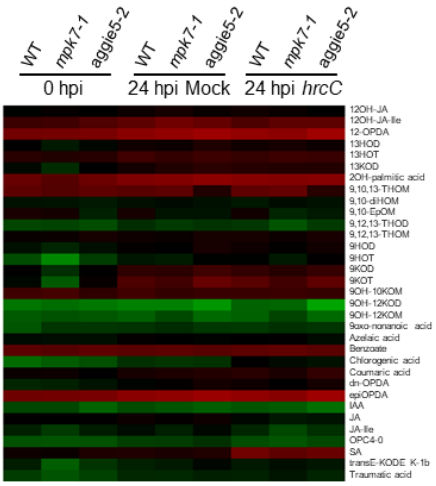

Figure 4.4 AGGIE5 and MPK7 regulates hrcC-induced late oxylipin reprogramming.

Heat map of *hrcC*-induced oxylipin reprogramming in Col-0 (WT), *mpk7-1* or *aggie5-2*. Four-week-old plants were hand-inoculated with *P.s.t. DC3000 hrcC* at 5×10^{-4} cfu/ml. The *in planta* bacterial growth was measured at 24 hours-post inoculation (hpi). The *Col-0* (WT), *mpk7-1* and *aggie5-2* mutant were included in the assay. The original content values were subjected to data adjustment by normalized genes/rows and hierarchical clustering was generated with the average linkage method using MeV4.9. Red color indicates relatively high concentration, and green indicates relatively low concentration.

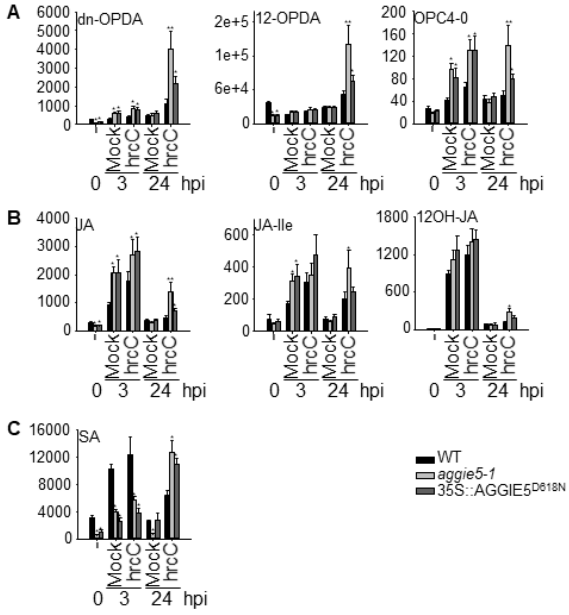

Figure 4.5 AGGIE5^{D618N} positively regulates hrcC-induced oxylipin reprogramming.

A. AGGIE5^{D618N} positively regulates JA precursors in MTI. **B.** AGGIE5^{D618N} positively regulates JA induction in MTI. **C.** AGGIE5^{D618N} negatively regulates early SA induction but positively regulates late SA induction in MTI.

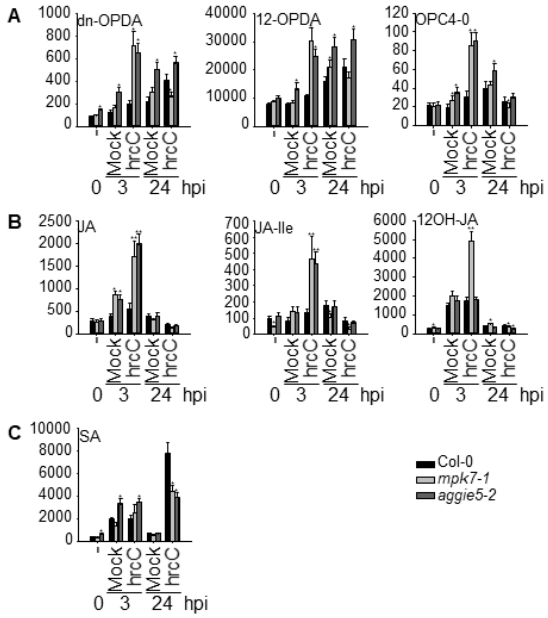

Figure 4.6 AGGIE5 and MPK7 negatively regulates hrcC-induced oxylipin reprogramming.

A. AGGIE5 and MPK7 negatively regulates JA precursors in MTI. **B.** AGGIE5 and MPK7 negatively regulates JA induction in MTI. **C.** AGGIE5 negatively regulates early SA induction in MTI, while AGGIE5 and MPK7 positively regulates late SA induction in MTI.

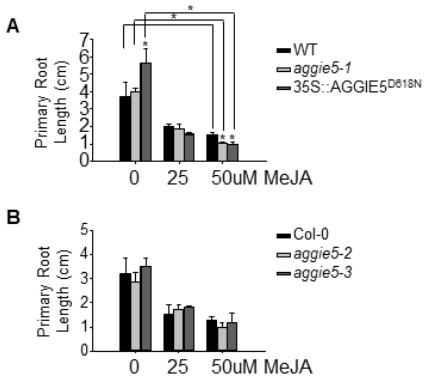

Figure 4.7 AGGIE5^{D618N} promotes MeJA-triggered root growth inhibition.

A. AGGIE5^{D618N} promotes MeJA-triggered root growth inhibition. Four-day-old seedlings were treated with 0, 25 or 50 uM MeJA for 6 days on ½ MS medium. The *pFRK1::LUC* transgenic plants (WT), *aggie5-1* mutant and homozygous lines of p35S*::AtAGGIE5*^{D618N}*-GFP* transgenic plants in WT background were included in the assay. The data are shown as means ± se from three biological repeats with Student's *t*-test. * indicates $p<0.05$ when compared to WT. **B.** MeJA-triggered growth inhibition is unaltered in *aggie5-2* and *aggie5-3* mutant. Four-day-old seedlings were treated with 0, 25 or 50 uM MeJA for 6 days on ½ MS medium. Col-0 (WT), *aggie5-2* and *aggie5-3* mutants were included in the assay. The data are shown as means ± se from three biological repeats with Student's *t*-test. * indicates $p<0.05$ when compared to WT. The above experiments were repeated 3 times with similar results.

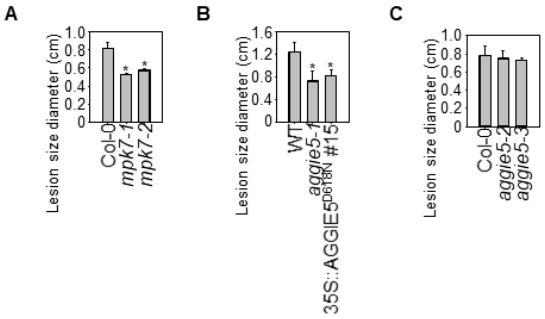

Figure 4.8 AGGIE5^{D618N} and MPK7 inversely regulates disease resistance to necrotrophic fungal pathogen *Botrytis. cinerea*.

A. The *mpk7-1* and *mpk7-2* mutants are more resistance to *B. cinereal* infection. Leaves of five-week-old plants were drop-inoculated with *B. cinerea* at the concentration of 2.5×10^5 spores/ml. Lesion size was measured 2 days post-inoculation (dpi). Col-0 (WT), *mpk7-1* and *mpk7-2* mutant were included in the assay. The data are shown as mean ± se from 15 infected leaves. **B.** The *aggie5-1* mutation increases susceptibility to *B. cinereal* infection. Leaves of five-week-old plants were drop-inoculated with *B. cinerea* at the concentration of 2.5×10^5 spores/ml. Lesion size was measured 2 days post-inoculation (dpi). The *pFRK1::LUC* transgenic plants (WT), *aggie5-1* mutant and homozygous lines of p35S*::AtAGGIE5*^{D618N}*-GFP* transgenic plants in WT background were included in the assay. The data are shown as mean ± se from 15 infected leaves. **C.** Resistance to *B. cinereal* infection are unaltered in *aggie5-2* and *aggie5-3* mutants. Leaves of five-week-old plants were drop-inoculated with *B. cinerea* at the concentration of 2.5×10^5 spores/ml. Lesion size was measured 2 days post-inoculation (dpi). Col-0 (WT), *aggie5-2* and *aggie5-3* mutant were included in the assay. The data are shown as mean ± se from 15 infected leaves. The above experiments were repeated 3 times with similar results.

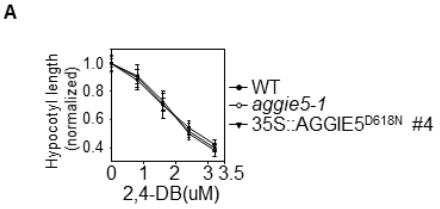

Figure 4.9 AGGIE5^{D618N} does not affect growth inhibition triggered by 2,4-DB.

A. AGGIE5^{D618N} does not affect growth inhibition triggered by 2,4-DB. Four-day-old seedlings were treated with 0, 0.8, 1.6, 2.4 or 3.2 uM 2,4-DB for 6 days on ½ MS solid medium. The *pFRK1::LUC* transgenic plants (WT), *aggie5-1* mutant and homozygous lines of p35S*::AtAGGIE5*^{D618N}*-GFP* transgenic plants in WT background were included in the assay. The data are shown as means ± se from from 20 seedlings. The above experiments were repeated 3 times with similar results.

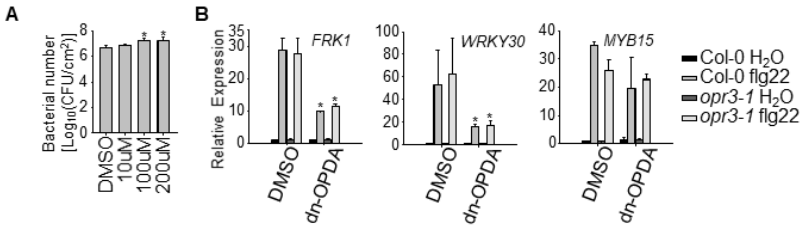

Figure 4.10 Application of dn-OPDA attenuates immune gene expression and negatively regulates disease resistance to virulence bacterial pathogen P.s.t. DC3000.

A. Application of 100 uM dn-OPDA on Arabidopsis leaves negatively regulates local disease resistance to virulence bacterial pathogen *P.s.t. DC3000*. Four-week-old Col-0 (WT) plants were hand-inoculated with 3% DMSO or 10, 100, 200 uM dn-OPDA (in 3% DMSO) 6 hours before inoculation of *P.s.t. DC3000* at 5×10 cfu/ml. The *in planta* bacterial growth was measured at 3 days-post inoculation (dpi). **B.** Application of 100 uM dn-OPDA negatively regulates endogenous MAMP-induced marker gene expression. Ten-day-old seedlings were treated with 100 nM flg22 for 60 min for qRT-PCR analysis after pretreatment with 3% DMSO or 100 uM dn-OPDA (in 3% DMSO). Col-0 (WT) and *opr3-1* mutant were included in the assay. The data are shown as means ± se from three biological repeats with Student's *t*-test. * indicates $p<0.05$ and ** indicates $p<0.01$ when compared to WT. The above experiments were repeated 3 times with similar results.

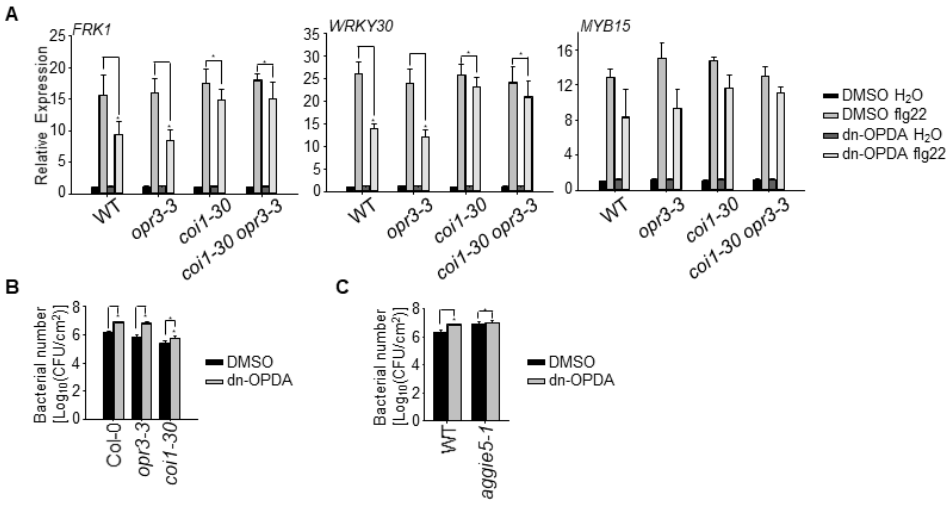

Figure 4.11 Dn-OPDA partially rely on COI1 but not OPR3 to attenuates plant defense to virulence bacterial pathogen P.s.t. DC3000.

A. Attenuation of dn-OPDA on immune gene expression is partially COI1-dependent but OPR3-independent. Ten-day-old seedlings were treated with 100 nM flg22 for 60 min for qRT-PCR analysis after pretreatment with 3% DMSO or 100 uM dn-OPDA (in 3% DMSO). Col-0 (WT), *opr3-3*, *coi1-30* and *coi1-30opr3-3* mutants were included in the assay. The coi*1-30* mutant is from next generation of *coi1-30*(+/-) and confirmed by PCR-based genotyping. The coi*1-30opr3-3* mutant are from next generation of coi*1-30*(+/-) *opr3-3* and confirmed by PCR-based genotyping. The data are shown as means ± se from three biological repeats with Student's *t*-test. * indicates $p<0.05$ and ** indicates $p<0.01$ when compared to WT. **B.** Attenuation of dn-OPDA on disease resistance to virulence bacterial pathogen *P.s.t. DC3000* is partially COI1-dependent but OPR3-independent. Four-week-old Col-0 (WT), *opr3-3*, and *coi1-30* plants were hand-inoculated with 3% DMSO or 10, 100, 200 uM dn-OPDA (in 3% DMSO) 6 hours before inoculation of *P.s.t. DC3000* at 5×10 cfu/ml. The coi*1-30* mutant is from next generation of *coi1-30*(+/-) and confirmed by PCR-based genotyping. The coi*1-30opr3-3* mutant are from next generation of coi*1-30*(+/-) *opr3-3* and confirmed by PCR-based genotyping. The *in planta* bacterial growth was measured at 3 days-post inoculation (dpi). **C.** Dn-OPDA could not enhance susceptibility in *aggie5-1*. Four-week-old *pFRK1::LUC* (WT) and *aggie5-1* plants were hand-inoculated with 3% DMSO or 10, 100, 200 uM dn-OPDA (in 3% DMSO) 6 hours before inoculation of *P.s.t. DC3000* at 5×10 cfu/ml. The *in planta* bacterial growth was measured at 3 days-post inoculation (dpi). The above experiments were repeated 3 times with similar results.

Table 4.1 Genotyping primers used in study in chapter 4.

Gene	Forward Primer	Reverse Primer
opr3-3	AATCCGTGTAGCCAACAACTG	CAGCCACATTCAAAGAAAAGG
opr3_F1		AACACACTACATTACATTATTGATAACA
coi1-30	TGGACCATATAAATTCATGCAGTC	CTGCAGTGTGTAACGATGCTC

Note: The T-DNA left and right border primers were selected accordingly to each mutant. For SALK lines, LBb1.3 (ATTTTGCCGATTTCGGAAC); for *opr3-1*, LB (TTGTTTTGGAGGATTTCATGC) and for *opr3-3*, LB_GW1 (GCTTTCGCCTATAAATACGACGGATCGT) was used respectively.

Table 4.2 qRT-PCR primers used in study in chapter 4.

Gene	Forward Primer	Reverse Primer
FRK1	ATCTTCGCTTGGAGCTTCTC	TGCAGCGCAAGGACTAGAG
WRKY30	GCAGCTTGAGAGCAAGAATG	AGCCAAATTTCCAAGAGGAT
MYB15	CTTGGCAATAGATGGTCAGC	TGAGTGTGCCATACGTTCTTG
At2g17740	TGCTCCATCTCTCTTTGTGC	ATGCGTTGCTGAAGAAGAGG
PR1	ACACGTGCAATGGAGTTTGTGG	TTGGCACATCCGAGTCTCATG
PAD4	TCTTCAGTTAAAGATCAAGGAAGG	GGTTGAATGGCCGGTTATC
PAL1	GTGGCAATGTGTGGCTTGT	ATTAGATTCCTTAACGCCGGAAT
VSP1	CAACCAAATCAGCCCATTG	TACTCAAGCCAAACGGATCG
AFB1	AGTGATTTGATGCTTCATCACTTGT	CAATGACTTCGACATTGAGCCTTGGCA
UBQ10	AGATCCAGGACAAGGAAGGTATTC	CGCAGGACCAAGTGAAGAGTAG

Note: The restriction enzyme sites are underlined, and the point mutation sites are underlined and in bold.

4.5 Discussion

Combining the *in vitro* AGGIE5 phosphorylation assay and the result of the transgenic plants, we conclude that D618N mutation negatively regulates AGGIE5 function in plant innate immunity and that AGGIE5 likely works as a negative regulator to limit dn-OPDA and some other oxylipins production in MTI to fine-tune plant defense against bacterial pathogens. We inspected that dn-OPDA is an important signal facilitating fine-tune of defense responses in nucleus. Dn-OPDA-regulated transcription reprogramming in Arabidopsis was shown to be dependent on JA signaling SCF-COI1 complex interacting with unknown complexes. Information on the role of AGGIE5 in dn-OPDA induction or accumulation is still limited, even in knockout plants, except for the mutant *aggie5-1*. This mutant exhibited severely increased dn-OPDA and JA induction possibly caused by a defect in the phosphorylation at a conserved MAPK phosphorylation site by a group C MPK MPK7, which was associated with the partial loss of flg22-triggered protection in Arabidopsis leaves against bacterial pathogen P.s.t. DC3000. We also hypothesized the phosphorylation at Thr-612 positively regulates AGGIE5 activity to suppress MAMP-induced oxylipin production and facilitate immune responses in Arabidopsis, which is worthy testing in the future. Overall, this study provides strong genetic evidence for the global roles of dn-OPDA in Arabidopsis immunity to bacterial pathogens.

In Arabidopsis, two sn-1-specific acyl hydrolases, Defective in Anther Dehiscence 1 (DAD1) and Dongle (DGL) have been reported to be plastid-localized lipases and to be essential for JA biosynthesis. However, both DGL RNA interference lines and the *dad1*

mutant maintain wild-type levels of 12-OPDA and JA during the early wound response as well as after Pseudomonas infection, suggesting that unidentified enzymes with sn-1 and sn-2 hydrolase activity are involved in wound-induced and pathogen-induced OPDA and JA synthesis (Ellinger et al., 2010). Moreover, it is reported that increased levels of oxylipins and salicylic acid favored closure of stomata in response to Pseudomonas syringae infection.

5. CONCLUSION

We identified one novel regulator of plant innate immunity on the basis of pathogen-induced immune gene expression screening of Arabidopsis EMS insertion mutant collections. The application of non-pathogenic strain DC3000 *hrcC* robustly elicits MAMP-induced defense responses, providing an alternative way to study MTI. The method combing traditional map-based cloning and bulk population sequencing is helpful for the genetic mutant examination. Compared with conventional genetic analysis, mapping-by-sequencing is more efficient. We can identify the causative mutations in two generations. Furthermore, we can identify some unusual mutations, like the *aggie5-1* (AGGIE5^{D618N}) case, although the phenotypes and mechanism may not be understood immediately and easily. Continuing screening will uncover more novel components involved in plant innate immunity.

AGGIE5 are essential to maintain normal immune gene induction and resistance to bacterial pathogens. Genome-wide transcriptional analysis revealed the transcription reprogramming is compromised in the *aggie5-1* mutant and transgenic plants expressing AGGIE5^{D618N}. AGGIE5 encodes a chloroplast/peroxisome-localized protein which possess both lipase and NTPase domain. Genetic analysis reveals that both intact lipase and NTPase motifs are required for functionality of AGGIE5 in plant immunity. In a yeast-two-hybrid screen, the group C MPK MPK7 is identified as the interactor of AGGIE5. Interestingly, *in vitro* assays indicated that MPK7 directly interacts with and phosphorylates membrane-resident AGGIE5. In addition, our genetic screen revealed that MPK7 also play an important role in plant resistance against bacterial pathogens.

Furthermore, the functionality of AGGIE5 in MTI depends on MPK7-mediated protein phosphorylation, suggesting that AGGIE5 as one of MPK7 client proteins regulates plant defense responses. Mutagenesis analysis revealed that specific phosphorylation sites of AGGIE5 by MPK7 are indispensable for its function in MTI. Moreover, the dn-OPDA did suppress MTI gene induction. Application of dn-OPDA in *opr3* mutants and *coi1-30* mutant provide insights that dn-OPDA attenuates immune genes expression relying on CO1 but not OPR3.

REFERENCES

Allen, G.J., Muir, S.R., and Sanders, D. (1995). Release of CA^{2+} from individual plant vacuoles by both insp(3) and cic ADP-Ribose. Science *268*, 735-737.

Andersson, M.X., Hamberg, M., Kourtchenko , O., Brunnstrom, A., McPhail, K.L., Gerwick, W.H., Gobel, C., Feussner, I., and Ellerstrom, M. (2006). Oxylipin profiling of the hypersensitive response in Arabidopsis thaliana - Formation of a novel oxo-phytodienoic acid-containing galactolipid, arabidopside E. Journal of Biological Chemistry *281*, 31528-31537.

Arnaud, D., and Hwang, I. (2015). A sophisticated network of signaling pathways regulates stomatal defenses to bacterial pathogens. Molecular Plant *8*, 566-581.

Asai, T., Tena, G., Plotnikova, J., Willmann, M.R., Chiu, W.L., Gomez-Gomez, L., Boller, T., Ausubel, F.M., and Sheen, J. (2002). MAP Kinase signalling cascade in Arabidopsis innate immunity. Nature *415*, 977-983.

Bent, A.F., and Mackey, D. (2007). Elicitors, effectors, and R genes: The new paradigm and a lifetime supply of questions. In Annual Review of Phytopathology, pp. 399-436.

Berridge, M.J. (1993). Inositol trisphosphate and calcium signaling. Nature *361*, 315-325.

Berriri, S., Garcia, A.V., Frey, N.F.D., Rozhon, W., Pateyron, S., Leonhardt, N., Montillet, J.L., Leung, J., Hirt, H., and Colcombet, J. (2012). Constitutively active mitogen-activated protein kinase Versions Reveal Functions of Arabidopsis MPK4 in Pathogen Defense Signaling. Plant Cell *24*, 4281-4293.

Bethke, G., Unthan, T., Uhrig, J.F., Poschl, Y., Gust, A.A., Scheel, D., and Lee, J. (2009). Flg22 regulates the release of an ethylene response factor substrate from MAP Kinase 6

in Arabidopsis thaliana via ethylene signaling. Proceedings of the National Academy of Sciences of the United States of America *106*.

Bohm, H., Albert, I., Fan, L., Reinhard, A., and Nurnberger, T. (2014). Immune receptor complexes at the plant cell surface. Current Opinion in Plant Biology *20*, 47-54.

Boller, T., and Felix, G. (2009). A renaissance of elicitors: perception of microbe-associated molecular patterns and danger signals by pattern-recognition receptors. In Annual Review of Plant Biology, pp. 379-406.

Boudsocq, M., Willmann, M.R., McCormack, M., Lee, H., Shan, L.B., He, P., Bush, J., Cheng, S.H., and Sheen, J. (2010). Differential innate immune signalling via Ca^{2+} sensor protein kinases. Nature *464*, 418-U116.

Broekaert, W.F., Delaure, S.L., De Bolle, M.F.C., and Cammue, B.P.A. (2006). The role of ethylene in host-pathoven interactions. In Annual Review of Phytopathology, pp. 393-416.

Browse, J. (2009). Jasmonate Passes Muster: A receptor and targets for the defense hormone. In Annual Review of Plant Biology, pp. 183-205.

Chinchilla, D., Zipfel, C., Robatzek, S., Kemmerling, B., Nurnberger, T., Jones, J.D.G., Felix, G., and Boller, T. (2007). A flagellin-induced complex of the receptor FLS2 and BAK1 initiates plant defence. Nature *448*, 497-U412.

Couto, D., and Zipfel, C. (2016). Regulation of pattern recognition receptor signalling in plants. Nature Reviews Immunology *16*, 537-552.

Dave, A., and Graham, I.A. (2012). Oxylipin signaling: a distinct role for the jasmonic acid precursor cis-(+)-12-oxo-phytodienoic acid (cis-OPDA). Frontiers in Plant Science *3*.

Dubiella, U., Seybold, H., Durian, G., Komander, E., Lassig, R., Witte, C.P., Schulze, W.X., and Romeis, T. (2013). Calcium-dependent protein kinase/NADPH oxidase activation circuit is required for rapid defense signal propagation. Proceedings of the National Academy of Sciences of the United States of America *110*, 8744-8749.

Ellinger, D., Stingl, N., Kubigsteltig, II, Bals, T., Juenger, M., Pollmann, S., Berger, S., Schuenemann, D., and Mueller, M.J. (2010). Dongle and Defective in anther dehiscence1 lipases are not essential for wound- and pathogen-induced jasmonate biosynthesis: redundant lipases contribute to jasmonate formation. Plant Physiology *153*, 114-127.

Farmer, E.E., Almeras, E., and Krishnamurthy, V. (2003). Jasmonates and related oxylipins in plant responses to pathogenesis and herbivory. Current Opinion in Plant Biology *6*, 372-378.

Fessler, M.B., and Parks, J.S. (2011). Intracellular lipid flux and membrane microdomains as organizing principles in inflammatory cell signaling. Journal of Immunology *187*, 1529-1535.

Feys, B.J., Moisan, L.J., Newman, M.A., and Parker, J.E. (2001). Direct interaction between the Arabidopsis disease resistance signaling proteins, EDS1 and PAD4. Embo Journal *20*, 5400-5411.

Feys, B.J., Wiermer, M., Bhat, R.A., Moisan, L.J., Medina-Escobar, N., Neu, C., Cabral, A., and Parker, J.E. (2005). Arabidopsis senescence-associated gene101 stabilizes and

signals within an enhanced disease susceptibility 1 complex in plant innate immunity. Plant Cell *17*, 2601-2613.

Glazebrook, J. (2005). Contrasting mechanisms of defense against biotrophic and necrotrophic pathogens. Annual Review of Phytopathology *43*, 205-227.

Gobel, C., Feussner, I., Hamberg, M., and Rosahl, S. (2002). Oxylipin profiling in pathogen-infected potato leaves. Biochimica Et Biophysica Acta-Molecular and Cell Biology of Lipids *1584*, 55-64.

Gobel, C., Feussner, I., Schmidt, A., Scheel, D., Sanchez-Serrano, J., Hamberg, M., and Rosahl, S. (2001). Oxylipin profiling reveals the preferential stimulation of the 9-lipoxygenase pathway in elicitor-treated potato cells. Journal of Biological Chemistry *276*, 6267-6273.

Halim, V.A., Altmann, S., Ellinger, D., Eschen-Lippold, L., Miersch, O., Scheel, D., and Rosahl, S. (2009). PAMP-induced defense responses in potato require both salicylic acid and jasmonic acid. Plant Journal *57*, 230-242.

Hartley, S.E., Eschen, R., Horwood, J.M., Gange, A.C., and Hill, E.M. (2015). Infection by a foliar endophyte elicits novel arabidopside-based plant defence reactions in its host, Cirsium arvense. New Phytologist *205*, 816-827.

Heese, A., Hann, D.R., Gimenez-Ibanez, S., Jones, A.M.E., He, K., Li, J., Schroeder, J.I., Peck, S.C., and Rathjen, J.P. (2007). The receptor-like kinase SERK3/BAK1 is a central regulator of innate immunity in plants. Proceedings of the National Academy of Sciences of the United States of America *104*, 12217-12222.

Hisamatsu, Y., Goto, N., Hasegawa, K., and Shigemori, H. (2006). Senescence-promoting effect of arabidopside A. Zeitschrift Fur Naturforschung C-a Journal of Biosciences *61*, 363-366.

Jeworutzki, E., Roelfsema, M.R.G., Anschutz, U., Krol, E., Elzenga, J.T.M., Felix, G., Boller, T., Hedrich, R., and Becker, D. (2010). Early signaling through the Arabidopsis pattern recognition receptors FLS2 and EFR involves Ca2+-associated opening of plasma membrane anion channels. Plant Journal *62*, 367-378.

Kachroo, A., and Kachroo, P. (2009). Fatty Acid-Derived Signals in Plant Defense. In Annual Review of Phytopathology, pp. 153-176.

Kadota, Y., Sklenar, J., Derbyshire, P., Stransfeld, L., Asai, S., Ntoukakis, V., Jones, J.D.G., Shirasu, K., Menke, F., Jones, A., *et al.* (2014). Direct Regulation of the NADPH Oxidase RBOHD by the PRR-Associated Kinase BIK1 during Plant Immunity. Molecular Cell *54*, 43-55.

Kang, S.N., Yang, F., Li, L., Chen, H.M., Chen, S., and Zhang, J. (2015). The Arabidopsis transcription factor Brassinosteroid Insensitive1-ethyl methanesulfonate-suppressor1 is a direct substrate of mitogen-activated protein kinase 6 and regulates immunity. Plant Physiology *167*, 1076-+.

Kourtchenko, O., Andersson, M.X., Hamberg, M., Brunnstrom, A., Gobel, C., McPhail, K.L., Gerwick, W.H., Feussner, I., and Ellerstrom, M. (2007). Oxo-phytodienoic acid-containing galactolipids in arabidopsis: Jasmonate signaling dependence. Plant Physiology *145*, 1658-1669.

Kupper, F.C., Gaquerel, E., Boneberg, E.M., Morath, S., Salaun, J.P., and Potin, P. (2006). Early events in the perception of lipopolysaccharides in the brown alga Laminaria digitata include an oxidative burst and activation of fatty acid oxidation cascades. Journal of Experimental Botany *57*, 1991-1999.

Lai, X.J., Yang, R., Luo, Q.J., Chen, J.J., Chen, H.M., and Yan, X.J. (2015). Glycerol-3-phosphate metabolism plays a role in stress response in the red alga pyropia haitanensis. Journal of Phycology *51*, 321-331.

Landgraf, P., Feussner, I., Hunger, A., Scheel, D., and Rosahl, S. (2002). Systemic accumulation of 12-oxo-phytodienoic acid in SAR-induced potato plants. European Journal of Plant Pathology *108*, 279-283.

Li, B., Jiang, S., Yu, X., Cheng, C., Chen, S.X., Cheng, Y.B., Yuan, J.S., Jiang, D.H., He, P., and Shan, L.B. (2015). Phosphorylation of trihelix transcriptional repressor ASR3 by MAP Kinase 4 negatively regulates Arabidopsis Immunity. Plant Cell *27*, 839-856.

Li, L., Li, M., Yu, L.P., Zhou, Z.Y., Liang, X.X., Liu, Z.X., Cai, G.H., Gao, L.Y., Zhang, X.J., Wang, Y.C., *et al.* (2014). The FLS2-Associated Kinase BIK1 Directly Phosphorylates the NADPH oxidase RbohD to control plant immunity. Cell Host & Microbe *15*, 329-338.

Lin, W.W., Lu, D.P., Gao, X.Q., Jiang, S., Ma, X.Y., Wang, Z.H., Mengiste, T., He, P., and Shan, L.B. (2013). Inverse modulation of plant immune and brassinosteroid signaling pathways by the receptor-like cytoplasmic kinase BIK1. Proceedings of the National Academy of Sciences of the United States of America *110*, 12114-12119.

Lin, Y.T., Chen, L.J., Herrfurth, C., Feussner, I., and Li, H.M. (2016). Reduced biosynthesis of digalactosyldiacylglycerol, a major chloroplast membrane lipid, leads to oxylipin overproduction and phloem cap lignification in Arabidopsis. Plant Cell *28*, 219-232.

Lippok, B., Birkenbihl, R.P., Rivory, G., Brummer, J., Schmelzer, E., Logemann, E., and Somssich, I.E. (2007). Expression of AtWRKY33 encoding a pathogen- or PAMP-responsive WRKY transcription factor is regulated by a composite DNA motif containing W box elements. Molecular Plant-Microbe Interactions *20*, 420-429.

Liu, S., Kracher, B., Ziegler, J., Birkenbihl, R.P., and Somssich, I.E. (2015). Negative regulation of ABA signaling by WRKY33 is critical for Arabidopsis immunity towards Botrytis cinerea 2100. Elife *4*.

Liu, Y.D., and Zhang, S.Q. (2004). Phosphorylation of 1-aminocyclopropane-1-carboxylic acid synthase by MPK6, a stress-responsive mitogen-activated protein kinase, induces ethylene biosynthesis in Arabidopsis. Plant Cell *16*, 3386-3399.

Lu, D.P., Wu, S.J., Gao, X.Q., Zhang, Y.L., Shan, L.B., and He, P. (2010). A receptor-like cytoplasmic kinase, BIK1, associates with a flagellin receptor complex to initiate plant innate immunity. Proceedings of the National Academy of Sciences of the United States of America *107*, 496-501.

Marcos, R., Izquierdo, Y., Vellosillo, T., Kulasekaran, S., Cascón, T., Hamberg, M., and Castresana, C. (2015). 9-lipoxygenase-derived oxylipins activate Brassinosteroid signaling to promote cell wall-based defense and limit pathogen infection. Plant Physiology *169*, 2324-2334.

Meng, X.Z., Xu, J., He, Y.X., Yang, K.Y., Mordorski, B., Liu, Y.D., and Zhang, S.Q. (2013). Phosphorylation of an ERF transcription factor by Arabidopsis MPK3/MPK6 regulates plant defense gene induction and fungal resistance. Plant Cell *25*, 1126-1142.

Meng, X.Z., and Zhang, S.Q. (2013). MAPK cascades in plant disease resistance signaling. In Annual Review of Phytopathology, N.K. VanAlfen, ed., pp. 245-266.

Montillet, J.L., Leonhardt, N., Mondy, S., Tranchimand, S., Rumeau, D., Boudsocq, M., Garcia, A.V., Douki, T., Bigeard, J., Lauriere, C., *et al.* (2013). An abscisic acid-independent oxylipin pathway controls stomatal closure and immune defense in Arabidopsis. Plos Biology *11*.

Mosblech, A., Feussner, I., and Heilmann, I. (2009). Oxylipins: structurally diverse metabolites from fatty acid oxidation. Plant Physiology and Biochemistry *47*, 511-517.

Mueller, S., Hilbert, B., Dueckershoff, K., Roitsch, T., Krischke, M., Mueller, M.J., and Berger, S. (2008). General detoxification and stress responses are mediated by oxidized lipids through TGA transcription factors in Arabidopsis. Plant Cell *20*, 768-785.

Nakajyo, H., Hisamatsu, Y., Goto, N., Yamada, K., Hasegawa, K., and Shigemori, H. (2011). Structure-activity relationships on senescence-promoting effect of Arabidopsides from *Arabidopsis thaliana*. Heterocycles *83*, 57-62.

Nakajyo, H., Hisamatsu, Y., Sekiguchi, M., Goto, N., Hasegawa, K., and Shigemori, H. (2006). Arabidopside F, a new oxylipin from *Arabidopsis thaliana*. Heterocycles *69*, 295-+.

Nilsson, A.K., Fahlberg, P., Johansson, O.N., Hamberg, M., Andersson, M.X., and Ellerstrom, M. (2016). The activity of hydroperoxide lyase 1 regulates accumulation of

galactolipids containing 12-oxo-phytodienoic acid in Arabidopsis. Journal of Experimental Botany *67*, 5133-5144.

Nomura, H., Komori, T., Uemura, S., Kanda, Y., Shimotani, K., Nakai, K., Furuichi, T., Takebayashi, K., Sugimoto, T., Sano, S., *et al.* (2012). Chloroplast-mediated activation of plant immune signalling in Arabidopsis. Nature Communications *3*.

Ochsenbein, C., Przybyla, D., Danon, A., Landgraf, F., Gobel, C., Imboden, A., Feussner, I., and Apel, K. (2006). The role of EDS1 (enhanced disease susceptibility) during singlet oxygen-mediated stress responses of Arabidopsis. Plant Journal *47*, 445-456.

Ogasawara, Y., Kaya, H., Hiraoka, G., Yumoto, F., Kimura, S., Kadota, Y., Hishinuma, H., Senzaki, E., Yamagoe, S., Nagata, K., *et al.* (2008). Synergistic activation of the Arabidopsis NADPH oxidase AtrbohD by Ca^{2+} and phosphorylation. Journal of Biological Chemistry *283*, 8885-8892.

Pedras, M.S.C., and To, Q.H. (2017). Defense and signalling metabolites of the crucifer *Erucastrum canariense*: Synchronized abiotic induction of phytoalexins and galacto-oxylipins. Phytochemistry *139*, 18-24.

Ranf, S., Eschen-Lippold, L., Pecher, P., Lee, J., and Scheel, D. (2011). Interplay between calcium signalling and early signalling elements during defence responses to microbe- or damage-associated molecular patterns. Plant Journal *68*, 100-113.

Roux, M., Schwessinger, B., Albrecht, C., Chinchilla, D., Jones, A., Holton, N., Malinovsky, F.G., Tor, M., de Vries, S., and Zipfel, C. (2011). The Arabidopsis Leucine-Rich Repeat Receptor-Like Kinases BAK1/SERK3 and BKK1/SERK4 Are Required for Innate Immunity to Hemibiotrophic and Biotrophic Pathogens. Plant Cell *23*, 2440-2455.

Saubeau, G., Goulitquer, S., Barloy, D., Potin, P., Andrivon, D., and Val, F. (2013). Differential induction of oxylipin pathway in potato and tobacco cells by bacterial and oomycete elicitors. Plant Cell Reports *32*, 579-589.

Schafer, M., Fischer, C., Meldau, S., Seebald, E., Oelmuller, R., and Baldwin, I.T. (2011). Lipase activity in insect oral secretions mediates defense responses in Arabidopsis. Plant Physiology *156*, 1520-1534.

Segonzac, C., and Zipfel, C. (2011). Activation of plant pattern-recognition receptors by bacteria. Current Opinion in Microbiology *14*, 54-61.

Stintzi, A., and Browse, J. (2000). The Arabidopsis male-sterile mutant, *opr3*, lacks the 12-oxophytodienoic acid reductase required for jasmonate synthesis. Proceedings of the National Academy of Sciences of the United States of America *97*, 10625-10630.

Stintzi, A., Weber, H., Reymond, P., Browse, J., and Farmer, E.E. (2001). Plant defense in the absence of jasmonic acid: The role of cyclopentenones. Proceedings of the National Academy of Sciences of the United States of America *98*, 12837-12842.

Suarez-Rodriguez, M.C., Adams-Phillips, L., Liu, Y.D., Wang, H.C., Su, S.H., Jester, P.J., Zhang, S.Q., Bent, A.F., and Krysan, P.J. (2007). MEKK1 is required for flg22-induced MPK4 activation in Arabidopsis plants. Plant Physiology *143*, 661-669.

Sun, Y.D., Li, L., Macho, A.P., Han, Z.F., Hu, Z.H., Zipfel, C., Zhou, J.M., and Chai, J.J. (2013). Structural basis for flg22-Induced activation of the Arabidopsis FLS2-BAK1 Immune Complex. Science *342*, 624-628.

Taki, N., Sasaki-Sekimoto, Y., Obayashi, T., Kikuta, A., Kobayashi, K., Ainai, T., Yagi, K., Sakurai, N., Suzuki, H., Masuda, T., *et al.* (2005). 12-oxo-phytodienoic acid triggers

expression of a distinct set of genes and plays a role in wound-induced gene expression in Arabidopsis. Plant Physiology *139*, 1268-1283.

Testerink, C., and Munnik, T. (2011). Molecular, cellular, and physiological responses to phosphatidic acid formation in plants. Journal of Experimental Botany *62*, 2349-2361.

Tsai, C.-H., Chen, C.-W., Boachon, B., Thomas, J., Weber, H., Mauch-Mani, B., and Zimmerli, L. (2009). Priming of Arabidopsis PAMP-triggered immunity by specific inhibition of the jasmonate response induced by coronatine. Plant Biology (Rockville) *2009*, 324-324.

Tsuda, K., Sato, M., Glazebrook, J., Cohen, J.D., and Katagiri, F. (2008). Interplay between MAMP-triggered and SA-mediated defense responses. Plant Journal *53*, 763-775.

Tsuda, K., Sato, M., Stoddard, T., Glazebrook, J., and Katagiri, F. (2009). Network properties of robust immunity in plants. Plos Genetics *5*.

van der Luit, A.H., Piatti, T., van Doorn, A., Musgrave, A., Felix, G., Boller, T., and Munnik, T. (2000). Elicitation of suspension-cultured tomato cells triggers the formation of phosphatidic acid and diacylglycerol pyrophosphate. Plant Physiology *123*, 1507-1515.

van Schooten, B., Testerink, C., and Munnik, T. (2006). Signalling diacylglycerol pyrophosphate, a new phosphatidic acid metabolite. Biochimica Et Biophysica Acta-Molecular and Cell Biology of Lipids *1761*, 151-159.

Vicente, J., Cascon, T., Vicedo, B., Garcia-Agustin, P., Hamberg, M., and Castresana, C. (2012). Role of 9-lipoxygenase and alpha-dioxygenase oxylipin pathways as modulators of local and systemic defense. Molecular Plant *5*, 914-928.

Vlot, A.C., Dempsey, D.A., and Klessig, D.F. (2009). Salicylic acid, a multifaceted hormone to combat disease. In Annual Review of Phytopathology, pp. 177-206.

Wagner, S., Stuttmann, J., Rietz, S., Guerois, R., Brunstein, E., Bautor, J., Niefind, K., and Parker, J.E. (2013). Structural basis for signaling by exclusive EDS1 Heteromeric complexes with SAG101 or PAD4 in plant innate immunity. Cell Host & Microbe *14*, 619-630.

Xiao, S., Gao, W., Chen, Q.F., Chan, S.W., Zheng, S.X., Ma, J.Y., Wang, M.F., Welti, R., and Chye, M.L. (2010). Overexpression of Arabidopsis Acyl-CoA binding protein ACBP3 Promotes starvation-induced and age-dependent leaf senescence. Plant Cell *22*, 1463-1482.

Xin, X.F., and He, S.Y. (2013). *Pseudomonas syringae* pv. *tomato* DC3000: A model pathogen for probing disease susceptibility and hormone signaling in Plants. In Annual Review of Phytopathology, N.K. VanAlfen, ed., pp. 473-498.

Xu, J., Xie, J., Yan, C.F., Zou, X.Q., Ren, D.T., and Zhang, S.Q. (2014). A chemical genetic approach demonstrates that MPK3/MPK6 activation and NADPH oxidase-mediated oxidative burst are two independent signaling events in plant immunity. Plant Journal *77*, 222-234.

Yamaguchi, T., Minami, E., and Shibuya, N. (2003). Activation of phospholipases by N-acetylchitooligosaccharide elicitor in suspension-cultured rice cells mediates reactive oxygen generation. Physiologia Plantarum *118*, 361-370.

Yu, X., Feng, B.M., He, P., and Shan, L.B. (2017). From chaos to harmony: responses and signaling upon microbial pattern recognition. In Annual Review of Phytopathology, Vol 55, J.E. Leach, and S.E. Lindow, eds., pp. 109-137.

Zhang, J., Li, W., Xiang, T.T., Liu, Z.X., Laluk, K., Ding, X.J., Zou, Y., Gao, M.H., Zhang, X.J., Chen, S., *et al.* (2010). Receptor-like cytoplasmic kinases integrate signaling from multiple plant immune receptors and are targeted by a *Pseudomonas syringae* effector. Cell Host & Microbe *7*, 290-301.

Zhang, J., Shao, F., Cui, H., Chen, L.J., Li, H.T., Zou, Y., Long, C.Z., Lan, L.F., Chai, J.J., Chen, S., *et al.* (2007). A *Pseudomonas syringae* effector inactivates MAPKs to suppress PAMP-Induced immunity in plants. Cell Host & Microbe *1*, 175-185.

Zhang, Z.B., Wu, Y.L., Gao, M.H., Zhang, J., Kong, Q., Liu, Y.A., Ba, H.P., Zhou, J.M., and Zhang, Y.L. (2012). Disruption of PAMP-induced MAP Kinase cascade by a *Pseudomonas syringae* effector activates plant immunity mediated by the NB-LRR Protein SUMM2. Cell Host & Microbe *11*, 253-263.

Zhao, H.Z., Jiang, M., Xie, C.F., Song, S.Y., Wang, J., Bai, G., and Luo, G.A. (2012). Metabolic fingerprinting of ACS7 mutant and wild-tyoe Arabidopsis thaliana under salt stress by ultra performance liquid chromatography coupled with quadrupole/time of flight mass spectrometry. Analytical Letters *45*, 1786-1798.

Zipfel, C., Kunze, G., Chinchilla, D., Caniard, A., Jones, J.D.G., Boller, T., and Felix, G. (2006). Perception of the bacterial PAMP EF-Tu by the receptor EFR restricts Agrobacterium-mediated transformation. Cell *125*, 749-760.

Zipfel, C., Robatzek, S., Navarro, L., Oakeley, E.J., Jones, J.D.G., Felix, G., and Boller, T. (2004). Bacterial disease resistance in Arabidopsis through flagellin perception. Nature *428*, 764-767.

APPENDIX

SUPPLEMENTAL DATA

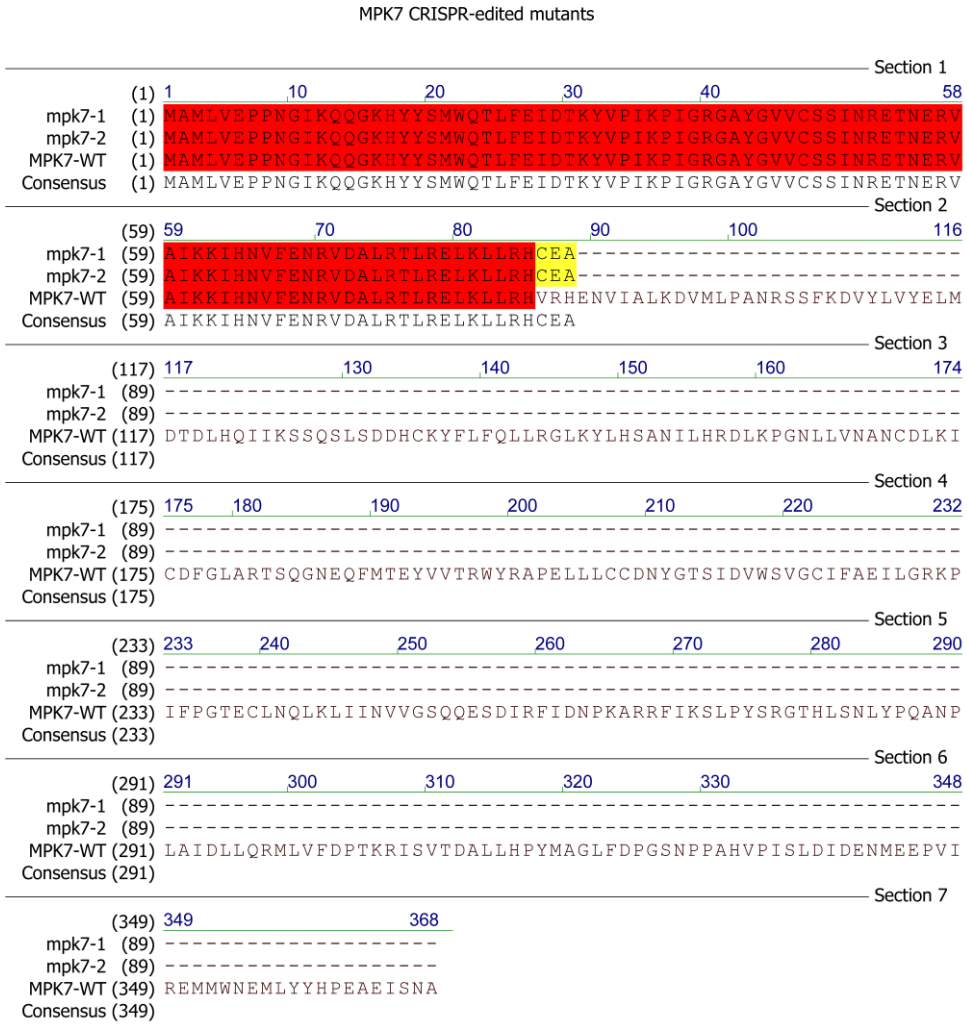

Supplemental Figure 1 Mutation in *mpk7-1* and *mpk7-2* mutants

Alignment of proteins of MPK7, *mpk7-1* and *mpk7-2000*